Electron Transfer in Protein-Carbon Nanotube Hybrid Structures

Adam Beachey

A thesis presented for the degree of

Doctor of Philosophy

School of Physics and Astronomy

Cardiff University

September 2017

Abstract

We have developed a method of site-specific attachment of proteins to pristine carbon nanotube (CNT) sidewalls using genetically encoded unnatural amino acids with functional moieties. Here, we incorporated an azido phenylalanine (AzPhe) group at different positions in the protein to assess the importance of different protein-CNT configurations. This site-directed mutation of the protein structure has provided routes for direct covalent attachment to the sidewall of the CNT, as well as providing a functional group for modification with another molecule such as pyrene for non-covalent CNT attachment.

We have employed a variety of techniques to study these nanoscale systems in order to gain an insight into the binding mechanism, the protein-CNT interaction dynamics and their electronic properties. Using atomic force microscopy (AFM), we found that the proteins bind regular patterns dictated by the position of the phenyl azide. By integrating CNTs into electrical transistor-like devices, we have performed electrical measurements across the CNTs to monitor the attachment of various proteins to the CNT sidewalls.

Using these protein-CNT systems, we have also been able to study the interaction between proteins and CNTs using Raman spectroscopy and total internal reflection fluorescence microscopy (TIRFM). Here we present evidence of covalent attachment of proteins to CNTs using Raman spectroscopy to study the changes in vibrational modes present in the CNTs. TIRFM has provided evidence of post-cross-linking activity of proteins on CNTs using super-folder green fluorescent protein (sfGFP) as a marker. By analysing the protein's fluorescent properties, we have produced evidence suggesting the importance of the orientation of the protein with respect to the CNT, which in turn determines the distance between the CNT interface and the active site of the protein.

The approach developed here provides a versatile and convenient generic approach to interfacing proteins, in defined orientations, to CNTs that holds promise for exploitation in bioelectronics tools and biomolecular sensors.

Acknowledgements

The past few years have been strange so the people I'll be thanking are those who helped me make sense of it. I'd like to thank my supervisors Emyr MacDonald, Martin Elliott and Dafydd Jones for pushing me along and guiding me through this PhD. Your support kept me going and your friendship made this a lot easier. True bros!

I have to thank Sam, Andy, Adam, Ben, Dan, Rachael and most importantly, Harley from the Biosciences group for making sure I had something to write about in this thesis. There have been many people to come through that group over the past couple of years and I'm happy to have worked with them and have the occasional beer with them. Thanks to Dave Jamieson and Oliver Castell for they're patience and perseverance through the countless hours of TIRF imaging. We got there in the end! Thanks to Matteo Palma and Mark Freely of Queen Mary University of London for all their help and guidance throughout and thank you to Monica Craciun of University of Exeter for the many Raman measurements.

Cheers to Chris Dunscombe and Andrew Harrison for all the help and guidance in fabricating my devices and providing all the electronics help when I needed it. Cheers to Dave Westwood and Matthew Hunt for making sure Fridays in the labs wasn't chore. And cheers to everyone in the School of Physics and Astronomy and anyone who made it to the Flute after a long Friday (and occasionally a Wednesday). There's too many of you to name and I'm too lazy to list you guys but you're all bros!

Now I'd like to say cheers to my Nanophysics family; Andry, Athraa, Rangeen, Isam and Watheq for putting up with me for all these years. You guys have been a second family to me and you encouraged me to succeed. I just encouraged you guys to come to the pub! Also, not to forget; cheers to Suze, who has been the truest of bros for the past couple of years. Thanks for keeping me sane. Much Love!

Before I mention my actual family, it's best I mention the boys and the lads (as they know, that's not gender specific). Cheers to Mikey, Nathan, Owain, Nomme, Jingham, Olly, Keelan and everyone else who's been putting up with me over the years. I realise this list would be a bit long if I wrote everyone's name.

Now I wouldn't have been able to get this far without my family pushing me and supporting me. My mums; Julie and Sarah, my dad, Ric, and the rest of the Beacheys and Leachs; Luke, Joe, Gemma and Joyce. You guys put me up when I needed it and helped me with everything. Somehow inspired me to pursue Science and Art! I've been told that's rare but it feels natural. Everything I do is for you guys!

List of Publications

Adam Beachey, Harley L. Worthy, Benjamin J Bowen, David Jamieson, Monica F. Craciun, J. Emyr Macdonald, Oliver K Castell, Martin Elliott D. Dafydd Jones. **Genetically encoded designed covalent interfacing of proteins with nanocarbon: a general strategy for functionally integrated regular nanoscale assembly.**

Contents

List of Figures

Abbreviations

SPM	**S**canning **P**robe **M**icroscopy
AFM	**A**tomic **F**orce **M**icroscopy
STM	**S**canning **T**unneling **M**icroscopy
TIRFM	**T**otal **I**nternal **R**eflection **F**luorescence **M**icroscopy
CNT	**C**arbon **N**ano**t**ube
MWNT	**M**ulti-**W**alled carbon **N**ano**t**ube
SWNT	**S**ingle-**W**alled carbon **N**ano**t**ube
sSWNT	**s**emiconducting **S**ingle-**W**alled carbon **N**ano**t**ube
mSWNT	**m**etallic **S**ingle-**W**alled carbon **N**ano**t**ube
sfGFP	**s**uper**f**older **G**reen **F**luorescent **P**rotein
cyt b_{562}	**c**ytochrome $_{562}$
AzPhe	p-**Az**ido-L-**Ph**enylalanine
SPAAC	**S**train-**P**romoted **A**zide-**A**lkyne **C**ycloaddition
CuAAC	**C**opper-promoted **A**zide-**A**lkyne **C**ycloaddition
DBCO	**di**benzyl**c**yclo**o**ctyne
DEP	**Die**lectro**p**horesis

Dedicated to all the bros, the lads, the boys, and the family...

Chapter 1

Introduction

1.1 Bioelectronics with Carbon Nanostructures

The development of electrical interfacing to single biomolecules or complexes in a living cell is key to several areas of fundamental science, such as electron transfer and physiology. It is also important in understanding the principles for developing novel biosensors for medical diagnostics. For instance, growth hormone secretion underlies basic biological action and many human diseases (e.g. obesity, diabetes, thyroid disease, dwarfism and gigantism or acromegaly) result from altered hormone secretion patterns or hormone sensitivity, while hormone abuse remains a pressing problem in both professional and amateur sport [1]. Growth hormone levels in the blood can vary by a factor of two or so over a 10-30 minute timescale[2]. Currently, single samples are sent to a laboratory with a turnaround time of a couple of days. Another important use for diagnostics is monitoring the single molecule interactions between the antibiotic resistance enzyme TEM β-lactamase and its inhibitor protein (BLIP), allowing us to detect antibodies present in infection[3][4]. These examples highlight an important area that would benefit enormously from the development of a real-time continuous diagnostic measurement technique having direct electrical readout.

In aiming to develop a generic platform that could be used for such real-time electrical sensors, one needs a stable material system having well-defined electrical behaviour, sensitive to its molecular environment, which can be easily interfaced to a range of proteins to act as molecular recognition sensors.

Carbon nanomaterials such as graphene and carbon nanotubes (CNTs) are good candidates as organic electronic materials to interface to protein with their high surface-to-volume ratio resulting in their electronic properties being highly sensitive to changes in their environment. CNTs in particular have the advantage of having a nanoscale structure with comparable dimensions to that of biological molecules. This has motivated much research into producing medical biosensors with a CNT interface[5][6]. Unlike most other methods currently used for biodetection, CNT based devices can be modified directly with biomolecules to be used as label-free active biosensors. This means we can create a platform for monitoring biological events without modifying the target molecules[7][8]. CNTs have the advantage of being bio-compatible with the ability to be functionalised with a wide variety of molecules. Chemical functionalisation of CNTs can enhance their bio-compatibility as well as their solubility making them easier to integrate into an electronic device platform. This has resulted in a wide range of device types in order to utilise the properties of the CNTs and the biomolecular functional group. These devices include electrodes modified with CNTs[8][9], CNT-based electrodes with adsorbed bio-molecules[10], covalent attachment of biomolecules[11] and various others. This gives us a broad range of possibilities for producing a device to understand this biomolecular electronic interaction; each with their own advantages and disadvantages.

One very important factor to consider when integrating biomolecules into an electronic device is the Debye screening length. This is the distance at which charge from the mobile carrier is screened from the conjugated material. If the distance between the biomolecule and the CNT is beyond this length, then there will be no charge transfer between structures[7][12]. For this reason, the distance between the structures should be made as small as possible, limiting the chance of charge screening. To do this, the size of the linker between the two must be made as

small as possible. Previous studies have shown some success with limiting this distance by funtionalising CNTs with a linker molecule of known length prior to the biomolecular integration [13][14][11]. This can be done using a covalent approach involving breaking a C=C double bond to form a covalent bond to the CNT surface,or a non-covalent approach which involves pi-stacking of a conjugated molecule onto the CNT surface.

By using the covalent approach, a defect site is introduced to the carbon material's surface via the conversion of an sp^2 hybrid orbital structure to an sp^3 structure with a highly reactive linker molecule at this defect site. This can be done using such reactive groups as aryl diazonium salts, (figure 1.1, (a))[15], or azomethine ylides[16]. Although this has proven to be an effective method to provide strong linker sites for biomolecular integration, the introduction of chemically induced defect sites across the entire structure of the CNTs can heavily detriment their conductive properties[15][17]. Another method sometimes used for covalent CNT functionalisation, is by sonicating them in a solution of hydrogen chloroauric acid, causing gold nanoparticles to form on the surface of the CNT (figure 1.1, (c)). These nanoparticles can readily bind to thiol groups either in alkane-thiols or those already present in a biomolecule [18] [19].

Alternatively, non-covalent approaches have been investigated which take advantage of the π orbital nature of the sp^2 carbon surface (figure 1.1, (b)). By choosing a reactive molecule with an aromatic hydrocarbon based structure, we are able to non-covalently stack these π orbital systems on the CNT surface via π-π stacking interactions. These interactions describe an electrostatic interaction resulting in a non-covalent attractive force between parallel aromatic rings [22]. This can effectively provide a reactive linker moiety across the CNT structure without inducing a structural defect. The most commonly used linker molecule for this purpose is 1-pyrenebutyric acid, which contains a pyrene molecule consisting of 4 benzene rings[23]. Another approach would be to functionalise the surface with single strand DNA (ssDNA) which contains bases with an aromatic ring structure. Reactive groups can easily be integrated at desired positions on the ssDNA, allowing for control over the distribution of reactive sites on the CNT[24][25].

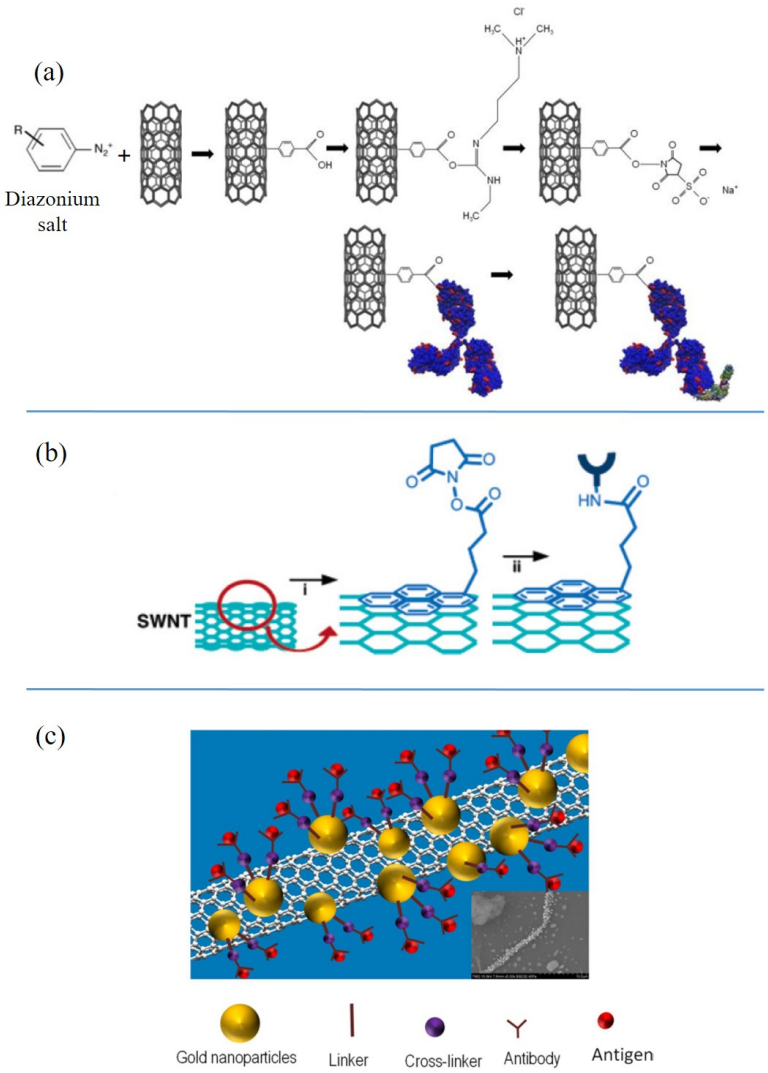

FIGURE 1.1: Three widely used methods of forming biomolecule-CNT hybrid structures; each of which involving pre-modification of the CNT structures.(a) Covalent linker molecules incorporated into the CNT structure via a reduction reaction with diazonium salts. This forms sp^3 defects along the CNT surface with carboxyl groups, which can be modified to bind to a target biomolecule [20]. (b) Reaction of SWNT with (i) 1-pyrenebutanoic acid succinimidyl ester to form a functional group which (ii) reacts with incoming biomolecule [21]. (c) A model of a CNT decorated with gold nanoparticles, allowing for functionalisation with thiol groups[19].

Much research has been successful in providing precise control over segregating CNTs according to their structure and electronic properties[26][27], as well as the deposition of CNTs with the ability to create nanoscale architecture on which to base these biosensors[28][29]. However, formulating a reliable method of biomolecular deposition in order to measure single molecule events has proved more of a challenge. One reoccurring factor which limits this in most cases is the lack of

control of the individual biomolecules, with little control over their position and orientation. Reliance on physical absorption via van der Waals forces leads to weak poorly-defined attachment. An ideal situation would be to determine the specific residue in the protein structure to form a stable, well-characterised bond to the CNT, giving us an idea of position compared with the active site of the molecule. Enzymes for example, come in a wide variety of structures with their own specific function, dictated by their active site. Once the enzyme's conjugate molecule interacts with this active site, this could cause an electrostatic change in the biomolecule. This change in the electronic dynamics can be thought of as a transfer of charge, which would originate in this active site. Therefore, the distance between the active site and the CNT is crucial in understanding how this energy transfer mechanism takes place. As previously mentioned, the Debye screening length can play an important factor here and hence it is desirable to limit the distance at which the charge needs to travel.

For the research presented in this thesis, we took an alternative approach to CNT functionalisation, by modifying the protein to incorporate the linker molecule instead of modifying the CNT surface. By incorporating the linker molecule directly into the protein structure, this allowed us to gain more control over the binding and orientation of the protein. This allows us to define how the protein binds through to the carbon surface without needing to functionalise the entire carbon structure. Modifying the protein instead of the CNT has the benefit of limiting the number of defects created to one per protein attached, as well as providing it a with a defined orientation allowing for a pre-defined distance between the CNT surface and the active site of the protein. This method of biochemical engineering relies on the process of site directed mutagenesis, which is used to make changes to the DNA sequence used to form the protein. This method of bio-engineering in turn allows us to incorporate an unnatural amino acid (uAA) into the chain of amino acids which makes up the protein[30]. The uAA allows us to include additional functionality which is not already present in the 20 natural amino acids.

Previous work from our group has shown this to be an effective method of binding various proteins to different substrates. Single molecule measurements have

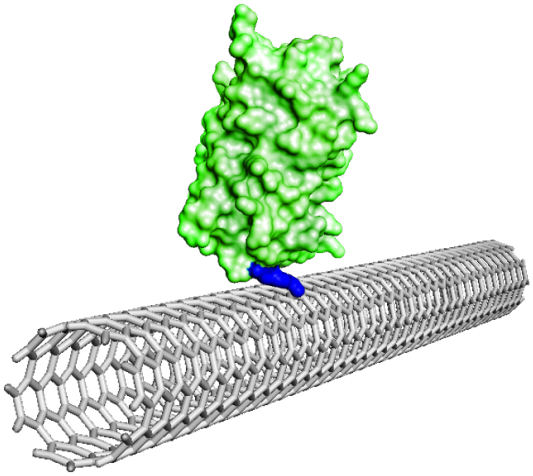

FIGURE 1.2: A model of a green fluorescent protein (GFP) modified with the unnatural amino acid, azido phenylalanine (in blue), to bind to a CNT.

been performed with scanning tunnelling microscopy (STM) of a cytochrome b_{562} variant with a thiol groups at opposite ends of the protein, which enables it to bind to a gold substrate and a platinum-iridium STM tip simultaneously[31][32]. Pre-defining the position of the linker interface molecule allowed for the electronic pathway to be analysed shedding new light on a nanoscale system.

Another example of uAA incorporation is in the antibiotic resistance protein TEM β-lactamase, where the uAA p-azido-L-phenylalanine (AzPhe) was introduced to the protein, giving it the functionality to bind to dibenzylcyclooctyne pyrene. This gave it the ability to stack onto a graphene substrate, resulting in a non-covalent interface with a pre-defined protein orientation[33].

With the use of uAAs, we have the ability to incorporate various biomolecules into nano-electronic systems, with the potential for transistor type biosensing technology. This would mean the biomolecule would act to gate the current flow in the nanomaterials with the sensitivity to detect individual quantum events. Most sensing technologies rely on analysing bulk statistics from analyte samples by measuring overall changes. Using this new method of developing protein-CNT hybrid structures, we can reliably bind proteins to CNTs with a higher degree of control

than alternative binding methods. Having this high degree of control over the orientation of the protein can be crucial for understanding mechanisms within these biomolecules at a single molecule level. By understanding the electron transfer in a single molecule or how it interacts with its interface material, we could potentially develop single molecule, sensing systems. This could be very important to pick out single molecule interactions for medical detection and monitoring drug delivery.

1.2 Thesis Outline

The work covered in this thesis branches from developing CNT based systems for electronic analysis and scanning probe studies, to the implementation of proteins with post deposition activity measurements. Using a variety of proteins at varying orientations, we have been able to investigate how they interact with CNTs to give us a clearer understanding of the viability of the uAA linker method. This is done using various techniques, including atomic force microscopy (AFM), Raman Spectroscopy and total internal reflection fluorescence microscopy (TIRFM). Simple transistor-like devices have been built to test the protein-CNT hybrids as a viable sensing device and give a clearer understanding into the electron flow at the interface.

In Chapter 2, I discuss the background theory behind CNTs and the proteins under investigation. I also discuss the theory and methods behind the uAA incorporation into the protein structure.

Chapter 3 provides an overview of the experimental techniques used and developed for this project including AFM, Raman spectroscopy, TIRFM, CNT dispersion and device integration.

In Chapter 4, I analyse and discuss the importance of site directed mutagenesis to define the orientation of the protein when cross linking to the CNTs. This is analysed using AFM, giving us convincing evidence of defined orientation of

different proteins. These proteins are then integrated into a device and the binding mechanism is monitored in real-time by measuring the resistance changes in a simple potential divider circuit.

Chapter 5 covers the optical studies of these protein-CNT hybrid structures. Here, I use Raman spectroscopy to study effect of protein cross-linking to the CNT structures by analysing their vibrational modes. I then go on to study the activity of the fluorescent protein, super folder green fluorescent protein (sfGFP), to understand how it behaves when bound to a CNT surface.

Finally, in Chapter 6 I provide an overview of the points discussed in this thesis with a summary of the outcomes and their importance to further the understanding of bioelectronics and nanomaterials.

Chapter 2

Background Theory

2.1 Introduction

In order to fully understand protein-CNT interactions, we must first establish the background theory regarding the nanotubes and the proteins in question. In this chapter I provide a brief introduction to CNTs in terms of their discovery, synthesis and properties. This is followed by an introduction to proteins where I provide information on the proteins used for this project. I have also provided further information on the linker molecule incorporation, which was briefly mentioned in the previous chapter.

2.2 Carbon Nanotubes

Since the early 20th century, carbon materials have been the focal point of much research for their unique mechanical and electrical properties. The discovery of CNTs emerged from the study of macroscopic carbon fibres formed via catalytic chemical vapour deposition. As research into growing these fibres continued, the growth of carbon filaments with a diameter less than 10nm was observed. These fibres had a cross section of concentric circular fibres with the innermost fibres behaving like CNTs[34] .

The breakthrough in CNT synthesis came in 1991, when Sumio Iijima produced multi-walled CNTs (MWNT) using arc discharge on graphitic rods. This was the turning point in bridging the gap between experimental observation and theoretical studies of 1D systems[35] .

2.2.1 Synthesis of CNTs

A few methods of CNT synthesis have been developed, each with their advantages. Synthesis via arc discharge or laser ablation uses very high temperatures (>3000°C), producing CNTs with a very high degree of structural perfection. A common method of synthesis is using chemical vapour deposition (CVD) which uses a lower temperature (>1000°C), resulting in a higher probability density of defects, however; this method can be done at atmospheric pressure and can result in a larger yield in comparison with other methods[36].

These methods of synthesis have made it possible to produce SWNTs and MWNTs. These nanotubes can reach lengths from hundreds of nanometres, to several micrometres, with SWNTs having a diameter of 0.4-2nm and MWNTs with a diameter of 2-100nm. It remains a challenge to grow SWNTs with a specific band gap, though some groups have managed this using metal nano-alloy catalysts in the growth process[37][38]. The common method of chirality separation is through the use of post-synthesis processes such as incorporating conjugated polymers with selective π-conjugated structures[39], able to attach to a certain chirality CNT, or more large scale techniques like size exclusion gel chromatography[27][26].

2.2.2 Electronic Structure of CNTs

Carbon (Z=6), is a group 4 element which means it has 4 available electrons in its outer orbital shell. These are split between the 2s and 2p orbitals. 3 of these electrons form a hybrid orbital structure between the s and p orbitals, forming an sp^2 orbital, which has a planar structure with each electron orbiting 120° away from each other. This explains the structure of the planar sheets of carbon, with

each carbon bonding to 3 other carbons at 120° to each other. The 4^{th} valence electron hybridises with the other additional valence electrons in the other carbon atoms orbitals, forming a de-localised π-band. This results in the formation of a 2D, planar lattice of hexagonally bonded carbon known as graphene.

Carbon materials make up a variety of structures with a range of electrical properties. Graphene is characterised as a zero band gap semiconductor or metal as the DOS is zero at the the Fermi level [36]. A CNT is essentially a sheet of graphene, seamlessly wrapped to form a cylinder [40]. However, the electrical properties of the nanotube can vary dramatically, depending on how this graphene sheet is wrapped. Figure 2.1 shows the ways in which this can happen where the structure is described by its chiral vector (n, m). Here, n and m are integers of the vector equation $R = na_1 + ma_1$. When n_1=n_2, this forms an armchair structure which is always metallic with the Fermi level lying within the valence band. Zig-zag structures (n_1,0) can be either semiconducting or metallic and a chiral structure ($n_1 \neq n_2$) is always semiconducting[36] .

For semiconducting SWNTs (sSWNTs), the optical excitation wavelength varies with chirality. The photo-absorption and photoluminescence of such materials depends on their electronic density of states (DOS). The DOS of a 3-D semiconducting material is continuous as a function of energy. For 2-D materials like graphene, one of the dimensions in k-space is confined meaning the DOS follows a step-like function. SWNTs are treated as 1-D materials with electronic confinement in two directions. This results in the DOS following an inverse square rule and therefore is a discontinuous function of the energy, forming spikes in the energy-DOS relationship known as Van Hove singularities[41][34].

These singularities give rise to the optoelectronic properties of sSWNTs, defining positions of multiple conduction and valence bands as shown in figure 2.2. Having such sharp transitions between energy bands means the nanotubes can be photo-excited at well-defined energies, thus meaning the nanotubes can be optically excited at certain wavelengths, defined by the chirality of the nanotube[42].

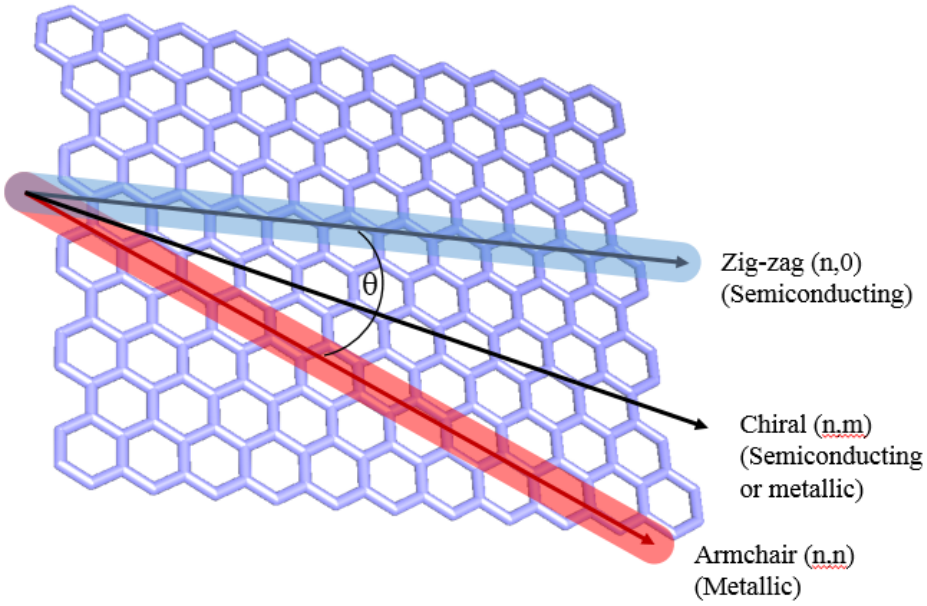

FIGURE 2.1: Graphical representation of sp^2 carbon. The arrows indicate the edges at which the graphene can be rolled up to form a CNT with different electrical properties. θ indicates the chiral angle.

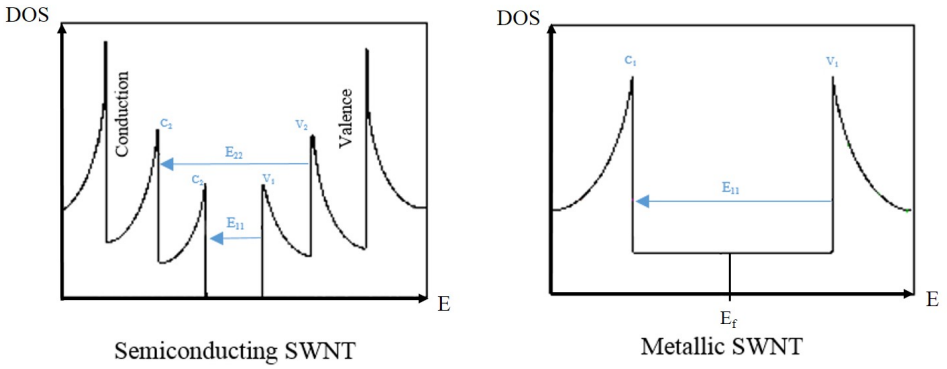

FIGURE 2.2: Plots of the density of states (DOS) against energy (E) for semiconducting and metallic SWNTs. The sharp features are known as Van Hove singularities.

For metallic SWNTs (mSWNTs), the DOS is non zero at the Fermi level which results in no band gap. However, its 1-D structure still means these singularities are present, where transitions between them produce photoluminescent properties. A study has shown that mSWNTs optically excite at around 500nm and emit in the near infra-red[43]. Excitation wavelengths of sSWNTs tend to be around

the optical red to infra-red region of the spectrum (550nm to 800nm) with some excitation wavelengths occurring around 300nm[44].

For photoluminescent and photocatalytic properties of CNTs, we should understand the idea of an electron-hole pair acting as one single quasiparticle known as an exciton. These are formed when electromagnetic waves interact with matter. In semiconductor materials, a photon with greater energy than the band gap is absorbed, exciting an electron from the valence band to the conduction band. The product of this is a positively charged hole in the valence band and a negatively charged electron in the conduction band, bound together by a Coulombic attraction forming an exciton.

2.3 Protein Structure and Biochemistry

Proteins are biomolecules which function as the tools that build, operate and maintain living organisms. They consist of a sequence of amino acids encoded by DNA, which defines how it folds and therefore, how it functions. This initial sequence of amino acids is known as the primary structure of the protein as shown in Figure 2.4. The secondary structure is formed by the interaction of the hydrogen bonds of neighbouring amino acids creating two types of stable structures known as alpha helices and beta sheets as shown in Figure 2.3. Within an alpha helix, the hydrogen bond network runs along the length of the helix, resulting in its coiled shape. Alternatively, the hydrogen bond network runs in between parallel beta sheets causing this ordered row of amino acids.From here the proteins fold themselves into a compact 3-D domain which shields most of the carbon rich, hydrophobic amino-acids from surrounding water molecules. This is known as the tertiary structure and the basis of monomeric proteins. Two or more domains within a single protein can assemble into a larger quaternary structure[45].

To understand how proteins or other biomolecules can be incorporated into nanoelectronics, we must understand the physical interactions that govern their structure and function. Amino acids are bound together with the formation of covalent

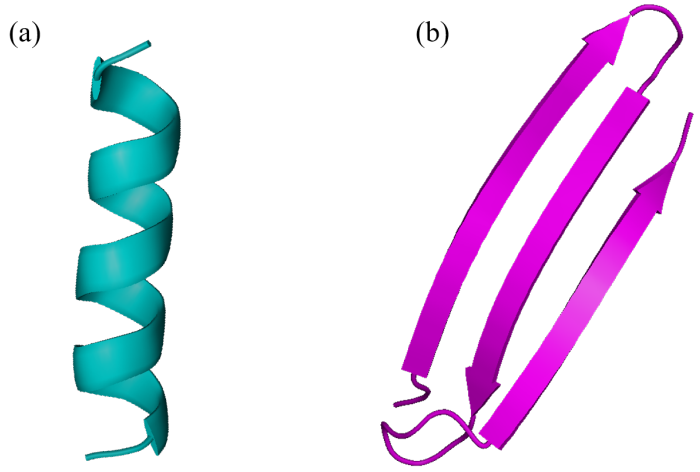

FIGURE 2.3: Models of the secondary protein structure constituents (a) alpha helix and (b) beta sheets.

(peptide) bonds between amino acids along the backbone, with their structure is defined a combination of electrostatics, hydrogen bonds, van der Waals interaction and hydrophobic interactions.

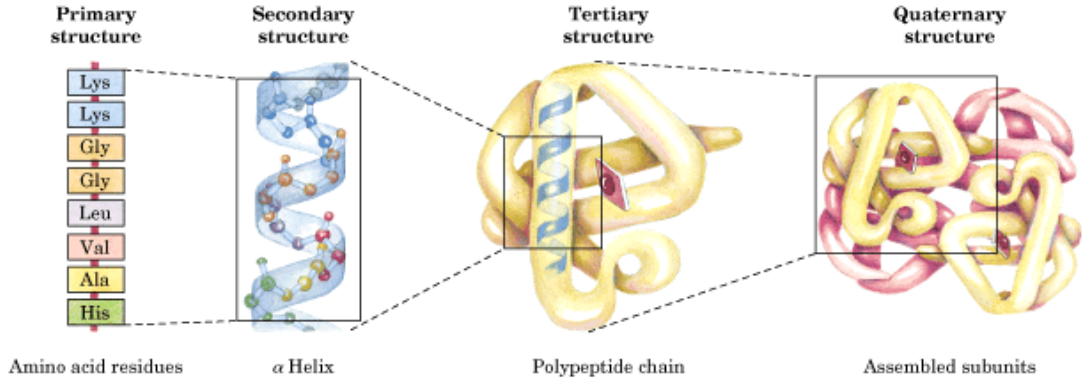

FIGURE 2.4: Levels of protein structure from the initial amino acid sequence to the fully assembled protein[46].

2.3.1 Hydrophobic Interaction

For proteins to form, the folding process must be thermodynamically favourable. According to the second law of thermodynamics, the total entropy of the system and its surroundings has to increase for a reaction to happen spontaneously. For biological systems, we can write the change in Gibbs free energy (ΔG) in terms

of the change in entropy (ΔS) and the change in enthalpy (ΔH) assuming the temperature (T) remains constant:

$$\Delta G = \Delta H - T\Delta S \tag{2.1}$$

Water molecules cannot induce dipoles in non-polar hydrophobic material and hence do not form bonds. However if they reorient, such that they can H-bond to neighbouring water molecules in an ice-like dynamic structure around the non-polar material surface, the number of H-bonds is close to that in bulk solution. Here the enthalpy H (or total energy U) is minimised. The increased order in this ultra-thin ordered layer contributes an decrease in entropy S, with G minimised at equilibrium. We compare two situations where the non-polar material is aggregated into a single globule with that where the same amount of non-polar material segregated into many smaller globules, the difference in Gibbs free energy being $\Delta G = G_{aggregated} - G_{segregated}$. $\Delta H \approx 0$ since there is not an appreciable difference in the number of hydrogen bonds in the two cases. However $\Delta S > 0$ since the entropy decrease due to ordering is smaller in the aggregated case because of the smaller total surface area. Hence $\Delta G = \Delta H$ - $T\Delta S$ will be negative. Equilibrium occurs when G is minimised i.e. when the total surface area of the hydrophobic surface is minimised[45][47].

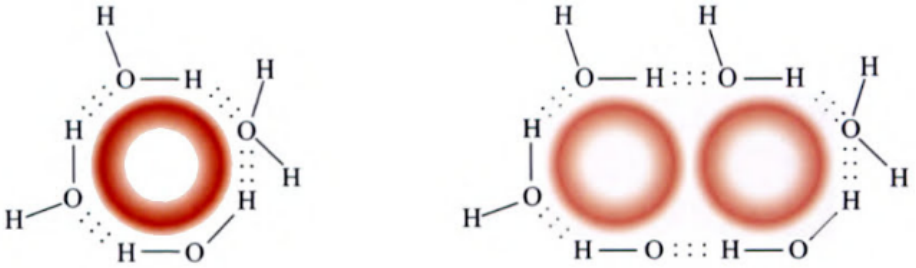

FIGURE 2.5: Hydrogen-bound water molecules around a non-polar molecule on the left. Energy is minimised by bringing these non-polar molecules together through what is known as the hydrophobic interaction to form the non-polar pair seen on the right[48].

This free energy driven phenomenon is known as the hydrophobic effect and is seen in many biological processes[45]. It is this process which drives the packing of the

protein chain to form a compact globule with a hydrophobic core and hydrophillic groups on the exterior.

2.3.2 Electrostatic Interactions

The interior of a protein is made up almost entirely of non polar residues or localised pairs of opposing charge, with the unpaired charged residues forming the external structure of the protein. We will only find charged residues within a protein if they are there to bind to charged atoms like Iron or Oxygen, such that the net local charge is close to zero[45]. This arrangement minimises G since water molecules can bind to polar residues around the periphery and do not come into contact with the non-polar interior. An unpaired charge within the hydrophobic core of a protein will be excluded, as can be seen from simple electrostatic considerations.

Consider the energy U of a sphere of radius R, charge q, in a medium of permittivity ϵ give by Coulomb's law:

$$U = \frac{1}{2}.\frac{e^2}{4\pi \cdot \epsilon \cdot R} \tag{2.2}$$

for water, $\epsilon_r \approx 80$, and for a protein, $\epsilon_r \approx 3$. If we take the radius of our ion to be $R \approx 3\mathring{A}$ and the charge e, to be the charge of an electron, then for a charged ion in contact with water, $U_{water} \approx 0.03$eV whereas for the same charge within the hydrophobic core of the protein, $U_{protein} \approx 0.8$eV. Therefore, to minimise energy, it is favourable for the charge to be on the exterior of the protein[45][47].

2.3.3 Proteins in Bioelectronics

The nanoscale size and well-defined function of individual proteins makes them well suited for incorporation into organic or inorganic structures for nanotechnology. However, due to this nanoscale size, it is unclear what the mechanisms of

energy transfer are between these molecules. There have been many studies which incorporate proteins and other biomolecules into nano-scale devices where their properties are utilised for biomedical targets [5], optoelectronics [49][50] and also used to build nano-structures[51][52]. From these investigations, it is clear that proteins can be successfully be implemented as active elements in nano-electronic devices. Therefore, it should be essential to try to understand the fundamental aspects of their electronic properties.

There have previously been investigations describing the current flow through individual protein molecules which can be described as an individual electron transfer process[31][53][54]. This showed how these molecules can be understood as independent components in electronic devices with the potential to probe the electronic dynamics within these molecules. These studies focused on cytochrome b_{562} (cyt b_{562}) which is a redox active molecule, believed to act as an electron transfer protein[55]. This study introduced the importance of orientation of the protein to it's conductive properties. By altering the geometry of the system, they changed the electron transfer characteristics which was strongly influenced by the inorganic ion core within the protein structure[31].

Another protein which has attracted a lot of attention is green fluorescent protein (GFP) which can be characterised as an electron transfer protein, known for its fluorescent properties[56]. This makes it the ideal candidate for optoelectronic studies as a potential selective light sensor. These two proteins are the main focus of this thesis with the addition of the antibiotic resistance protein, TEM β-lactamase[57].

2.3.4 Green Fluorescent Protein

There are three proteins under investigation in this thesis to help understand the flexibility of the processes used and electron transfer between these molecules and CNTs. The primary focus of this study with be on an improved version of

the GFP, which is isolated from the jellyfish Aequorea Victoria [58]. GFP comprises of 11 β-sheets forming a β-barrel model with an α-helix running through it's centre. The chromophore, located in the middle of the β-barrel, is a p-hydroxybenzylideneimidazolinone formed by re-arranging Ser65, Tyr66 and Gly67 within the protein. The tight β-barrel surrounds the chromophore, shielding it from much energy transfer between it and the surrounding molecules. This means the chromophore should retain its fluorescence and avoiding quenching. As the name suggests, the protein fluoresces in the green region of the optical spectrum[56].

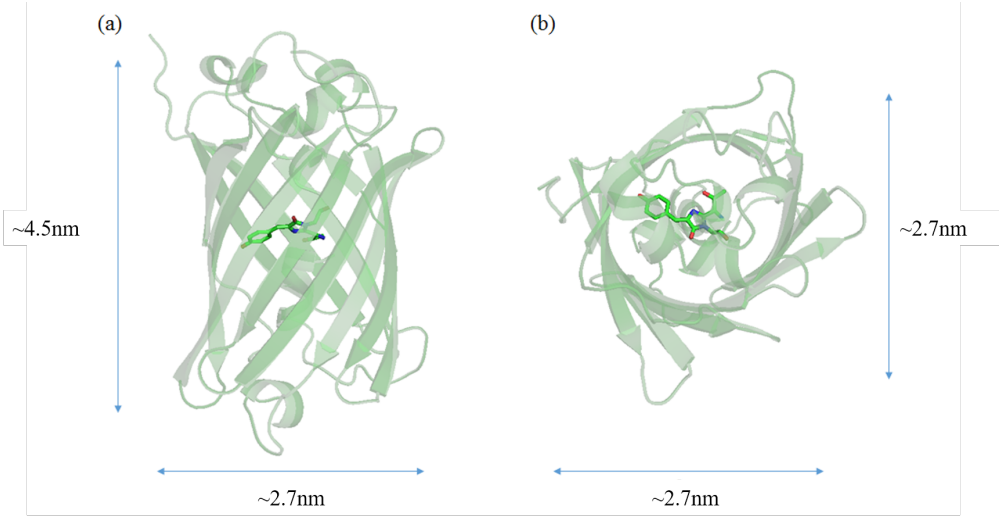

FIGURE 2.6: Graphical representation created in PyMol, of the structure of sfGFP from (a) a side on view, and (b) a top down view. The chromophore is highlighted in the centre of the β-barrel.

The variant used in this investigation is the super folder GFP (sfGFP) which folds more efficiently when fused to other proteins making it more robust and tolerant to its environment. It has a major excitation peak at 475nm and an emission peak at 508nm. The structure of sfGFP is shown in Figure 2.6.

These fluorescent properties and robust structure of sfGFP makes it an ideal protein to study electron transfer between proteins and CNTs.

2.3.5 Cytochrome b_{562}

Cyt b_{562} is a redox-active protein produced in Escherichia coli (E-coli) which is thought to function as an electron transfer protein. The exact mechanism of the electron transfer in this protein is still uncertain although, previous work has shown strong dependence on the environmental properties and the redox haem central cofactor[55][59]. This has since led to studies of environmental effects and orientation dependent investigations when bound to conductive surfaces[32][31] .

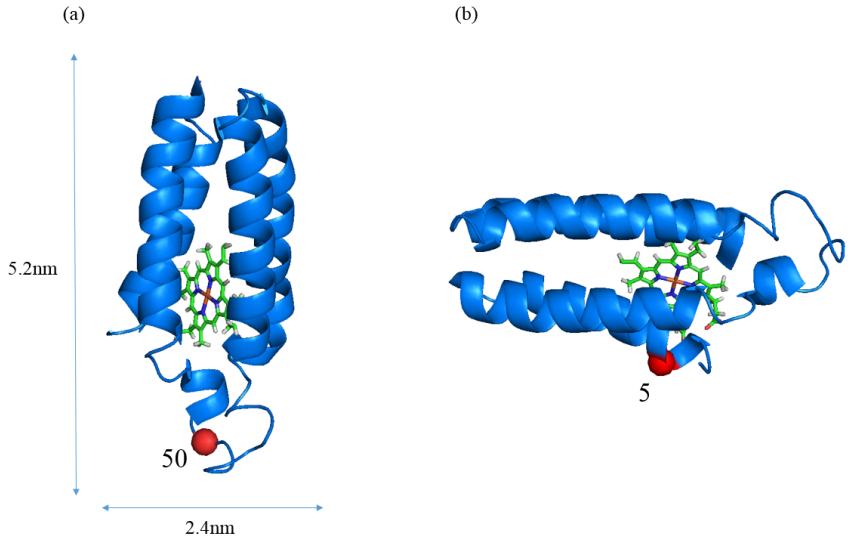

FIGURE 2.7: Graphical representation created in PyMol of the structure of cytochrome b_{562} in (a) the long axis arrangement and (b) the short axis arrangement. The positions of linker sites are marked in red.

Cyt b_{562} is an ideal target for engineering for nanotechnology as it is extremely stable under a large range of pH from 2.5 to 10.5, as well as being stable at temperatures up to 55°C.

For the purpose of the experiments, the protein was engineered to incorporate mutated residues at opposite side of the protein to for long axis (LA) and short axis (SA) configurations as shown in Figure 2.7. This allows us to define the linker proximity to the haem centre and therefore, the distance between the haem and the conductive substrate.

2.3.6 TEM β-lactamase

TEM β-lactamase is part of a group of enzymes responsible for resistance to β-lactam antibiotics such as penicillin. It does this through the hydrolysis of the amide bond of the β-lactam ring, causing breakdown of the antibiotic. This property makes TEM an ideal candidate to study antibiotic resistance, as well as being a bio-sensory target to monitor the build up of β-lactam antibiotic molecules[57].

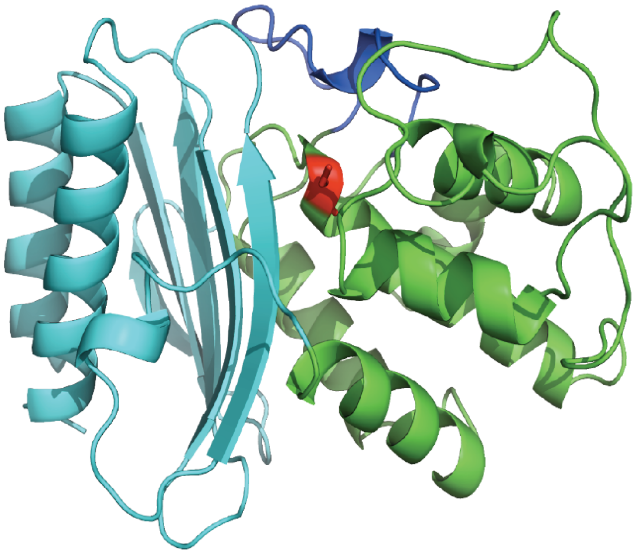

FIGURE 2.8: Graphical representation created in PyMol, of the structure of TEM β-lactamase with the α domain displayed in green and the α/β domain in cyan.

The structure of of TEM, shown in Figure 2.8, consists of two domains: an α domain which is made up of six α-helices, and a α/β domain that is made up of the N and C-termini regions.

2.4 Protein Engineering

Proteins are made up of a sequence of amino acids. In nature, there are 20 different amino acids which form the many various protein structures; each with their own unique function. However, having only 20 natural amino acids means chemical diversity of these molecules is limited, which limits additional functionality[45]. In order to functionalise carbon allotropes with proteins, additional groups must be

added to the protein, without inhibiting its structure or function. In order to do this, we must introduce unnatural amino acids (uAA) which serve as analogues of natural amino acids, with an additional bound functional group. These uAAs mimic the specific post-transnational modifications which happen naturally[30] .

In order to introduce the uAA to the protein sequence, the tRNA, used to form the primary structure of the protein, is mutated to include a TAG stop codon. This codon will stop the transition to form the protein unless the uAA in question is introduced[60]. This uAA will replace the TAG codon allowing the protein to form. With the uAA in place, the protein will fold with the functional group in a desired position on the protein structure.

In this study, the uAA used for funtionalising the proteins is the photo reactive molecule p-azido-L-phenylalanine (AzPhe).

2.4.1 Azido Phenylalanine

AzPhe is an analogue of the natural amino acid phenylalanine, that contains an azide functional group at the para position of the benzene group[30]. These azide groups are sensitive to light with a wavelength lower than 310nm, which is in the UV region of the spectrum. When exposed to this UV wavelength, the azide group consisting of 3 nitrogen, loses a N_2 group, leaving a reactive nitrene species with 2 lone pairs of electrons. This can then be used to cross link to other functional groups via the process of click-chemistry, in order to incorporate additional functionality.

Alternatively, the presence of this nitrene radical can cause a reaction with the sp^2 carbon surface, forming a bond across the C=C double bond in the carbon structure, resulting in a tetrahedral sp^3 carbon structure with a covalently bound nitrene-phenylalanine group as shown in figure 2.9[33].

By incorporating this AzPhe group into the proteins, we can selectively covalently cross-link proteins in defined orientations to CNTs with a short linker by simple

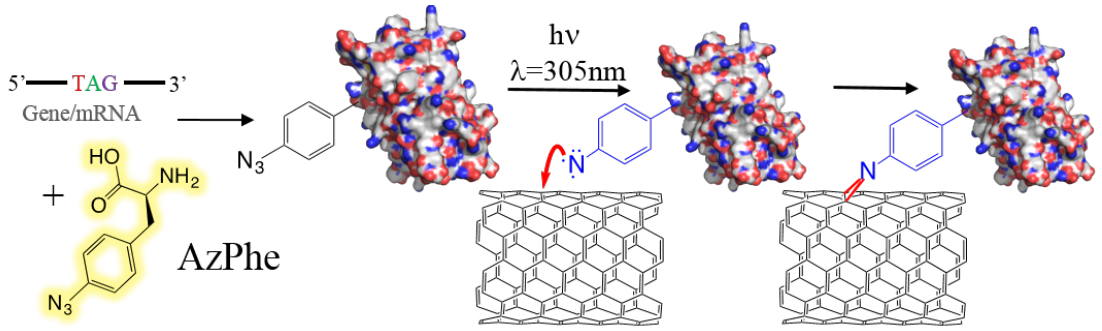

FIGURE 2.9: An overview of the photochemical insertion of a protein with an AzPhe linker molecule to a CNT sidewall.

exposure to high energy UV light. This can be done without the need to pre-treat the CNTs, giving us a one to one defect to chemical bond ratio, effectively limiting the number of defects introduced to the CNT. An alternative to this would be to use a method where no defects would be introduced, via the use of a pyrene based linker molecule.

2.4.2 Pyrene

Pyrene is a molecule consisting of 4 aromatic rings in a planar structure giving it a π orbital electron structure capable of stacking onto the π orbital structure of a CNT though what is known as π-π stacking. By using this as the linker molecule, this would provide a way of non-covalently binding these proteins onto a defect free CNT.

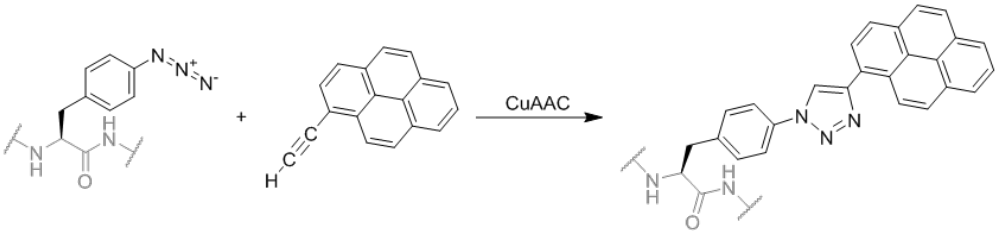

FIGURE 2.10: Chemical reaction for the addition of pyrene to an AzPhe group via copper(I)-catalysed alkyne-azide cycloaddition (CuAAC) to form a pyrene-AzPhe short linker moiety.

To incorporate a pyrene molecule into a protein, it needs to link to the AzPhe molecule. However, pyrene by itself does not readily bind with the azide group.

To overcome this problem, the pyrene is usually functionalised with dibenzylcyclooctyne (DBCO)[61], to form DBCO-pyrene via a reaction of DBCO amine and pyrene butanoic acid. This then allows strain promoted azide-alkyne cycloaddition between the azide group on the AzPhe and the alkyne of DBCO[33]. Although this is an effective method of incorporating the pyrene moiety into the protein, it does introduce an additional molecule in between the pyrene and the AzPhe, resulting in a longer linker molecule than simply using the azide linker alone. To solve this, the pyrene as anchored onto the AzPhe molecule with the help of a copper(I) catalyst via a process called copper(I)-catalysed alkyne-azide cycloaddition (CuAAC). This forms a pyrene-AzPhe short linker moiety without the DBCO molecule as seen in figure 2.10. The reason this isn't always the preferred method of attaching the pyrene moiety is that the prolonged exposure of the protein to a copper(I) catalyst can cause the protein to misfold[62]. To stop the catalytic reaction, ethylenediaminetetraacetic acid (EDTA), is added to absorb the cations and quench the reaction.

2.4.3 Single Strand DNA

Deoxyribonucleic acid, or DNA, is a linear polymer which is made up of a sequence of four different base structures, connected by a sugar-phosphate backbone. The four bases; adenine, cytosine, guanine and thymine, are non-polar structures containing aromatic rings which gives them a de-localised π electron structure. They form specific based pairs with adenine and thymine forming one pair, and guanine and cytosine forming the other. These pairs are held together by weak hydrogen bonds, which allows them to be reversibly broken in biochemical processes. The overall structure is bound together though a polar sugar phosphate backbone as shown in figure 2.11. Like with proteins, the charged polar molecules form the exterior of the DNA structure with the non-polar molecules on the interior, protected from water[45].

DNA is a useful structure to help incorporate into CNT systems, providing an alternative route to non-covalent functionalisation, as well helping solubilise them

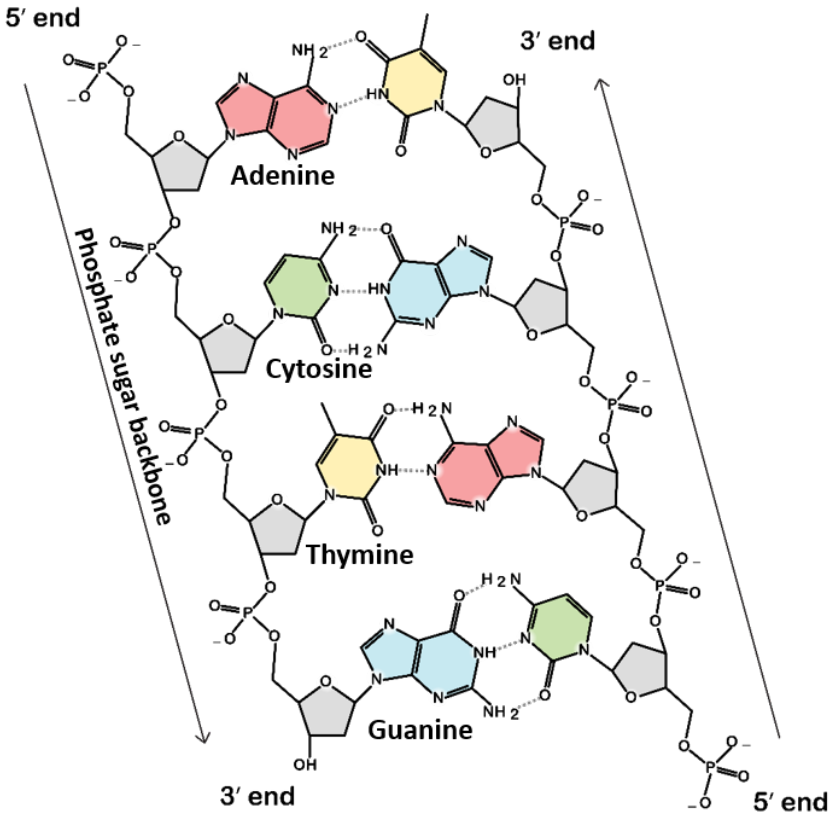

FIGURE 2.11: DNA structure with sugar phosphate backbone (grey) along the outer structure and base pairs of adenine (red) with thymine (yellow), and cytosine (green) with guanine (cyan), on the inside of the structure.

in water[63][64]. Using single strand DNA (ssDNA), that is DNA which hasn't been paired up with its conjugate base pair structures, we can take advantage of the aromatic bases to stack onto a CNT sidewall through π-π stacking. This will leave the polar backbone on the exterior of the CNT, allowing for charge interactions with water and helping its solubility. We can functionalise this backbone by incorporating reactive moieties like acetylene, which is a triple bond carbon molecule, which can bind through to an azide, present on a functionalised protein, using CuACC (this will be discussed in chapter 4).

Chapter 3

Experimental Techniques

3.1 Introduction

In order to study the electronic interactions between proteins and CNTs, a range of different experimental techniques were employed. This ranged from the use of scanning probe microscopy (SPM) to characterise and confirm protein-CNT interactions, to producing transistor-like CNT devices to study their electronic interactions with proteins. Various other tools were used such as Raman spectroscopy to study molecular interactions, and total internal reflection florescence microscopy (TIRFM), which can selectively excite fluorophores in proteins such as GFP, allowing us to study protein activity before and after CNT conjugation.

In this chapter, I describe the techniques used, from the characterising microscopies and spectroscopy, to the CNT dispersion in solution. Here I will cover the theory behind the various techniques used and the the ways in which they were implemented. I have also described the CNT dispersion and deposition methods I have developed as there was no prior experience in this within my group.

3.2 Scanning Probe Microscopy

A commonly used set of tools for the imaging and analysis of nanoscale systems come in the form of SPM. These tools not only allow us to form topographical maps of nanoscale structures; they also provide defined control over nanoscale systems and allows us to obtain mechanical and even quantum mechanical information of organic molecules and solid-state components.

3.2.1 Atomic Force Microscopy

Atomic force microscopy (AFM) is one of the most widely used techniques to study the topography and mechanical properties of nanoscale structures. The AFM was invented by G. Binnig, C.F Quate and Ch. Gerber in the early 1980s and first implemented in experimental use in 1986 [65]. In the same year, Binnig earned the Nobel Prize in physics for the development of the STM.

An AFM uses a sharp tip an the end of a cantilever which interacts with a surface to scan over it. The tip is deflected as it scans the surface due to variations in its topographical height. This deflection is monitored by reflecting a laser beam off the cantilever and onto a position-sensitive photo-detector. As the tip scans over the surface, the level of deflection is measured and a image is produced on a computer[65][66].

AFM has the advantage over its precursor, the STM, that by using the defection of the tip to map out the surface, it doesn't need to be a conducting surface for it to work. It can be used to study insulators as well as conductors and it can be used to measure mechanical properties and manipulate nanoscale structures with nanometre resolution.

As the tip approaches the surface, it experiences an attractive force due to the potential energy of the atoms in the surface as shown in figure 3.1. At very short distances, there is a repulsive force on the tip. There are 3 different modes for the

AFM which each have their advantages and disadvantages; contact mode, tapping mode (or intermediate mode) and non contact mode[67].

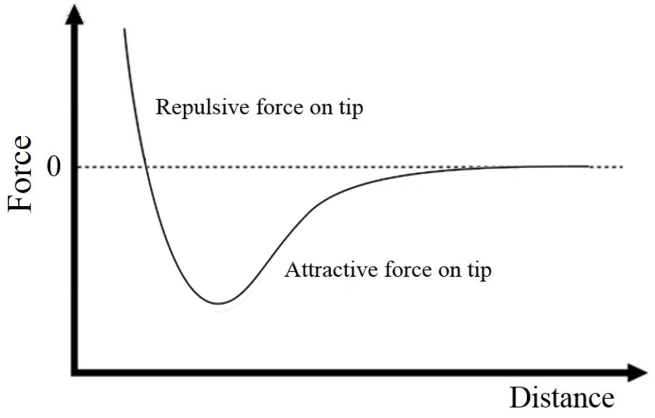

FIGURE 3.1: Diagram displaying the potential energy felt between the AFM tip and the sample.

Contact mode AFM relies on the tip maintaining constant contact with the surface meaning it will be applying a force as it scans. This has its advantages as it can provide high resolution images of the surface whilst providing a method of manipulating the structure with nanoscale control.

Non-contact mode AFM, the tip is lifted a few nanometres away from the surface within the range of van der Waals forces where it still feels an attractive force. The tip is driven by a small piezo element, set to oscillate the cantilever near its resonant frequency as it scans over the surface. The attractive force from the sample dampens the oscillating tip and the changes in amplitude is used as a feedback parameter in a feedback loop, producing a topographical image. This method is non invasive, but has its disadvantages over contact mode[68]. In ambient conditions, non-contact mode can image small unbound molecules on the sample's surface such as water, whereas contact mode will image the underlying surface without seeing the contamination.

Tapping mode AFM is an intermediate between contact and non-contact mode. For this mode, the tip oscillates near its resonant frequency close to the surface allowing it to tap the surface as it scans. Like the non-contact mode, the forces between tip and sample causes a dampening in the oscillation which is translated as

an image. The difference between the drive frequency and the dampened frequency of the cantilever can be also be recorded as a change of phase. This can be an important tool when imaging the change in a material as softer materials can dampen the oscillations more than a hard material. Although the tip still makes contact with the surface, it is a less invasive mode than contact mode and for that reason is the most commonly used mode for AFM[68][67].

During this project, the CNTs are functionalised with soft biological molecules, for which a non invasive AFM mode is desired. For this reason, non-contact mode and tapping mode are the preferred modes as they provide topographical images with minimal interaction with the surface.

3.3 Raman Spectroscopy

Raman Spectroscopy has proved to be an extremely powerful tool used to probe low frequency modes within a system such as vibrational, rotational modes in the molecular structure. It has been widely used to probe carbon allotropes such as graphene and CNTs, revealing many fundamental features of their structure, both physical and electronic[69].

With this in mind, it is also an ideal tool to analyse the binding mechanism which occurs between proteins and CNTs. This is done by studying the changes in the Raman spectra that occur when the CNTs are functionalised. Such changes can cause suppression or enhancement of existing modes as well as the introduction of new vibrational modes introduced through the addition of a protein.

Raman spectroscopy is a non-destructive method used to characterise the vibrational modes of materials using inelastically scattered light, also known as a Raman Effect. This effect, first described by Chandrasekhara Venkata Raman in 1928, describes the interaction where an incident photon is absorbed by a material and re-emitted at a different energy. This change in energy is equal to the energy which is required to excite a molecule to a higher vibrational mode. These vibrational

modes are quantized, the quanta commonly referred to as phonons. There energy quanta depend on the bonding environment of the vibrating atoms and hence, Raman frequencies can shed light on the structure and bonding [70][66, 71, 72].

By studying the Raman spectra produced from carbon nanotubes, a large number of properties can be obtained and studied. Data regarding quality, electronic structure, diameter and even the chirality of the CNTs can be obtained from this method[69][73].

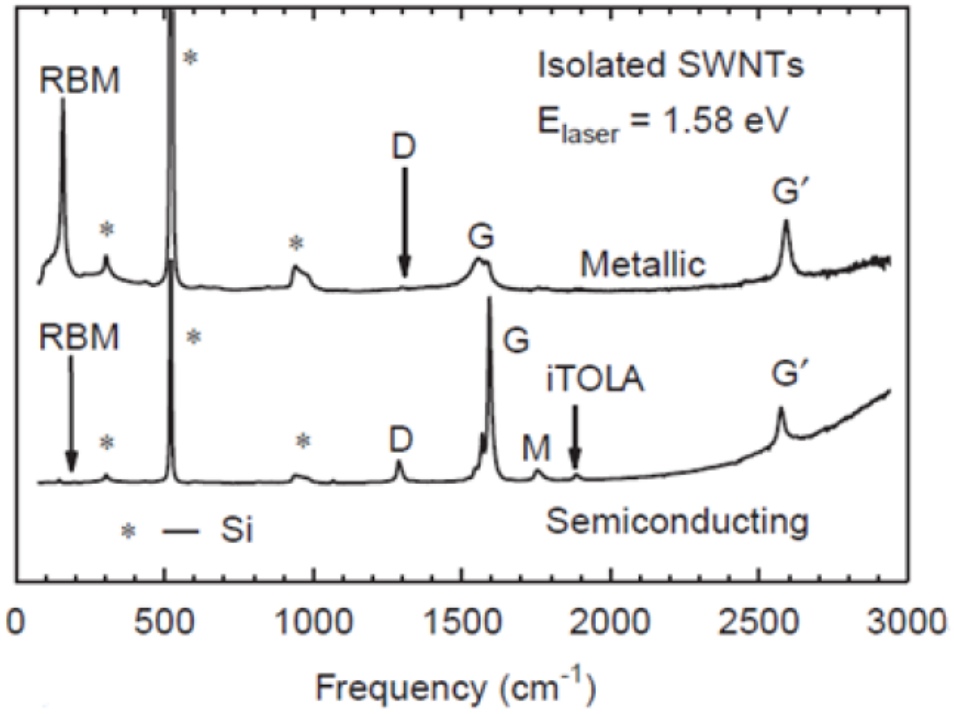

FIGURE 3.2: Raman spectra for metallic and semiconducting SWNTs. These spectra shows the radial breathing mode, the D-mode, G-mode and G'-mode, as well as some weak double resonance modes such as the M-mode[69].

The Raman scattering modes can be split into two groups; the primary modes and the secondary modes. The primary modes arise from a single mode interaction where a photon interacts with a single vibrational mode, and re-emits a photon. These modes are formed from the combination of the breathing modes for σ and π orbitals in the CNT structure. The secondary modes arise from one or two phonon, double resonances, which could arise from multiple modes[70].

The Raman spectra of a pristine CNT would be dominated by these primary modes which, for a CNT, would be the radial breathing mode (RBM) and the graphite-mode (G-mode) as seen in figure 3.2[69].

The RBM arises from the expansion and contraction of the entire circumference of the CNT structure. This is a first order mode which tends to dominate the spectrum at lower frequencies around 248cm^{-1}, but is dependent on the diameter of the tube. This means that the diameter can be deduced by knowing the frequency of this RBM[69].

The G-mode arises from the graphitic carbon and occurs at all sp^2 carbon sites. It involves the in-plane stretching and contracting of C-C bond sites. As it relies on the sp^2 bonds of carbon, then a six fold ring is not necessary for this mode to occur. For CNTs, an additional peak appears here corresponding to an additional mode arising from the folding of the CNT. For SWNTs, this peak appears around a frequency of 1582cm^{-1}[69][73].

Two additional modes worth mentioning are the D mode and it's overtone, the G$'$ mode which appear around 1340cm^{-1} and 2670cm^{-1} respectively. The D-mode is a breathing mode near the Brillouin zone boundary. This arises from the presence of a structural defect which would essentially mean a break in a σ bond orbital. This mode occurs around 1355cm^{-1} and can only occur in the presence of a six fold aromatic ring structure[69][73][74].

CNTs were dispersed in 1%wt SDS solution and drop cast onto SiO_2 substrates and left to dry. The samples were then rinsed under a flow of DI water to remove any loose particles, then immersed in ethanol for 60 min to remove surfactant molecules. These samples were sent for Raman spectroscopy measurements, performed by Prof. Monica Craciun in the Centre for Graphene Science at University of Exeter. For this, a 532nm laser was used with a 2μm spot size.

3.4 Total Internal Reflection Fluorescence Microscopy

There are many optical properties of CNTs which could tell us the more about their electronic structure such as absorption properties, extinction and florescence. This could then in turn tell us how the binding of a protein changes these attributes and therefore, affects the electronic structure of the CNT. However, due to the nanoscale diameter of these structures, it proves difficult to study these with conventional microscopy techniques [71].

Despite proteins like GFP also having a nanoscale structure, their fluorescent properties allow them to be studied using fluorescence microscopy in the visible region of the spectrum. To study how these fluorescent properties are affected by the interaction with CNTs, total internal reflection fluorescence microscopy (TIRFM) was employed.

TIRFM is used to selectively excite fluorescent molecules in a region above a solid substrate within 100nm above the surface. This presents advantages over conventional optical microscopies such as confocal microscopy, as it can be used to study surface bound molecular florescence in a sample with a very high signal to noise ratio[75].

Once a solution of florescent molecules is deposited on a surface, the molecules are free to move around the surface. Some molecules may bind to the substrate while others travel around the solution making it difficult to measure single molecule florescence. By limiting the depth of the observable region, TRIFM can pick out these bound molecules and other low lying molecules within a solution, allowing for single molecule measurements without background florescence from the rest of the solution[76].

This limitation in the depth of the observable region is achieved by shining light through a known thickness of a material with a known refractive index to cause total internal reflection. At the surface interface of the glass, there is a transition

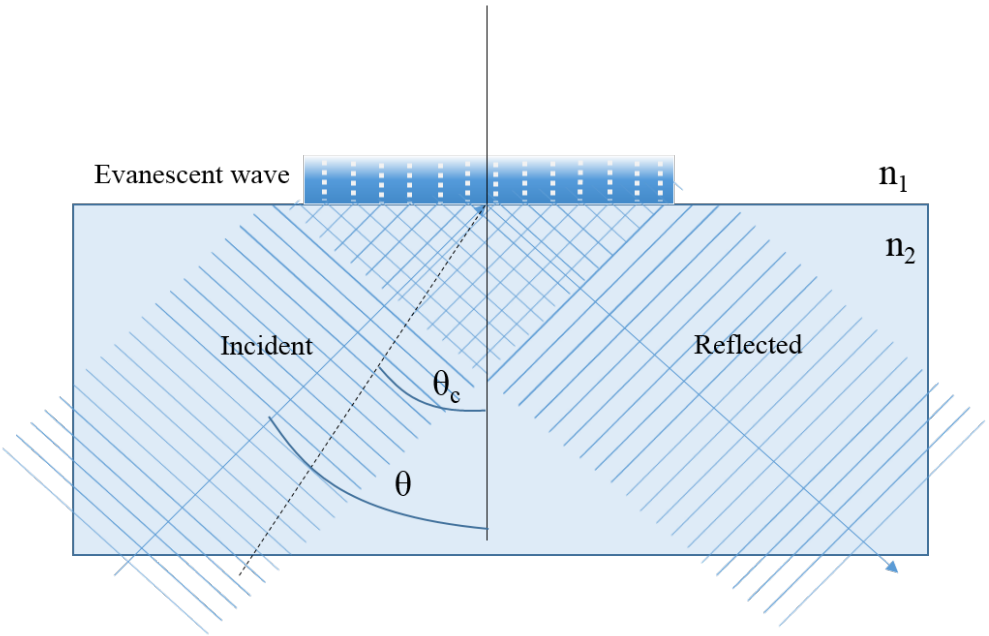

FIGURE 3.3: Schematic of principles behind TIRF. Refractive index n_2 is greater that n_1. Incident angle θ must be grater than θ_c for total internal reflection to occur. The exponentially decaying evanescent wave is used to excite the fluorophores above the surface.

in refractive index, where the glass meets the solution/air. When the angle of the incident light θ is greater than the critical angle θ_c, total internal reflection occurs at this interface as shown in figure 3.3. Here, the amplitude of the incident wave equals the amplitude of the reflected wave. However, due to the finite width of the incident light beam, there is a degree of interference at the interface. From this, an evanescent wave is formed across the interface. For this wave to obey Maxwell's equations and the conservation of energy, it must be a non vanishing field which decays exponentially with distance. This is what gives rise to this small finite depth to the observable region and provides the energy to selectively excite individual fluorophores within the solution[76].

With this in mind, TIRFM can be used to excite the fluorophores of a known excitation wavelength, and apply an optical filter to only allow wavelengths that correspond with the emission wavelength of the particle under observation.

3.5 Carbon Nanotube Dispersion and Deposition

Multiple methods of dispersion of both SWNTs and MWNTs were investigated in order to form solutions of separated CNTs for controlled depositions. The first method was to make use of organic solvents; in particular di-methylformaimide (DMF), which is a common solvent for this purpose[77]. The second method uses a surfactant to prevent the nanotubes from aggregating and to achieve single strands of nanotubes. For this method, the nanotubes are dispersed in 1wt% sodium dodecyl sulfate (SDS) in de-ionised water solution[78]. These methods both have their advantages, but our experimental results show that the SDS solution formed the better dispersion with longer individual nanotubes with less aggregation. It is important to achieve individual nanotubes in the dispersions to analyse single nanotube characteristics, and to have a better chance of observing protein attachment using scanning probe techniques.

Additionally, in this section I discuss a third dispersion technique which involves wrapping CNTs in short strands of DNA to disperse in a water solution to produce protein-DNA-CNT hybrid systems.

The nanotubes used for this investigation were provided by Sigma Aldrich and were grown using chemical vapour deposition. The data provided from Sigma Aldrich states that the SWNTs have an average diameter of 2.0nm, and the MWNTs have an average diameter of 9.5nm.

3.5.1 Dimethylformamide Solvent Dispersion

DMF is an colourless organic solvent, commonly used for separating and suspending CNTs. When in powder form, CNTs form large aggregates due to electrostatic forces and van der Waals forces. Using a combination of dispersing the CNTs in an organic solvent with ultrasonication, used to overcome these binding forces, we can separate CNTs and suspend them in solution, ready for deposition.

For the original experiments, the nanotube solutions produced consisted of 1mg nanotubes (SWNT or MWNT), and 10ml of DMF. The solvent has excellent wetting properties and proved to work very well to disperse the CNTs during sonication in an ultrasonic bath. After an hour of low power sonication, the solutions would appear fully dispersed forming an opaque black suspension. The MWNTs appeared to be more soluble than SWNTs, as they did not separate in solution over long periods of time, whereas the SWNTs separated from the solution almost immediately after sonication as seen in figure 3.4. A reason for this could be that the SWNTs are of very high purity and therefore have a poor hydrogen bonding ability[79]. This could be caused by fracturing of the MWNTs during sonication. SWNTs are more flexible than MWNTs, making them less prone to fracturing under sonication. The breaking of the CNTs can cause open bonds at the ends which can readily bind to molecules in the solvent. As the SWNTs are less prone to fracturing, they maintain their length and therefore, maintain a higher surface area for binding. This could therefore cause them re-aggregate and separate from the DMF[80].

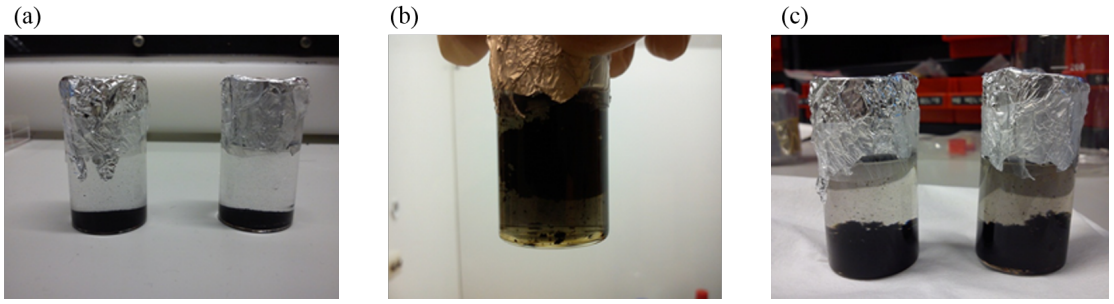

FIGURE 3.4: SWNTs in DMF. (a) Solutions before sonication. (b) A solution 1 minute after sonication. This shows the SWNTs starting to separate. (c) Solutions 1 day after sonication.

Similar results were found here for dispersion of MWNTs in ethanol[79]. CNTs are hydrophobic structures which would make them difficult to disperse in solution without their tendency to aggregate through hydrophobic interactions. The previous studies show that pristine tubes had lower hydrogen bonding than functionalised tubes, as functionalising the structures can form hydrophillic surfaces, thus increasing the level of dispersion in solvent.

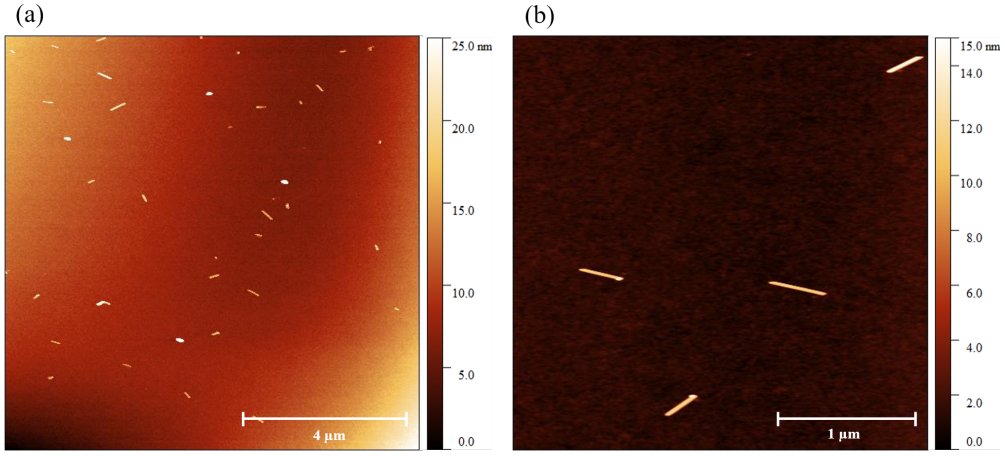

FIGURE 3.5: AFM images showing MWNT dispersion in DMF cast onto SiO_2 substrates. (a) Large scan showing a number of short MWNTs. (b) Smaller scan over short MWNTs (around 500nm in length).

From the images in figure 3.5, it is clear that the MWNTs are present, but exist as very short tubes generally less than 0.5μm. The details of the MWNTs supplied by Sigma Aldrich state that they should be of length 2.5 to 20μm.

This suggests that the tubes may have been fractured during the preparation of the solutions, and/or, the long tubes are bound together as aggregates due to increased surface area and therefore, higher number of van der Waals bonds. The ultra-sonication is the crucial process, producing localised shear stressed between adjacent nanotubes, which ultimately determines the overall level of dispersion. This process needs to supply enough energy to the tubes to overcome the binding energy between them, while supplying less energy than the energy needed to fracture the tubes.

Sediment formed by drop casting each solution onto SiO_2 and allowing to dry, was imaged under an AFM. Figure 3.6 shows long MWNTs wound into bundles of complex aggregates whereas the SWNTs seemed to form a web of partially aligned tubes with a higher aspect ratio. This has been found to happen in previous studies[80].

It seems that the longer tubes in both solutions are present but the dispersion procedure is insufficient at separating these tubes from each other. This is likely

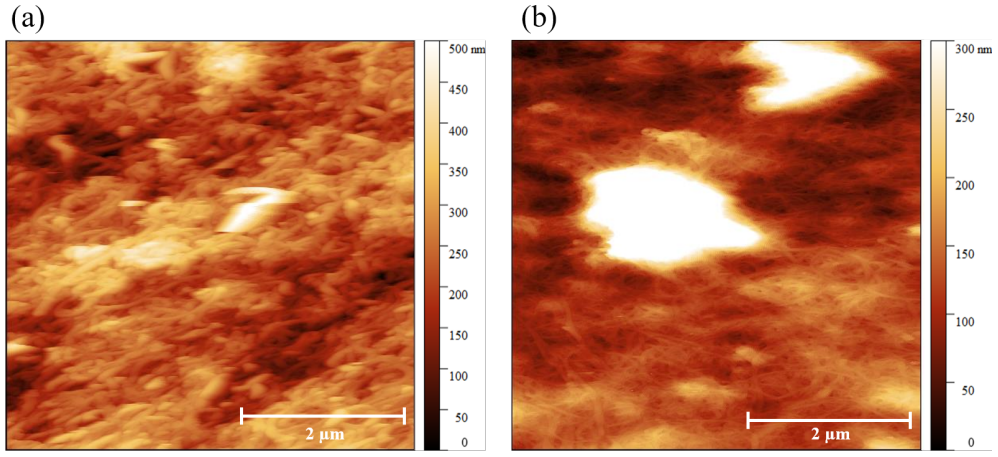

FIGURE 3.6: AFM images showing (a) MWNT bundles forming a large mesh of aggregates and (b) SWNTs forming webs of tubes bound by van der Waals forces

to result from the van der Waals force between the tubes being greater for longer tubes.

The next step was to try to separate the larger bundles of tubes away from the individual tubes in the hope of finding long individual tubes. To do this, the solutions were centrifuged. 1ml of each MWNT solution was taken and centrifuged at 10,000g for 6 minutes, then decanted into separate vials. The solid left behind was re-dispersed in DMF and the process was repeated two more times. The resulting solutions were then diluted with DMF until a clear solution is produced[81]. The SWNT solutions did not need to be diluted after centrifuging as they produced a clear, colourless supernant.

As the images in figure 3.7 clearly show, this method of dispersion was more effective with the SWNT samples, producing numerous individual nanotubes over 1μm in length. However, these were rare and proved difficult to find without slight aggregation.

DMF can be used to disperse carbon nanotubes and form a film of tubes and under certain circumstances, form semi-aligned aggregates. However, for the purpose of carbon nanotube biosensors, long, individual nanotubes need to be found in order to bridge electrodes. To produce individual nanotubes on a substrate, the surface

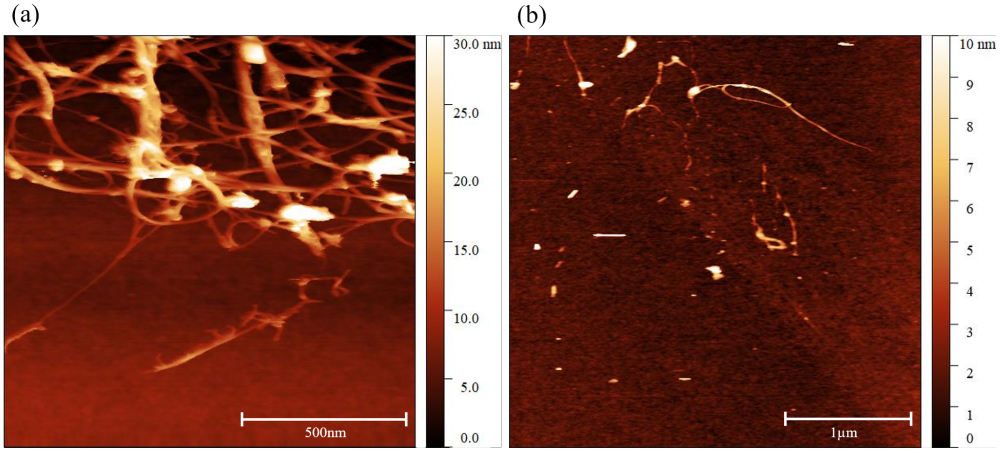

FIGURE 3.7: AFM images showing SWNT samples after solutions were centrifuged to remove very large aggregates.(a) Edge of aggregated region of SWNTs. (b) Large scan of sample showing very little individual SWNTs.

energy of the tubes must be reduced and the entropy of the system needs to decrease. To do this, a surfactant is used.

3.5.2 Sodium Dodecyl Sulphate dispersion

Surfactants such as SDS are compounds that are used to lower the surface tension between different liquids or a liquid and a solid[78]. An example of this is the emulsification of fat in water when soap is added.

These amphiphilic molecules are comprised of a hydrophobic tail group which binds itself to a solid, in this case a carbon nanotube, and a hydrophilic functional group which interacts with the water, lowering the surface tension at the interface. At a certain concentration, the surfactant forms micelles, called the critical micelle concentration. Once the surfactant surpasses this concentration, it acts as an emulsifier, which then acts to reduce the free energy of a system. This acts to stabilise the system while reducing the surface tension in solution. With this in mind, it is the perfect molecule to help the dispersion of carbon nanotubes and the separation of long individual nanotubes[78].

For the purpose of separating nanotubes, only a small concentration of SDS is needed. Larger concentrations would lead to micelles forming over the entire surface of the nanotube, which may greatly affect the binding of additional molecules (proteins), and will increase the resistance of the nanotube. The effect of surfactants on the binding of proteins to the surface is not well understood. One idea is that the hydrophilic head groups of the surfactants would interact with the hydrophobic surface of the proteins, holding them in a stable position[82]. This would still have the problem of an increased, undefined resistance across the nanotube. However, a solution to this has been found as all traces of the surfactant can be removed with a combination of rinsing in de-ionised water and ethanol. Previous studies done by Zhang et.al have shown with the use of X-ray Photoelectron Spectroscopy (XPS), that sufficient rinsing of these samples with ethanol can removed traces of SDS molecules from the nanotubes[83].

For these experiments, the most common SDS solution used for the purpose of dispersing SWNTs comprises of 1wt% SDS in de-ionised water. Concentrations are sometimes quoted in terms of the critical micelle concentration (CMC), which is the concentration at which the surfactant molecules combine to form a micelle structure. This is required to disperse the nanotubes so the concentration of surfactant should be larger than 1 CMC[84].

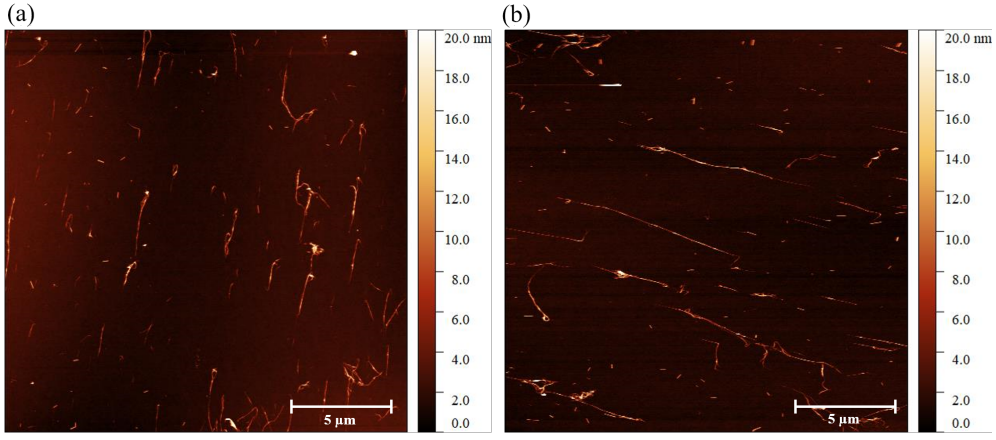

FIGURE 3.8: AFM images showing SWNT dispersion in SDS cast onto SiO_2 substrates. The alignment of the CNTs follow the direction of the droplet's movement when drying. (a,b) Large scans showing more individual SWNTs than that which was found in the DMF solutions. (a) SWNTs aligned along y-axis. (b) Long SWNTs aligned along the x-axis.

If the concentration is too low, then the SDS won't form micelles so the nanotubes won't disperse. If the concentration is too high, then the surfactant will bundle together reforming large aggregates[84]. SDS does not negatively affect the nanotubes and can be washed away with de-ionised water or ethanol[83].

Typical solutions were made up of 1mg/ml SWNTs in 1wt% SDS solution. These solutions were sonicated until a black suspension is achieved. This is followed by ultracentrifugation at 10,000g for 30 minutes in order to separate larger aggregates from the individual CNTs. The supernatant from this solution is then taken and diluted until solution becomes clear.

3.5.3 sSWNT and mSWNT Suspensions

For the majority of the work presented in this thesis, the CNTs are separated into solutions containing metallic SWNTs (mSWNT) and semiconducting SWNTs (sSWNT). These CNTs, which were grown by arc discharge and suspended in an aqueous ionic surfactant solution (1% wt SDS) were provided by NanoIntegris. These solutions contain 0.01mg/ml CNTs and were separated into suspensions of sSWNTs and mSWNTs.

3.5.4 DNA suspensions

The aim of the previous two CNT dispersion methods is to solubilise the nanotubes for deposition, which is then followed by post deposition biomolecule functionalisation. However, it can be advantageous to form protein-CNT hybrids in solution, minimising the post deposition processing steps, whilst maintaining a stable environment for the protein. Using organic solvents can introduce a hostile environment for the protein, causing it to denature. On the other hand, surfactant solutions will form micelles around the CNT structures, preventing proteins from attaching to their surface.

Introducing DNA can provide a solution to this problem. Similarly to the use of surfactants, DNA can be used to wrap around the CNT structure with its hydrophobic base molecules π-stacking to the sp^2 carbon surface, and the hydrophilic sugar phosphate backbone on the outside. This acts to reduce the entropy in the surrounding water, increasing its solubility and reducing CNT aggregation. The difference between the use of surfactants and DNA is that DNA can be pre-modified to incorporate functional groups as described earlier in Chapter 2. Another advantage it has is the DNA only stacks along the areas of the CNTs where sp^2 carbon is present. This means that if we were to have open ended CNTs, the DNA would only cover the sidewalls of the nanotube, leaving the ends exposed for end-on functionalisation. This method of functionalisation can be done in a buffer solution which provides a stable environment to introduce proteins and create protein-CNT hybrid structures in solution.

For my experiments, I used variants of $(GT)_{20}$, which is a repeated guanine-thymine structure consisting of 20 base pairs. The solutions are made up of 0.1mg CNTs in 0.1ml deionised water. This is then mixed with 50μl DNA solution (1mg/ml in water), followed by 850μl of NaCl solution (0.1M in water). The NaCl component helps to mask the electrostatic interactions between the CNTs under sonication, however these tubes will re-aggregate quickly. The mixture is then sonicated in ice for 2 hours, keeping the temperature low to minimise the energy between the DNA and CNT structures. The solution is then centrifuged at 10,000g to remove the insoluble material leaving a solution of DNA-wrapped CNTs.

AFM studies of $(GT)_{20}$ wrapped SWNTs can be seen in figure 3.10. Here you can see an uneven structure covering the SWNT which in some cases, looks like it may consist of multiple layers of DNA. These studies show that the DNA is successful in separating CNTs without the need for surfactants, which also provides a method of alternative biomolecular functionalisation.

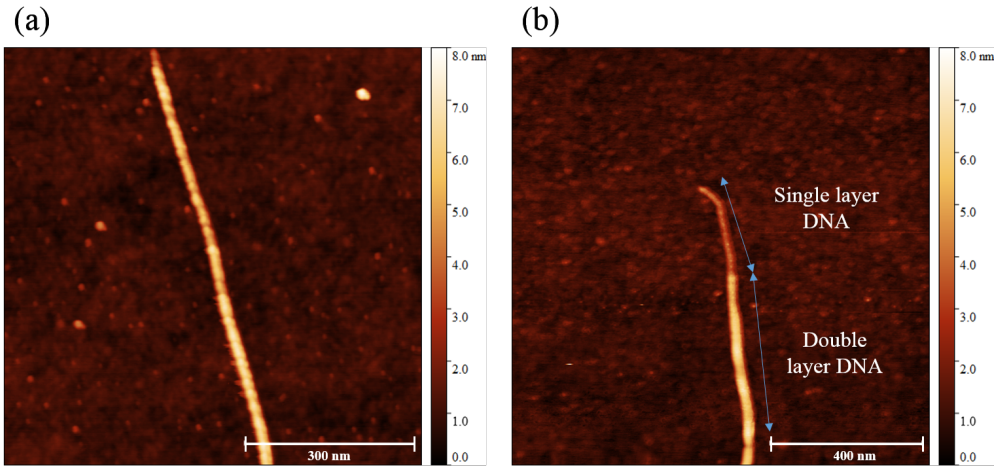

FIGURE 3.9: AFM images of $(GT)_{20}$ wrapped SWNTs on SiO_2. (a) View along the length of a SWNT wrapped in DNA, showing non-uniform heights along the structure. (b) Image of the end of a SWNTs wrapped in DNA, showing two different thicknesses along the structure suggesting multiple layers of DNA.

3.6 Electrode Fabrication

Electrodes patterns were defined by photolithography onto SiO_2 substrates. The electrodes are produced using a 10nm Chromium adhesion layer and a 70nm Gold layer, which is evaporated onto the substrates using an Edwards E306 Belljar evaporator.

The work shown in this thesis makes use of two different electrode designs. For the majority of the experiments, the effect of protein-CNT interactions is monitored using webs of nanotubes across electrodes with a long channel.

The second electrode design for this thesis is a narrow point set of electrodes, which were used to bridge low numbers of CNTs with the purpose of studying single nanotubes and single molecule interactions. For each set of electrodes, I produced a range of source-drain separation distanced from 2μm to 10μm.

3.7 Dielectrophoresis

In order to bridge the electrodes with CNTs, the technique of radio frequency dielectrophoresis (DEP) was employed[85]. This method is proven to effectively

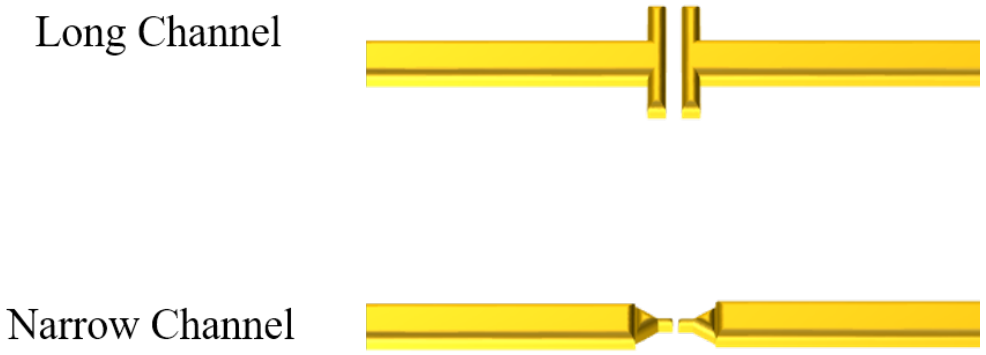

FIGURE 3.10: The two different electrode designs used in this project, comprising of either long channel or short channel gold electrodes connected to contact pads.

filter s-SWNTs from m-SWNTs. In this process, uncharged dielectric or conductive matter is placed inside an electric field where the field will induce a dipole moment within the matter. This is independent of the conductivity of the matter in question. When a non-uniform electric field is applied across the system, a Coulomb force F will be introduced:

$$\overrightarrow{F} = \overrightarrow{P}(\overrightarrow{\nabla E}) \tag{3.1}$$

Here, the force on the matter F is proportional to the dipole moment P of the matter, and the gradient of the electric field. Therefore, a uniform electric field will induce no net force on the matter[28].

For the purpose of separating s-SWNTs from m-SWNTs, we must consider a system where the nanotubes are suspended within a droplet of water or solvent, over two electrodes, connected to an AC waveform generator [86]. The DEP force F is given by the following equation:

$$\overrightarrow{F} = 2\pi V_{\epsilon m} K_{(\omega)} \nabla(\overrightarrow{E^2_{rms}}) \tag{3.2}$$

The force is proportional to the volume $V_{\epsilon m}$, the square of the gradient of the electric field $\nabla(\overrightarrow{E^2_{rms}})$, and the Clausias-Mosotti factor $K_{(\omega)}$. This factor $K_{(\omega)}$ is a function of the dielectric constants ϵ of the matter, and the frequency ω applied across the electrodes[28][87].

$$K_{(\omega)} = Re\left\{\frac{\epsilon_p^* - \epsilon_m^*}{\epsilon_p^* + 2\epsilon_m^*}\right\} \tag{3.3}$$

where,

$$\epsilon^* = \epsilon + \frac{\sigma}{i\omega} \tag{3.4}$$

Here, p and m relate to the particle and medium in question and σ_0 is the conductivity. The dielectric constant for water ranges from $75\epsilon_0$ to $80\epsilon_0$. For s-SWNTs, the dielectric constant ranges from $2\epsilon_0$ to $5\epsilon_0$, and for m-SWNTs the dielectric constant is ∞. Therefore, as the dielectric constant of water is in-between that of s-SWNTs and m-SWNTs, by altering the frequency applied, a crossover frequency ω_c between positive DEP force and negative DEP force exists. For s-SWNTs, this frequency is in the order of 100 kHz.

By applying this theory to a SWNT-FET system, the DEP force will push the m-SWNTs onto the electrodes, while the s-SWNTs undergo negative DEP and can then be rinsed away[28]. This process can also aid alignment of the nanotubes as the E-field induces a torque T across the length d of the tube in the direction of the E-field.

$$\overrightarrow{T} = \overrightarrow{P} \times \overrightarrow{E} = q\overrightarrow{d} \times \overrightarrow{E} \tag{3.5}$$

Figure 3.12 shows a device made up of two gold electrodes spaced 10μm apart after undergoing DEP with a SWNT solution. As you can see, there is a great degree of alignment of the nanotubes in the direction of the applied electric field.

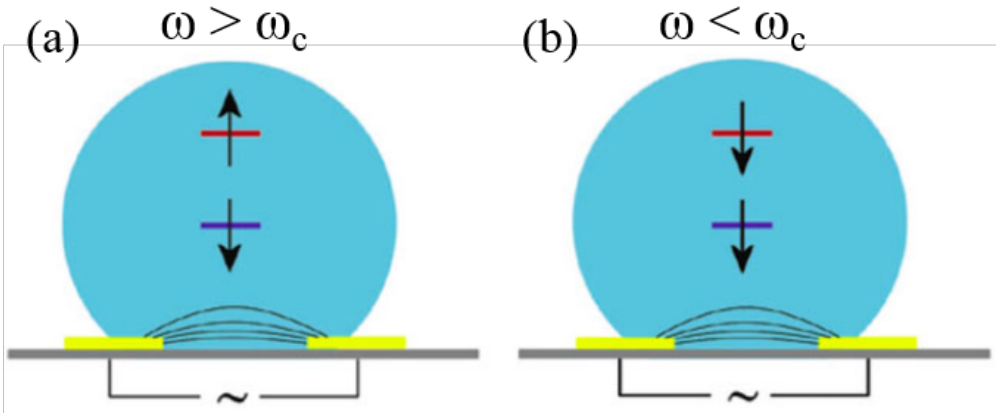

FIGURE 3.11: Diagrams of droplets containing CNTs across two electrodes, connected to an AC function generator. Here the red line represents the sSWNT and the blue line represents the mSWNT. ω and ω_c are the applied frequency and the crossover frequency respectively. (a) shows negative DEP with respect to the sSWNT, and (b) shows positive DEP for both sSWNT and mSWNTs. [28]

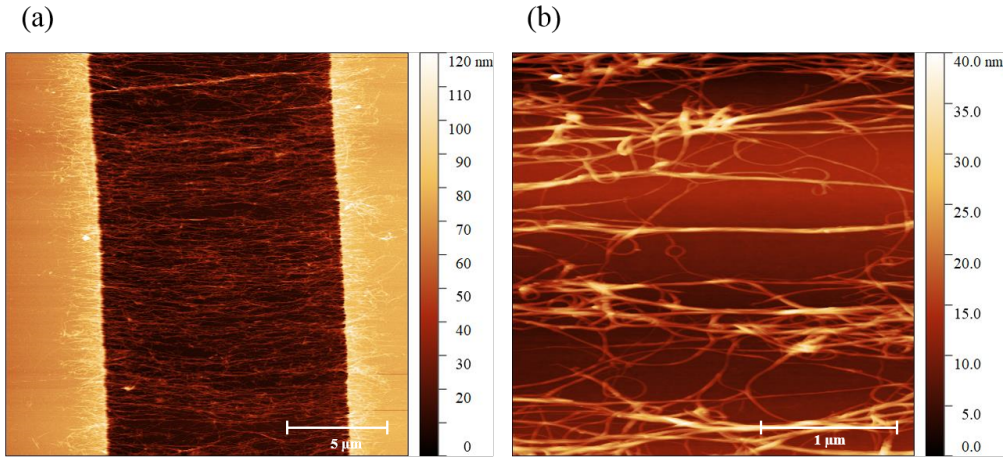

FIGURE 3.12: AFM images of a set of gold electrodes separated by a 10μm gap after undergoing DEP in a SWNT solution.(a) shows a section of the long channel with bridging SWNTs. (b) a close up section of the gap between the electrodes showing alignment of CNT structures.

The density of CNTs is greatest in the gap relating to the position of the highest potential gradient when DEP is applied [88][29]. This can also be seen in figure 3.13, which shows two examples of much narrower sets of electrodes separated by a 2μm gap. Again we can see the nanotubes have aligned to the direction of the field lines. With these narrow devices, we are able to limit the number of CNTs to as little as one bridging nanotube, which could have the potential to measure single molecule interactions with the nanostructure.

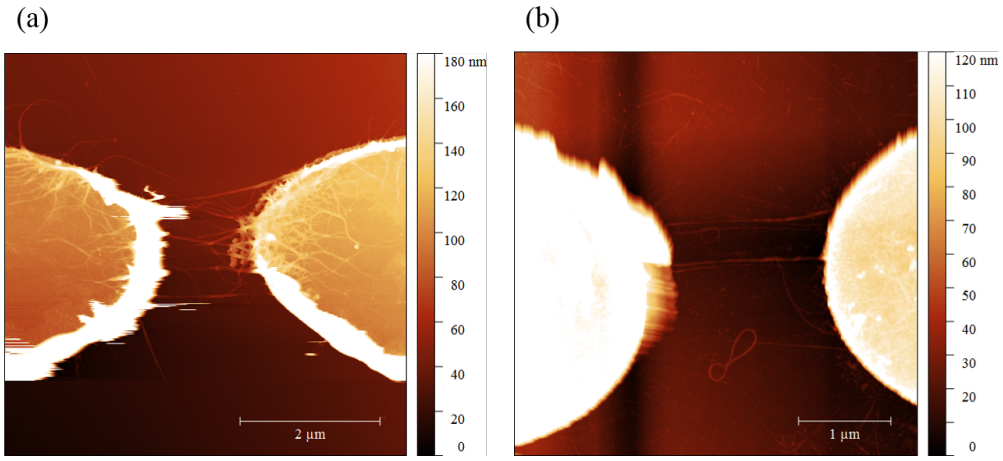

FIGURE 3.13: AFM images of narrow channel gold electrodes with a 2μm gap after undergoing DEP in a SWNT solution. There is visible alignment of the CNTs with the field lines produced during DEP. (a) large number of SWNTs deposited in 2μm gap after 30s of DEP. (b) Lower number of SWNTs deposited by reducing the time of applied DEP to 10s.

By using the method of DEP, CNTs can be aligned across two electrodes to forming a platform to perform electrical transport experiments, allowing us to monitor protein-CNT interactions in real-time.

3.8 Summary

In this chapter, I have described the main experimental techniques that I have applied to my research. I have given a brief introduction to SPM techniques and optical techniques, describing their role in characterising interactions between proteins and CNTs.

Furthermore, I have described the methods I have developed for CNT dispersion and deposition. Here, I have discussed the advantages I have found with sufractant-CNT dispersion over organic solvent dispersion. I found that using surfactants provides the solutions with higher dispersion and less aggregation. This has allowed for effective deposition across neighbouring electrodes with separation distances up to 10μm. To achieve this, I have also described the process of DEP as a highly effective method of aligning and bridging CNTs across neighbouring electrodes.

All these procedures have allowed me to investigate the protein-CNT interaction, and progress in the development of reliable and reproducible protein-CNT hybrid structures.

Chapter 4

Carbon Nanotube Sidewall Functionalisation

4.1 Introduction

Creating a functional platform to study bio-molecular activity is a key focus of this thesis. CNTs are ideal nanostructures to serve as an interface material for bioelectronic purposes, with good biocompatibility, high sensitivity and the ability to react with a wide range of chemical linker molecules. We have been successful in modifying proteins with a functional linker group to bind to the sidewall of a CNT as described in chapter 2.

Here we demonstrate defined protein-CNT interactions with chosen orientations and inter-molecular distances, through the use of AFM. We also show that protein attachment can be monitored by measuring the resistance change under UV illumination. By choosing the orientation of the protein, we can define the distance between the active component within the protein and the π-electron system of the CNT allowing for intimate electronic interactions.

In order to build a platform for bio-sensing, we bridged CNTs across a pair of electrodes, forming a device with similar function and properties to a field effect

transistor (FET). In this case, the CNTs act as the channel material with the proteins and molecules that bind to them, effectively gating the current flow across the device. We discuss the viability of this method as well as its versatility. We also demonstrate the attachment of proteins non-covalent linker methods including pyrene linker molecules and DNA-CNT hybrid structures.

4.2 Azide Chemistry Covalent Attachment of Proteins

4.2.1 Position Defined Covalent attachment

Proteins were prepared with the uAA, p-azido-L-phenylalanine in order to covalently cross link to the side wall of the CNTs. The linker is situated in predetermined positions within the protein allowing exquisite control over the orientation of the structure when bound to the CNT surface. Knowing how the protein is linked to the CNT allows us to have a better insight into how they electronically interact. This is important to know when developing a bio-molecular sensor, especially in terms of single molecule measurements.

The first step in this investigation was to study how the proteins bind to the carbon surface and whether their orientation can be controlled as the theory would suggest. This was done by analysing the height of different protein molecules when attached to CNTs using AFM, and comparing this to the protein model.

In this section, I discuss the data gathered for analysis of sfGFP, cyt b_{562} and TEM β-lacatmase with the linker molecule placed at various positions. The position of the AzPhe linker molecule is denoted as a number corresponding to its position in the amino acid chain that makes up the protein as shown in Figure 4.1.

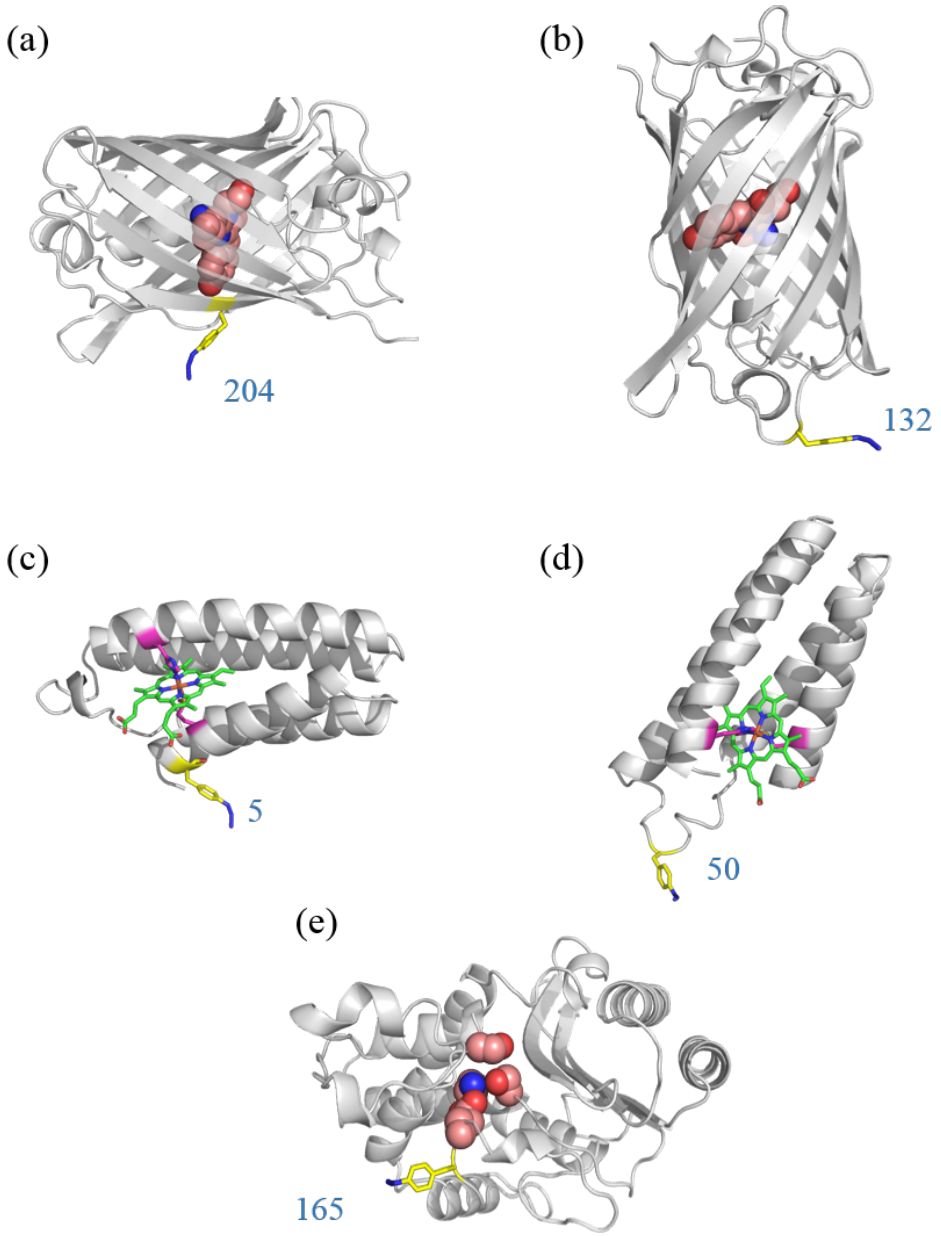

FIGURE 4.1: Structures of modified proteins with AzPhe group shown in yellow and blue. (a)sfGFP-204AzPhe, (b)sfGFP-132AzPhe, (c) cyt b_{562} -5AzPhe, (d)cyt b_{562} -50AzPhe, (e)TEM-156AzPhe.

4.2.1.1 Experimental Setup

SWNTs in SDS solution were deposited on a variety of substrates for different purposes including SiO_2 substrates for general distribution and height analysis, as well as on electrodes for electrical studies and quartz cover-slips for optical studies. For each experiment, the samples were analysed using tapping mode AFM to determine the distribution and quality of the attached proteins.

For the majority of the height analysis studies, samples of SWNTs on SiO_2 were prepared and rinsed in ethanol for 1 hour to ensure all surfactant is removed before protein attachment. The modified proteins were prepared in a dark environment as the azide group in the AzPhe is highly susceptible to degradation in ambient light.

The protein solutions were drop cast onto the SWNT samples with concentrations ranging from 10nM for low densities of proteins to 1μM for higher densities. All proteins with AzPhe reactive groups were diluted in 50mM tris buffer at pH 8. Samples with protein solutions were then illuminated with 305nm light at an intensity of 18Wm^{-2} for 5 minutes to cross-link the proteins to the SWNTs. The excess solution was then rinsed away with a flow of de-ionised water for 1 minute, ensuring all unbound proteins were removed from the samples, then dried under a flow of N_2 gas.

These samples were studied using tapping mode AFM to produce topographical images in which the heights and distribution of the bound proteins were analysed.

4.2.1.2 Results and Discussion

I conducted a number of control tests in which unmodified proteins, denoted as "wild type" (wt) proteins, were deposited on SWNT samples. This provided us with a comparison to AzPhe modified proteins, showing evidence that the linking of the protein is through this position defined group.

Figure 4.2 shows images of wt-cyt b_{562} control tests on SWNTs under AFM. There is some visible debris which could be bound protein molecules, however, there is no coherent shape or structure which would suggest there is no defined binding taking place. In comparison, Figure 4.3 shows more regular, defined structure of bound molecules on the CNTs. Here we can also see the molecules are all of similar height and width, which would suggest that they are bound in a defined way as the protein in question has a linker at one end of an elongated structure. This provides strong evidence that these bound molecules are cyt b_{562}-50AzPhe

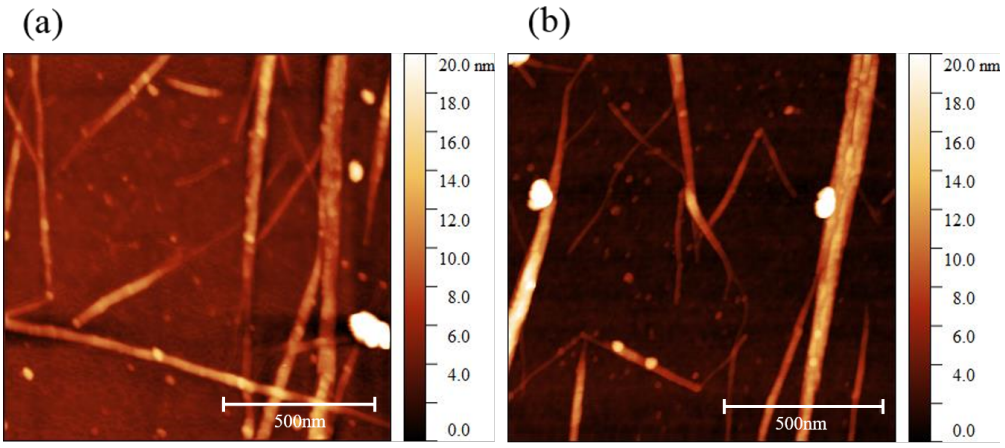

FIGURE 4.2: AFM image of 1μM wt-cyt b_{562} on sSWNTs after 5 minutes incubation followed by rinsing with a flow of de-ionised water. (a) We see some aggregates and what could be proteins binding to the CNTs. (b) Again som aggreagates but little structure to bound debris.

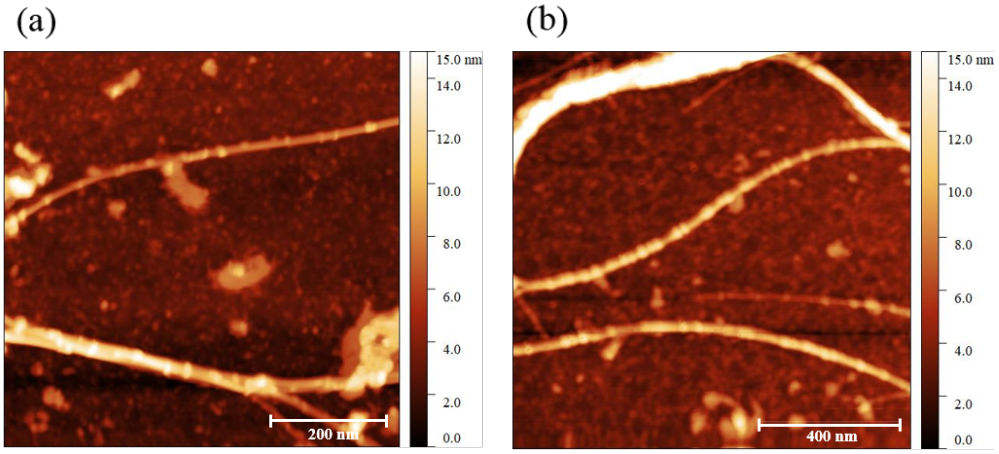

FIGURE 4.3: AFM image of 1μM cyt b_{562} -50AzPhe on sSWNTs after incubation with under 305nm UV illumination followed by rinsing with a flow of de-ionised water. (a) lagre aggregates and a number of proteins bound to CNTs with no noticeable defined spacing between them. (b) Defined high concentration of proteins bound to CNTs with most proteins bunching together with little spacing between them.

with the orientation defined by the azide. As additional control, the experiment was repeated for cyt b_{562}-50AzPhe deposition without UV illumination, resulting in little to no bound proteins to the CNT surfaces as seen in Figure 4.4.

Further evidence of photo induced cross-linking can be seen when comparing wt-sfGFP to a modified variant as seen in Figure 4.5 and Figure 4.6 respectively.

It is clear from Figure 4.6 that there is defined binding for proteins to SWNTs with

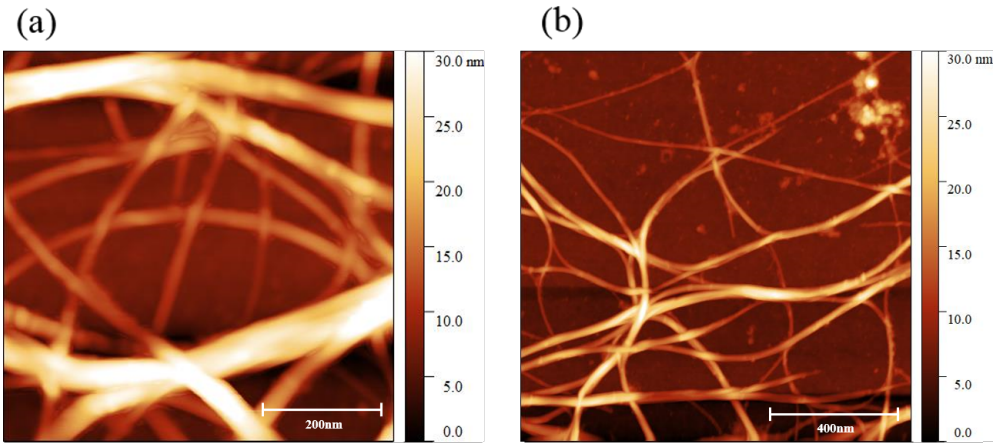

FIGURE 4.4: AFM image of sSWNTs after 5 minutes incubation in cyt b_{562}-50AzPhe solution without UV illumination, followed by rinsing with a flow of de-ionised water. (a) Webs of CNTs with no visible proteins bound. (b) Large scan showing visible debris but no clear evidence of protein-CNT attachment.

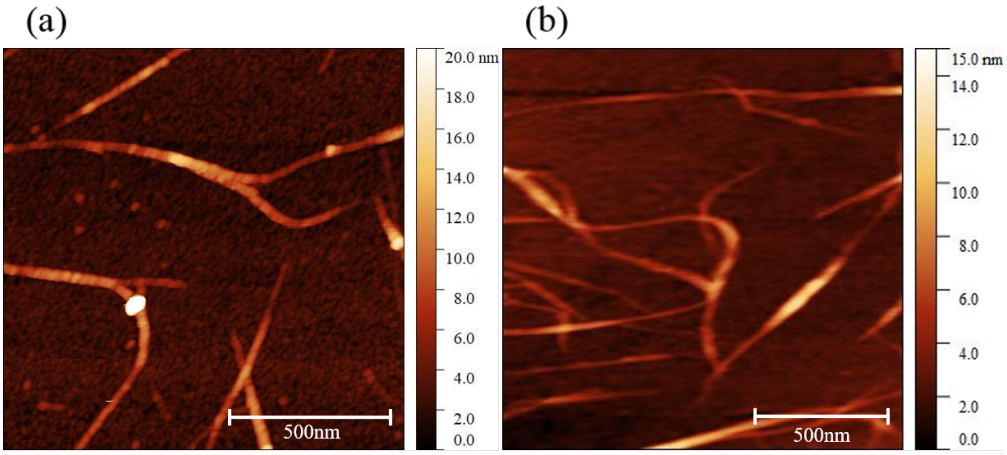

FIGURE 4.5: AFM image of 1μM sfGFP on sSWNTs after 5 minutes incubation followed by rinsing with a flow of de-ionised water. (a) sSWNTs with some visible attachment but little definition. (b) Again some visible debris attached to the CNTs but very little definition.

very little proteins binding to the substrate surface, suggesting that the proteins have chemically bound to the SWNTs.

TEM-165Az has proven to bind effectively to SWNTs under UV illumination showing regular structure along the nanotubes with high stability under multiple scans with AFM. It can be seen from Figure 4.7 that the wild type protein tends to stick along the CNTs however there is no defined structure or orientation with high concentrations of aggregates forming along the CNTs.

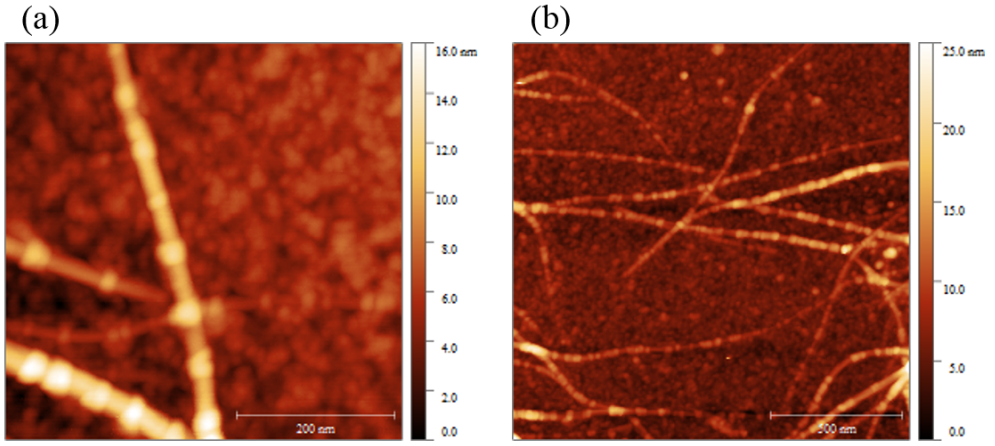

FIGURE 4.6: AFM image of 1μM sfGFP-204AzPhe on sSWNTs after incubation with under 305nm UV illumination followed by rinsing with a flow of de-ionised water. (a) Visible attachment of sfGFP to CNTs with highly defined structures. (b) Large scale scan showing high degree of protein coverage on CNTs in random distributions.

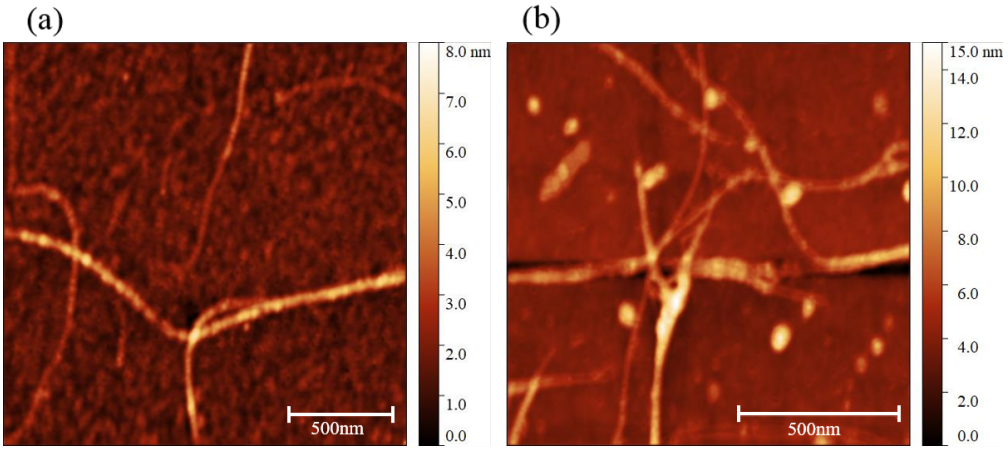

FIGURE 4.7: AFM images showing a comparison between (a) TEM-165AzPhe bound to SWNTs with good coverage and definition, and (b) wtTEM on SWNTs showing uneven coverage and lots of aggregation.

These control tests allow us to say with some confidence that the attachment of each of these proteins in question is defined through the AzPhe linker group. This result was also demonstrated using Raman spectroscopy, which is explained in chapter 5. Further analysis was done in order to prove that the orientation of the proteins can be controlled by this linker group. To do this, variants of sfGFP and cyt b_{562} were developed with the AzPhe implemented at adjacent positions on the protein allowing us to compare their heights when bound along their short axis

or their long axis. From Figure 4.1, you can see the short axis variants; sfGFP-204AzPhe and cyt b_{562}-5AzPhe, as well as the long axis variants; sfGFP-132AzPhe and cyt b_{562}-50AzPhe. The results of this can be seen in Figure 4.8.

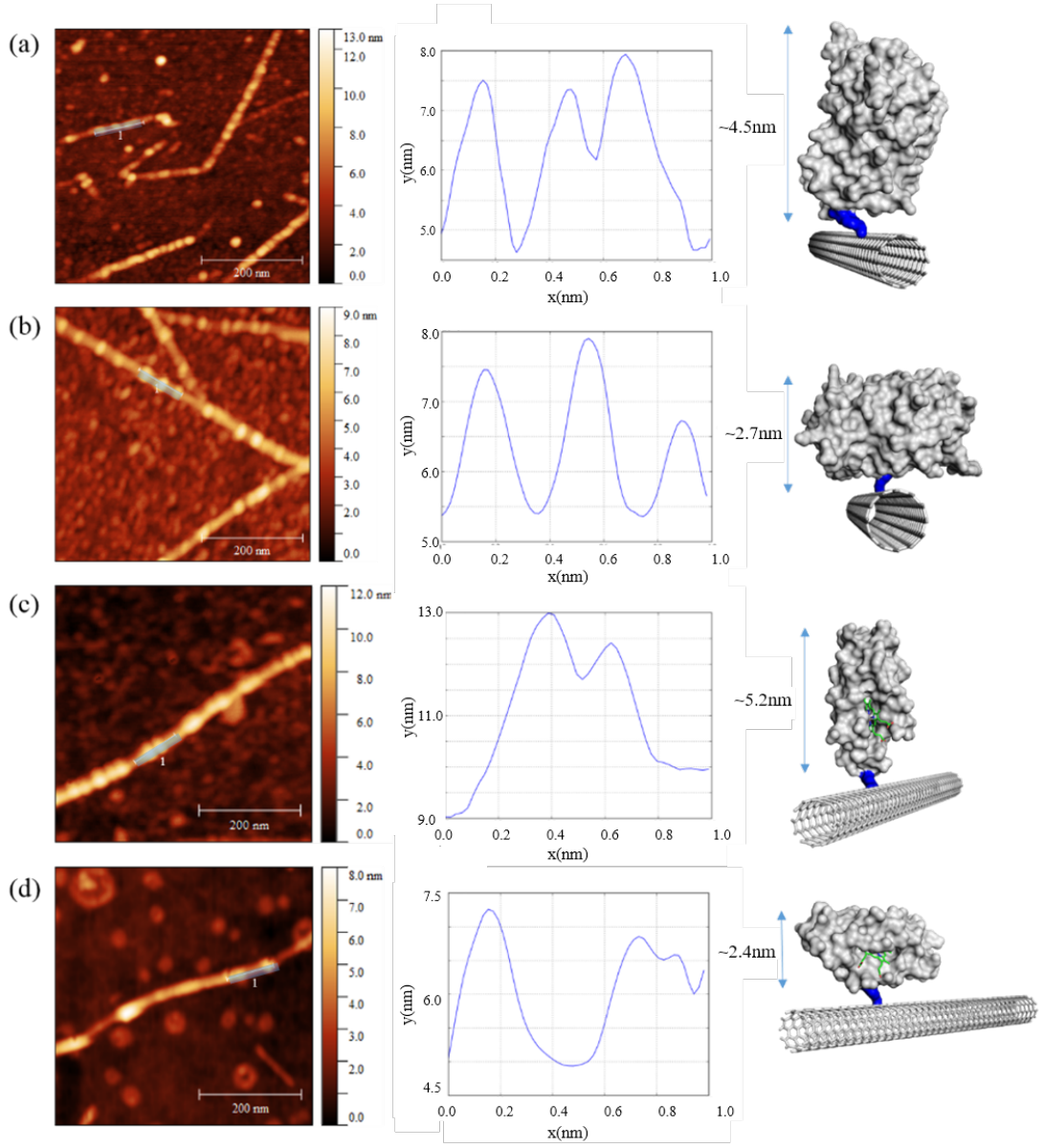

FIGURE 4.8: AFM images of proteins on SWNTs with respective profiles of the highlighted blue regions, showing the topography along the length of the nanotube for (a) sfGFP-132AzPhe, (b) sfGFP-204AzPhe, (c) cyt b_{562} -5AzPhe, (d) cyt b_{562}-50AzPhe. The plots shown in the centre are the profiles for their respective AFM images. The models on the right hand side show how the proteins stack on the SWNTs with their predicted heights taken from models and measured in the molecular modelling program, PyMol.

There are a number of interesting points that can be taken from studying the AFM images for the various proteins. Figure 4.8 shows a clear difference in

heights between the protein variants with the long axis proteins standing taller on the CNTs than their short axis counterparts. This was an expected result with sfGFP-132AzPhe having an average height of (3.11±0.92)nm compared with sfGFP-204AzPhe with an average height of (2.45±0.82)nm (see Figure 4.9). The long axis variant of cyt b_{562} has an average height of (3.19±0.52)nm, compared with the short axis variant standing at about (2.56±0.55)nm (see Figure 4.10), although the orientation of this particular protein made it difficult to obtain a reliable average height. The SA-cyt b_{562} variant appears to stack end to end long the CNT structure, forming a chain of proteins which effectively coat the sidewall of the CNT. Apparent heights were taken from the drop off where the protein chain ends and the CNT becomes visible. This is predominantly seen in the short axis variants of the proteins with cyt b_{562}-5AzPhe aligning its long axis parallel along the length of the CNTs, and sfGFP-204AzPhe in most cases, binding with the long axis sitting perpendicular to the length of the CNT. This meant the variation of heights was not the only result taken from these studies, as we can see visible alignment of the proteins when bound to the CNTs.

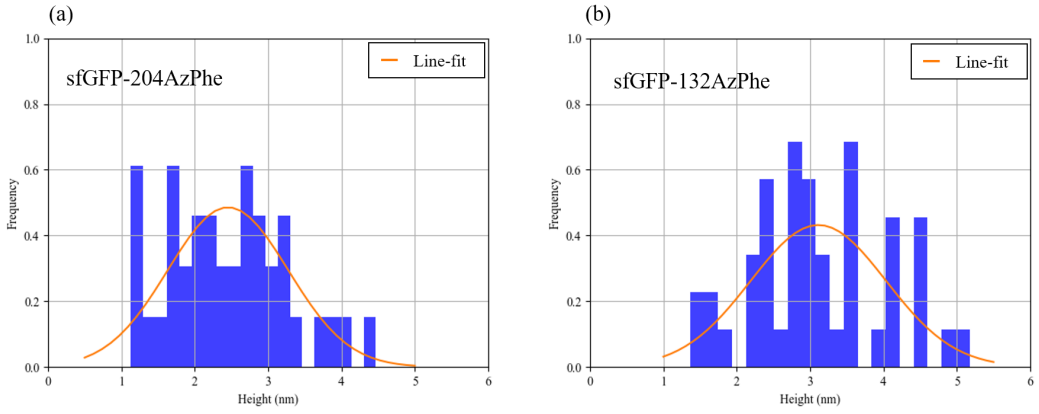

FIGURE 4.9: Histograms of heights of sfGFP-AzPhe attached to SWNTs with a normalised line fit applied to each. (a) Short axis sfGFP with an average height of (2.45±0.82)nm taken from 39 proteins. (b) Long axis sfGFP with an average height of (3.11±0.92)nm taken from 46 proteins

This alignment could possibly be an effect of the inherit dipole moment within the protein structure. The structure of sfGFP is mainly defined by the β-barrel as seen in figure 4.1. The dipole moment of β-sheets are defined by their hydrogen bonding network which act between neighbouring sheets. This would result in the dipole

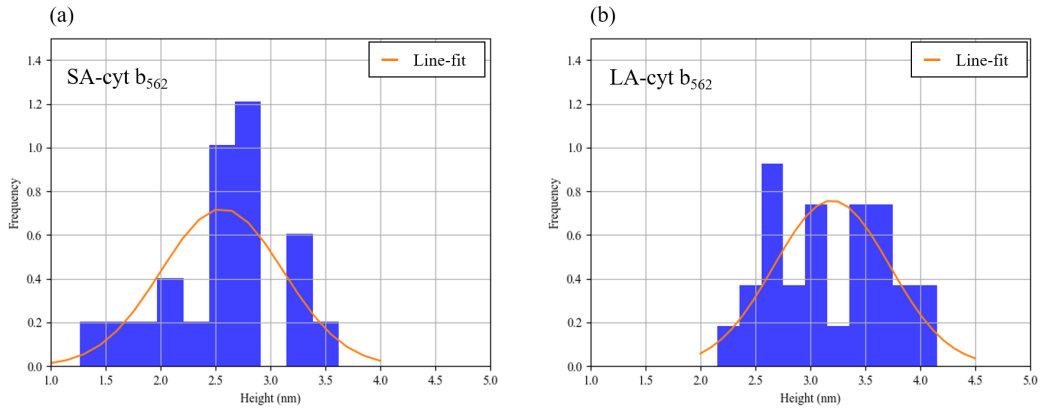

FIGURE 4.10: Histograms of heights of cyt b_{562}-AzPhe attached to SWNTs with a normalised line fit applied to each. (a) Short axis cyt b_{562} with an average height of (2.56±0.55)nm taken from 21 proteins. (b) Long axis cyt b_{562} with an average height of (3.19±0.52)nm taken from 27 proteins

moment acting perpendicular to the direction of the sheets. Any induced dipole moment in the CNT structure would align along the length of the structure which could suggest that the perpendicular alignment of sfGFP-204AzPhe on SWNTs arises from alignment of dipole moments.

The heights don't all agree with the predicted heights shown in Figure 4.8, with both the long axis variants measuring a bit shorter than predicted. This may be due to the stability of the protein standing on its end being lower than of it were on its side. Using AFM, we would assume that measuring the heights of soft matter could introduce an error which could also be a factor in measuring heights to be shorter than predicted. Nevertheless, this study has shown a clear difference between long and short axis variants of these two different proteins, demonstrating a high degree of control over the attachment.

From all of the images gathered for these protein-CNT experiments, there doesn't seem to be any specific pattern to the attachment with most proteins binding in random positions along the CNTs. There does seem to be a tendency for the proteins to aggregate close to each other which is very apparent in the SA-cyt b_{562} variant. It is unclear at the moment as to why this variant aggregates more than the others.

Only one variant of TEM β-lactamase was studied in this investigation. The variant, TEM-165AzPhe was successfully attached to the CNTs with regular heights and structure showing clear specific attachment. Due to the lack of available proteins, heights were only taken from 10 proteins attached to mixed SWNTs and therefore, a histogram was not made. The average measured height of the molecule is (1.88±0.61)nm from 10 proteins which doesn't agree with the theoretical model height of about 4.5nm, although more data is needed to draw conclusions from this. The binding of TEM to CNTs demonstrates the versatility of this method of protein attachment and the potential of producing a biosensor platform for antibiotic detection.

4.2.2 Monitoring Covalent Attachment

Under irradiation of 305nm light, the engineered proteins covalently bind to CNTs, disrupting the electron network as well as acting as a bio-molecular dopant, which can greatly affect the electron flow through the CNTs. By integrating the CNTs into a transistor-like device using DEP, these changes in electronic transport can be measured in real time.

The binding events can be monitored by measuring the change in resistance across the CNTs upon UV irradiation. The electronic structure of the CNTs makes them highly sensitive to small changes within their local environment. When a protein solution is introduced, a combination of environmental changes causes an increase in the CNTs resistance. The rate of change or resistance increases upon UV illumination as a result of photo-chemical cross linking.

4.2.2.1 Experimental Setup

Electrodes were fabricated with a separation of 2-5μm to bridge CNTs. Separate devices were prepared for sSWNTs and mSWNTs to compare their properties for this type of system. CNTs were deposited across the electrode gap using DEP, producing webs of partially aligned nanotubes. For sSWNT samples, DEP was

performed by drop-casting a solution of CNTs in SDS solution onto the electrodes and applying $3V_{pp}$ at a frequency of 100kHz for 30 seconds, across them. mSWNTs use a higher frequency of 1-5MHz for a positive DEP force, which ensures any sSWNTs in the solution undergo negative DEP. The excess CNT solution is then washed away from he devices in a flow of de-ionised water and annealed on a hot plate at 100^oC for an hour to reduce the contact resistance between the gold electrodes and the CNTs.

The typical resistance across these devices are about 100Ω to 1kΩ for high densities of CNTs. The number of CNTs can be reduced by limiting the time or the potential applied during DEP with very low densities achieving resistances of 20kΩ and up. High densities have the advantage of being more stable and resistant to electrical breakdown with low noise. However, this can limit the protein to CNT ratio due to dense packing of aggregates which can affect the signal measured across the device. Lower density devices have better sensitivity for single molecule detection but are prone to high levels of noise and electrical breakdown due to build up of charge withing the CNTs. Therefore, devices with mid range resistances are preferred for better sensitivity with good signal to noise ratio.

For real time measurements of the resistance across the CNT devices as proteins are bound, a simple potential divider circuit was set up with the purpose of measuring the voltage change across a series resistor as the resistance across the CNT device varies. A voltage applied using a wave form generator and the voltage across the series resistor is monitored using a lock-in amplifier, allowing us to monitor electrical changes with high sensitivity with a high signal to noise ratio. The resistance of the CNT device, denoted as R_{CNT} is given by the following potential divider equation:

$$R_{CNT} = R_1.(\frac{V_{in}}{V_{out}} - 1) - R_{fg} \tag{4.1}$$

Here, R_1 is the resistance of the series resistor, V_{in} is the voltage applied to the circuit, V_{out} is the voltage measured across the resistor and R_{fg} is the internal

resistance of the wave form generator.

Initial experiments showed that CNTs are highly susceptible to atmospheric changes under UV light exposure which can greatly alter the resistance across the devices. Studies conducted by various groups have shown that irradiating SWNTs with UV-light can enhance oxygen adsorption over both pristine SWNTs and ones with structural defects [89][90]. This could be a chemisorption event in which the oxygen molecule binds across a C=C double bond or a physisorption event in which the oxygen becomes weakly bound to the surface of the CNT. Molecular adsorption can have large effects on the electrical structure of the CNT, acting as a dopant and an structural defect, causing a change in its conductance properties. This can be seen in Figure 4.11 as an increase in the resistance across the CNT device under UV illumination in air.

After the CNT devices is illuminated with UV light, they begin to recover, with molecules slowly de-adsorbing from the SWNTs with a long recovery time of 12 to 24 hours where it finally reaches its original state. As it relaxes, the dopant molecules are released and electrons within the SWNT slowly recover from an exited state as they overcome a potential barrier. This recovery time can be reduced by heating up the sample, providing energy to overcome the potential barriers and increase the rate of molecular de-adsorption [90].

To ensure this UV-light enhanced oxygen adsorption was limited in our experimental setup, the experiment was conducted in an oxygen free environment with low humidity. This was done by placing our circuit inside an air tight box with a nitrogen source and drain. This meant the box could be flushed with a constant flow of nitrogen, providing an oxygen limited environment. A humidity and temperature sensor was added to the box to monitor the conditions throughout the experiment. The box also kept any ambient light from affecting the system, reducing the margin for error.

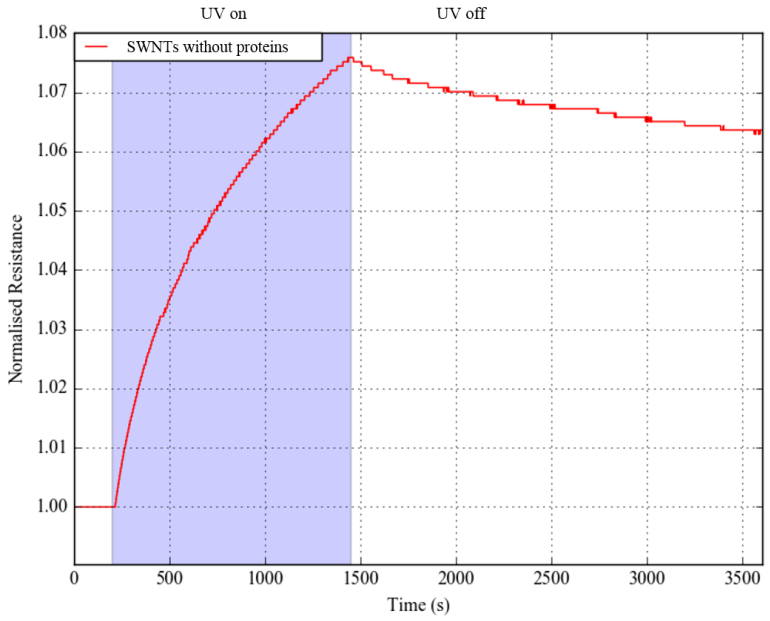

FIGURE 4.11: Resistance plot over time in air using mixed SWNTs. 305nm UV light was switched on at 200s causing a rise in the resistance across the device. Once the UV is switched off, the device starts to recover.

4.2.2.2 Results and Discussion

Each device had a different number of CNTs bridging which meant there was variation in resistances between devices. Therefore, the change in resistance caused by the protein attachment during the experiments is displayed as a normalised figure where the value of the resistance at a particular time is normalised to the initial resistance of the device. The first set of experiments were done on mixed SWNTs for monitoring the attachment of TEM-165AzPhe under UV illumination. The results are shown in Figure 4.12. Here we notice the initial large increase in resistance as the droplet is added which can be understood as a result of large environmental changes with a degree of confinement and molecular interactions within the solution. The temperature difference between the solution and the sample can play a big part in the observed resistance change. The solutions used are kept refrigerated to preserve protein structures whereas the devices are kept at room temperature. The large increase caused by the droplet being added can be partially due to the drop in temperature of the device. As it reaches thermal equilibrium, the rate of change in the measured voltage decreases. After the device

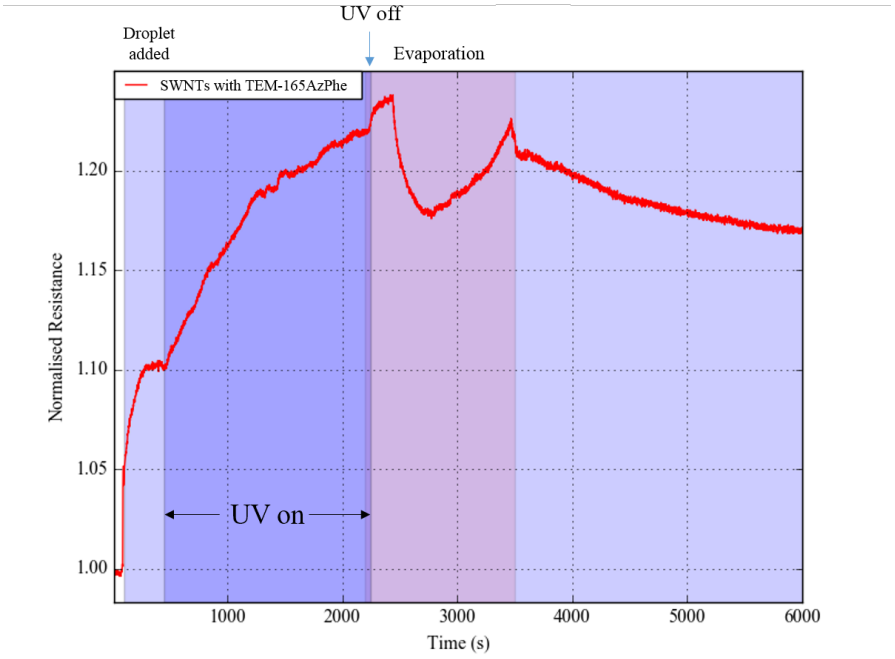

FIGURE 4.12: Resistance plot over time for TEM-165AzPhe on mixed SWNTs in buffer solution. The sample was illuminated with 305nm UV light

has reached this equilibrium, it is illuminated with UV light causing a convincing increase in the resistance, caused the formation of sp^3 bond orbitals as the azide molecule bonds across C=C double bonds, disrupting the π electron structure of the CNTs. Cross-linking reactions continue to take place as the UV is on, with the rate of change in resistance slowly decreasing as the CNTs become coated in protein molecules leaving less and less space for additional cross linking events. Just before the UV source is turned off, there is a small increase in resistance before it sharply drops and settles at a new resistance before relaxing. This is caused by the droplet evaporating, which deposits a large concentration of proteins and salts on the surface causing the initial increase, followed by the environmental changes when the solution evaporates, resulting in sharp variations in the resistance. Although this result is not ideal to show protein attachment, it does demonstrate the effect of UV illumination on the photo-cross-linking reaction.

Once this initial experiment was done, a number of improvements were introduced to the set up, including O-rings to suspend larger volumes of solution on the devices and the use of sorted SWNTs so that sSWNTs and mSWNTs could be compared. We tested this setup on different proteins and control tests on buffer solutions to

ensure it was the AzPhe causing the resistance change under UV illumination. Figure 4.13 compares the effect of UV illumination on buffer solution and cyt b_{562}-50AzPhe solution. Here we see the same effect as seen in the TEM-165AzPhe experiment where UV exposure causes a rise in resistance for the protein solution relating to the photo-cross-linking to the CNTs. Interestingly, the UV light does not appear to affect the resistance in the buffer solution test. When compared with the preliminary tests in air, we can attribute this change in resistance to the absorption of molecules in the atmosphere under UV illumination. However this effect does not appear to take place in solution. The continuous rise in resistance tells us that these devices take quite a while to reach equilibrium and the sSWNTs are very sensitive to these environmental changes. There is some periodic noise in this particular plot, which arises from a slight mismatch in frequency between the wave-function generator and the lock in amplifier causing a beat frequency in the recorded signal. Due to limited resources, this experiment was not repeated, but corrections to the experimental setup were made for further experiments.

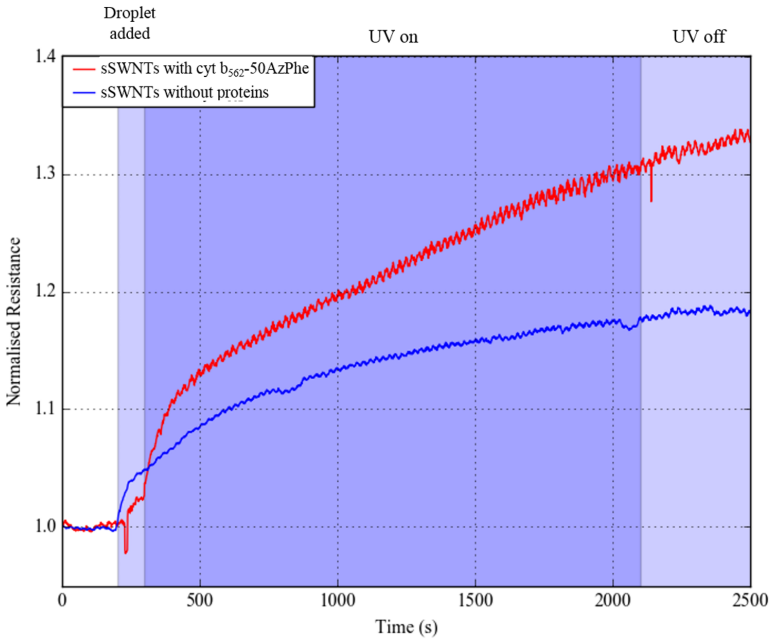

FIGURE 4.13: Resistance plot over time during incubation in solution under UV light. Here is a comparison between the resistance changes with a buffer solution and a solution containing cyt b_{562}-50AzPhe on sSWNTs. The noise seen in both curves is a beats frequency arising from a frequency mismatch between the wave function generator and the lock in amplifier.

Further experiments were performed with sfGFP-204AzPhe on sSWNTs and mSWNTs in Figures 4.15 and 4.16 respectively. The results from these experiments clearly demonstrate the immediate effect the UV illumination has on the chemical reaction cross-linking these molecules. For sSWNTs, the overall change in resistance is more gradual than with the metallic device, showing longer periods of time to reach a static equilibrium. However, the semiconducting device displays a resistance change of over double its original value. This was to be expected as the proteins not only form surface defects in the CNT structure, but also cause a shift in the density of states in the system. This effect could be similar to that of chemical dopants semiconductor technology which would effectively alter the electronic properties of the sSWNTs. GFP in particular, is known to be an electron donor molecule[91].

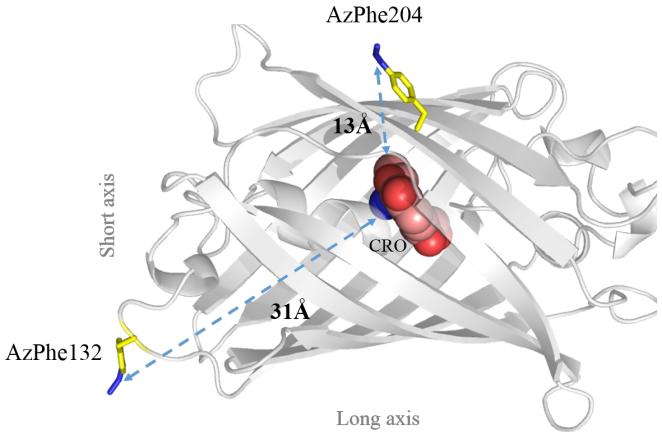

FIGURE 4.14: Diagram of sfGFP with the positions of the 132 and 204 AzPhe molecules with respect to the chromophore.

Furthermore, the position of the AzPhe in the 204 variant is about 13$\mathring{A}$ to the chromophore of the protein which may have an effect on the electronic interaction between the CNT and the protein's fluorophore (See figure 4.14). The effect of the linker's proximity to the fluorophore will be discussed further in chapter 5.

On the other hand, the mSWNT device is far more stable displaying clear evidence of photo induced protein cross-linking. Equilibrium within the solution is achieved relatively quickly for the buffer, although the protein solution still shows a steady rise in resistance even without UV illumination. This could be a result of proteins

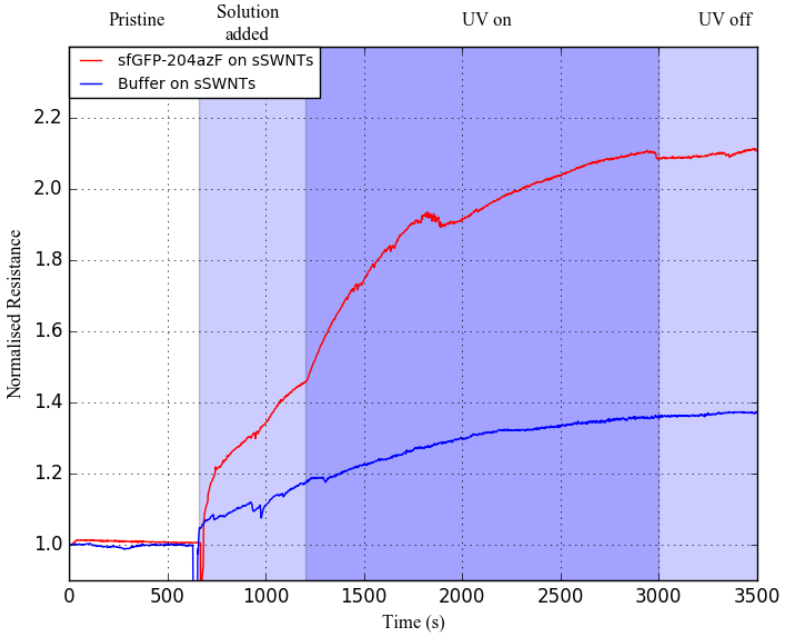

FIGURE 4.15: Resistance plot over time of sSWNTs during incubation in solution under UV light. Here is a comparison between the resistance changes with a buffer solution and a solution containing sfGFP-204azPhe on sSWNTs.

within the solution physisorbing to the CNT sidewalls, disrupting the π electron orbitals.

Using AFM, we can image the CNTs before and after photo-cross-linking of the proteins giving us an idea of the overall coverage of protein molecules on the resulting device. An example of this with sfGFP-204AzPhe on a sSWNT device is shown in Figure 4.17.

In each of these experiments, we see a definite rise in the electrical resistance of the SWNT devices after protein attachment. Once the devices are left to relax (which takes between 12 and 24 hours as mentioned earlier), the functionalised CNTs have a higher resistance then when they were pristine. This demonstrates the strong effect introducing these sp^3 defects has to the electronic structure of the CNT.

Despite experimental difficulties arising from lack of resources including proteins and electrodes for these devices, we have managed to demonstrate the immediate effect the covalent attachment has had on the electronic properties of the CNTs.

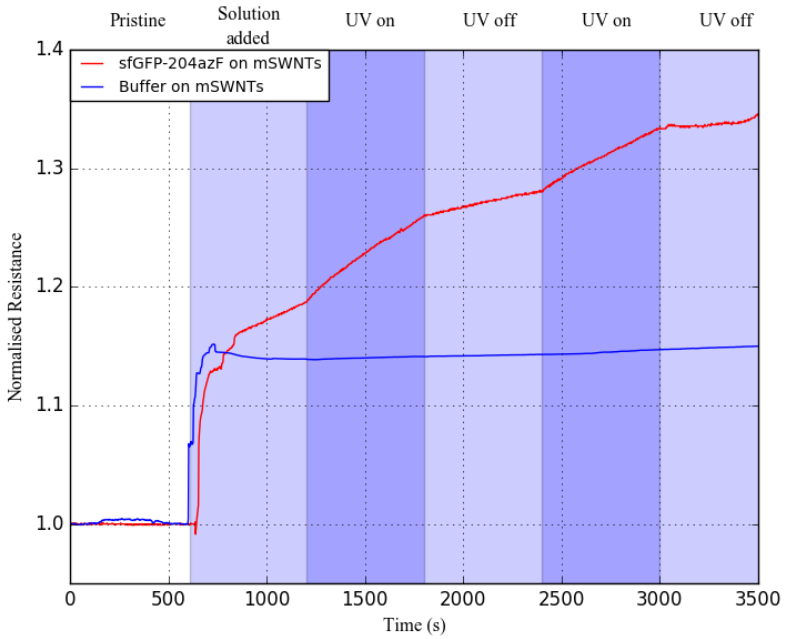

FIGURE 4.16: Resistance plot over time. Here is a comparison between the resistance changes with a buffer solution and a solution containing sfGFP-204azPhe on mSWNTs.

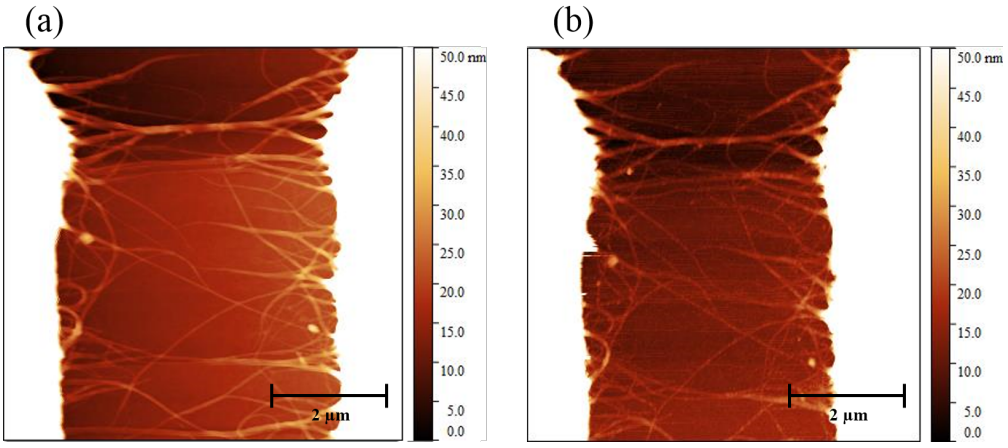

FIGURE 4.17: AFM image of SWNT device (a) before addition of proteins and (b) after photo cross-linking of sfGFP-204AzPhe.

This has proved to be an useful tool to probe in-situ attachment of proteins to CNT, although there are difficulties in quantitatively monitoring this attachment.

4.2.3 Photoresponce of sfGFP at Longer Wavelengths

One interesting aside regarding the covalent attachment of sfGFP to sSWNTs was the observation of a photoresponse at a wavelength close its activation wavelength. By shining light near this activation wavelength, sfGFP will fluoresce causing an energy transfer event. With such close proximity to the CNT, there is a high probability that some of the energy released from the sfGFP molecules will transfer to the CNTs, affecting their electronic properties. As previously mentioned, GFP acts as an electron donor upon light activation, which would therefore dope the CNT, resulting in a shift in the density of states.

The activation wavelength of sfGFP-204AzPhe is around 480nm, as seen from Figure 4.18, and emits at around 510nm giving the protein its green glow.

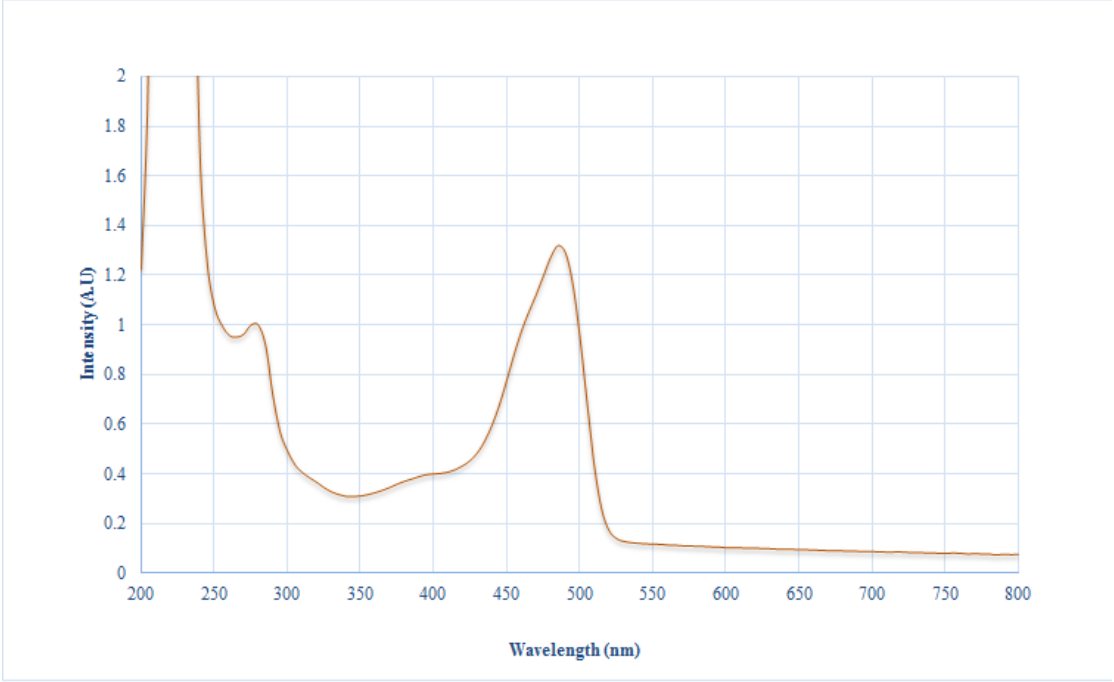

FIGURE 4.18: Plot of light absorbance for sfGFP-204AzPhe over a range of wavelengths.

We used the same potential divider circuit to measure the shift in potential difference across the device as it is illuminated with light at the protein activation wavelength. Here, a 480nm LED was implemented in place of the 305nm UV LED, and positioned 1cm away from the SWNT-sfGFP device, ensuring complete device illumination and reducing the margin for error. Each sample was rinsed

with de-ionised water and dried with a flow of nitrogen after the initial photo cross-linking experiment, ensuring that all non-specifically bound proteins were washed away. These devices were then left overnight to settle to a stable state before taking measurements. All experiments were conducted at room temperature with a forward bias of 100mV.

Figure 4.19 shows the photo-response when illuminating a sSWNT device with sfGFP-204AzPhe bound, compared with a device without proteins. The samples were illuminated for 60 seconds, 5 minutes apart. From the plots, you can see a clear, sharp response under illumination for the protein functionalised CNTs. This indicates that the proteins are still active post CNT functionalisation. One possible explanation for this is that sfGFP acts as an electron donor under exposure to 480nm light which would indicate a n-doping event. If this is the case, it seems to have reduced the number of holes in the CNT electronic structure, resulting in an increase in the resistance across the device. This photo-response has caused a very small shift in resistance compared with the cross-linking experiment which is expected as no additional defects are being produced, making this purely a charge transfer phenomenon.

One thing to notice from this plot, is that after the light source is switched off, there is no switching effect with the resistance dropping back to its initial level. Instead, it appears to remains relatively steady, which could suggest that that the initial excitation has resulted in resonantly transferred excitons to the CNTs. This is characteristic of light induced doping, causing charge traps at defect sites in the nanotube structure. This is highly probable as the photo induced cross-linking reaction forms one defect site per protein bound, creating a charge trapping site at the point of protein-CNT interaction[10][92]. The resistance slowly returns to its original level after a number of hours in ambient conditions as the charge gradually dissipates, tunnelling from the trap through a potential barrier.

Another group has observed similar results with charge trapping sites formed between CNTs and layered a porphyrin hybrid[10]. Here, Chen et.al. attributes

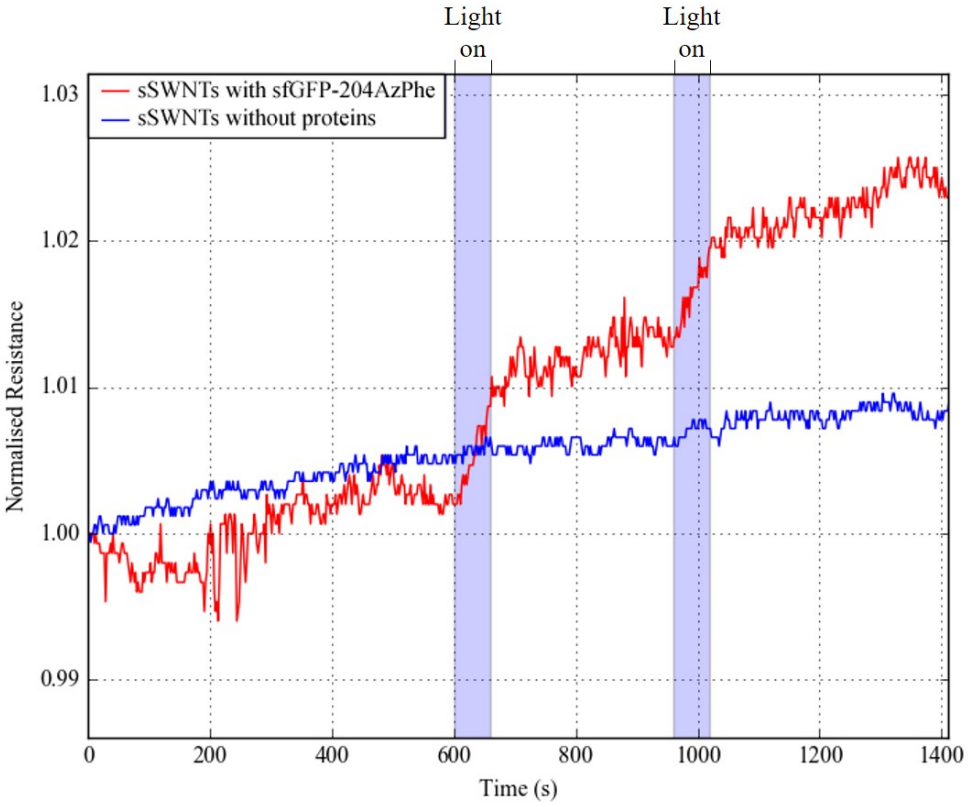

FIGURE 4.19: Plot of the effect of a 480nm light induced photo-response on a sSWNT device with and without sfGFP-204AzPhe attached. The 480nm illumination takes place in the regions coloured in pale blue.

charge trapping to a Coulomb blockade regime with the charge tunnelling through the potential barrier formed between the trap and the nanotube.

4.3 Non-Covalent Linker Methods

As I mentioned in chapter 2, by implementing the AzPhe moiety in the proteins structure, we get an additional degree of control over the protein, opening up different linker possibilities in addition to covalent photo-cross-linking. We have been successful in engineering the protein to include a pyrene linker, able to non-covalently link to the CNT sidewall via π-π stacking, as well as functionalising short stand DNA with a functional group to link to a protein with an alternative uAA incorporation.

The protein hybrid structures were made in small quantities so therefore, we did not have much material to conduct these experiments. Nevertheless, we were able to test these non-covalent CNT attachment methods and in this section, I'll briefly demonstrate their use and discuss their potential in developing protein-CNT hybrid nanostructures.

4.3.1 Pyrene Chemistry Non-Covalent Attachment of Proteins

Pyrene attachment is an attractive method for non-covalent cross-linking to CNTs as it doesn't cause a structural defect in the nanotube upon attachment. Instead, the pyrene molecule with its π orbital structure will readily stack onto the sidewall of a CNT through π-π stacking. This may have a significant impact on the electronic properties for a number of reasons. First of all, incorporation of an additional molecule to the AzPhe functional group would increase the protein-CNT distance, reducing the electron interaction between the protein and the CNT. Secondly, by not introducing a surface defect to the CNT structure, we reduce the chance of charge trapping, altering the way these systems behave when compared with the covalently bound proteins.

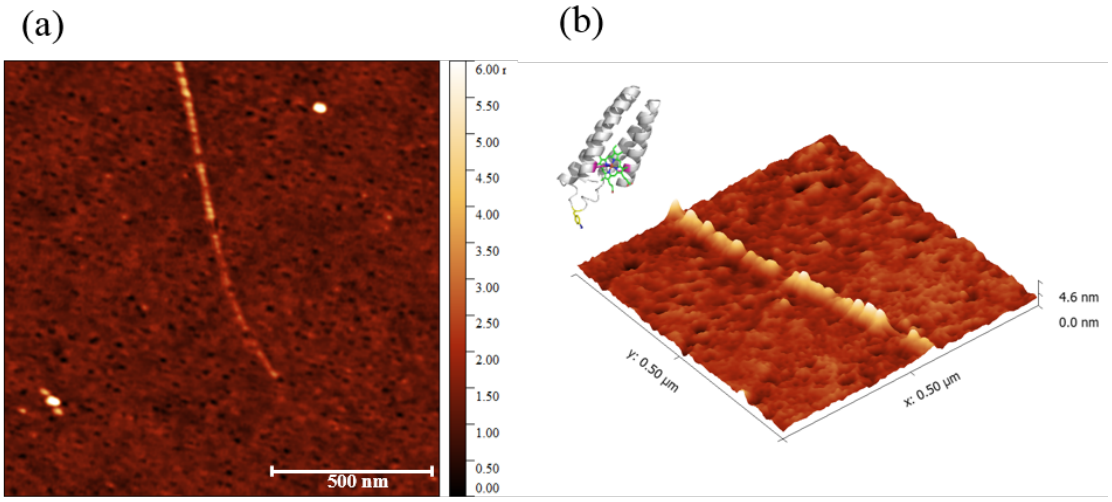

FIGURE 4.20: An AFM image of cyt b_{562}-5AzPhe (long axis) on a SWNT. (a) A typical AFM image from top down. (b) This is a 3D representation of a section of the protein-CNT structure taken from the same image.

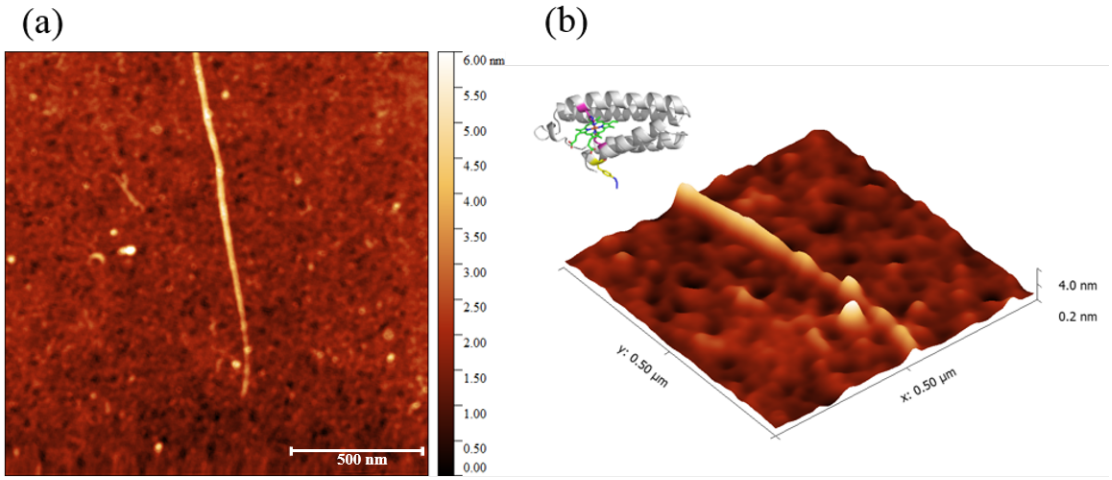

FIGURE 4.21: An AFM image of cyt b_{562}-50AzPhe (short axis) on a SWNT. (a) A typical AFM image from top down. (b) This is a 3D representation of a section of the protein-CNT structure taken from the same image.

By simply drop casting protein-pyrene solution onto pristine SWNT samples, we are able to link these bio-molecules to the nanotubes without the need for UV illumination. Figures 4.20 and 4.21 demonstrate the effective binding of the long and short axis variants of cyt b_{562} respectively. Notice that they stack along the CNTs in the same manner as their covalently attached counterparts, meaning that this method of stacking is characteristic of these orientations of cyt b_{562}. It is also further evidence of the exquisite control over the orientation of the bound protein, with the short axis stacking end to end, and the long axis variant standing perpendicular to the CNT.

4.3.2 DNA-Functionalised Protein Attachment

Forming protein-CNT hybrids in solution with a DNA functionalised linker is quite an attractive prospect with the ability to modify the DNA with various functional groups, additional control over the structure of the DNA at the nanoscale, as well as having surfactant free solutions. Although my work with DNA-CNT structures only covers preliminary attachment studies, I will demonstrate the capabilities of such a system and discuss the potential it has for building nanoscale bioelectronic structures.

For this study, I have investigated 2 different methods of protein-DNA cross-linking by incorporating either acetylene or azide linker moieties into the DNA sequence.

4.3.2.1 DNA-Acetylene Functionalisation

Solutions of $(GT)_8$-U(acetylene)-$(GT)_4$-G-U(acetylene)-T-$(GT)_7$ wrapped around SWNTs, suspended in de-ionised water, were produced with Mark Freely in the department of chemistry at Queen Mary University of London. The acetylene group is an alkyne C_2H_2 molecule which means the carbons are bound via a triple bond. This can undergo copper(I)-catalysed azide-alkyne cycloaddition (CuAAC) with an azide molecule in the presence of a copper(I) catalyst, forming a 1,2,3-triazole[62]. This is the same process in which we bind pyrene to the AzPhe moiety in a protein as I described in chapter 2.

The key note to take on board during this reaction is the effect of the toxicity of the copper (I) catalyst to the protein over time[62]. This reaction must go on long enough to ensure sufficient binding between the proteins and the DNA-CNTs, but not too long as it can cause degradation of the protein structure.

To produce solutions of protein-DNA-CNT nanostructures, we first added 0.8μl of 20mM $CuSO_4$, 1.3μl of 50nM tris(benzyltriazolylmethyl)amine (TBTA), and 10μl of 100mM amino guanadine buffer solution to 4 separate tubes. Here, the $CuSO_4$ acts as a source of Cu(II) which can be reduced to Cu(I) when reacted with ascorbic acid. This is added later on to activate the reaction. The TBTA acts to stabilise the Cu(I) oxidation state which enhances its catalytic effect in the azide-acetylene cycloaddition reaction.

The next step was to add 40μl of 1mg/ml DNA-SWNT solution to each tube along with 10μl of 1μM cyt b_{562}-50AzPhe. This protein was chosen for this experiment due to its stability under harsh conditions as proved with the previous pyrene reactions. Once the was done, 5μl of 100mM ascorbic acid was added to each tube to initiate the reaction. The 4 solutions were left to react over different periods of time to give us an idea of the optimal time for reaction. The reactions were

performed for 15, 30, 45 and 60 minutes, after which the reactions were quenched with 300μl of de-ionised water and 10μl ethylenediaminetetraacetic acid (EDTA). The EDTA absorbs the cations from the copper reaction, which helps to quench the chemical reaction.

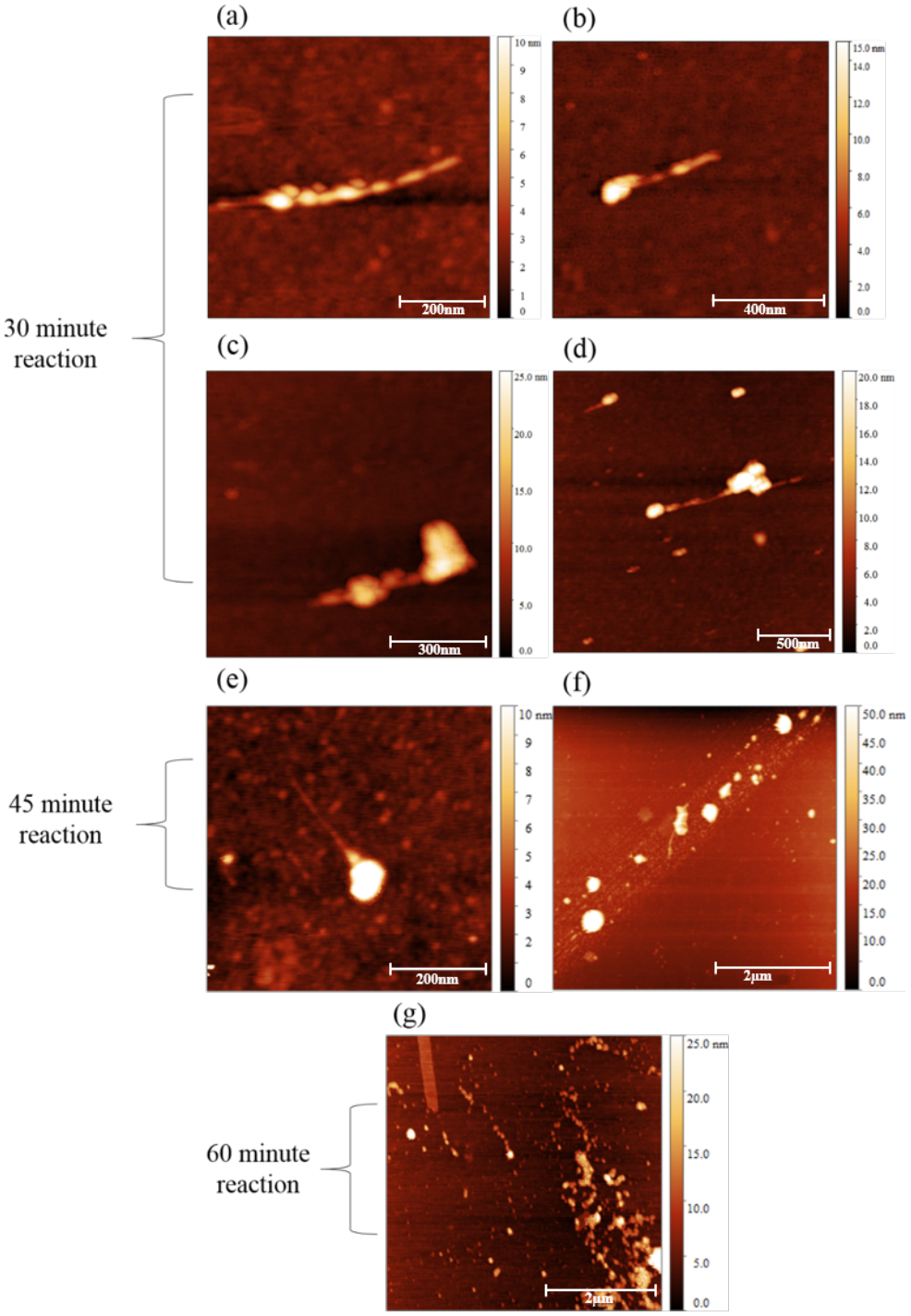

FIGURE 4.22: AFM images of SWNT-DNA-acetylene structures after CuAAC reaction with cyt b_{562}-50AzPhe at different time intervals. (a,b,c,d) 30 minute reaction. (e,f) 45 minute reaction. (g) 60 minute reaction

Finally the solutions were filtered in a centrifuge at 13,300g for 30 minutes and drop cast onto SiO_2 for AFM analysis. This led to some success in Cu-activated cross linking for the 30 and 45 minute reactions as seen in figure 4.22. No SWNT structures were found from the 15 minute reaction sample, which could have come from a problem when processing the sample.

Here, we can see the 30 minute reaction has yielded protein-DNA-SWNT hybrid structures with, in some cases, seemingly well formed protein structures. There are also some large aggregates which is a strong indication that the optimum reaction time is around 30 minutes or less. The 45 minute reaction produced what looks like protein aggregates attached to the DNA-SWNT structure, indicating structural degradation of the protein over this time period. The 60 minute reaction sample showed what looked like total degradation of the proteins, leading to large aggregated structures all over the surface of the substrate.

These experiments did not yield high numbers of success protein-DNA-SWNT hybrid structures. Combining this with the toxicity problem the copper(I) catalyst poses, we concluded that this is not the optimal approach to take to form these hybrid structures. Therefore we opted for a copper-free alternative using azide functionalised DNA oligos.

4.3.2.2 DNA-Azide Functionalisation

For these experiments, we used U(azide)-$(GT)_{20}$ wrapped around SWNTs which allowed us to bind through to an alkyne linker group in the protein. This process allows us to chemically link these molecules without the need for copper or UV treatment though a reaction known as strain-promoted azide-alkyne cycloaddition (SPAAC)[93][94][95]. To do this, we incorporate the uAA, s-cyclooctyne-L-pyrrolysine (SCO) into the protein. Here the alkyne group is under ring strain, allowing for it to readily react with an azide group under physiological conditions as seen in figure 4.23.

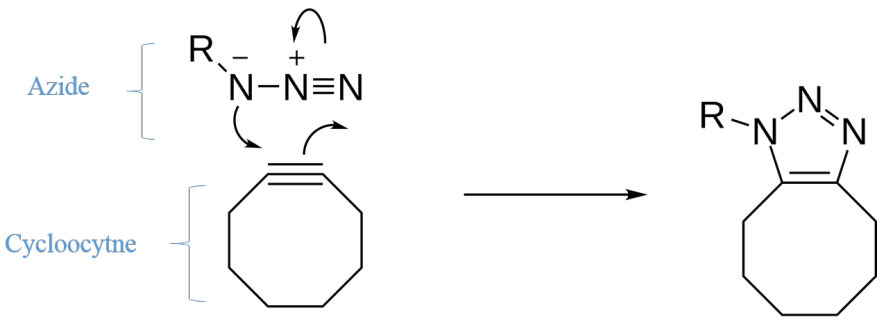

FIGURE 4.23: SPAAC reaction mechanism forming a triazole link without the need for a copper catalyst.

As the reaction is determined by the internal energy of the strained molecule, this is a relatively slow reaction which can take a number of hours. With this in mind, we ran this reaction for different time trials to allow us to determine the optimum time for a successful click reaction and ensure sufficient non-covalent binding of proteins to DNA-CNTs.

Mixtures were made up of 100nM sfGFP-204SCO and 0.1mg/ml DNA-SWNTs in equal parts and left for time trials of 1, 3 and 5 hours. The resulting hybrid structures were centrifuged through 3000Da filters to remove smaller particles from the bulk solution. These were then analysed using AFM, seen in figure 4.24.

The analysis showed mixed results with high coverage of proteins along CNTs in some cases, and very little coverage in others. The 1 hour reaction showed some evidence of binding with some aggregated structures attaching to the end of the DNA-CNT. When looking at the structure of the DNA oligo which coats the CNTs, one notices the azide linker group is at the end of the molecule. This means its available space for binding is determined by its separation from the neighbouring oligo. With that in mind, the easiest place fro proteins to access this linker molecule would be at the end of the DNA chain, positioned at the end of the SWNT. We achieved a higher coverage of proteins along DNA-CNTs after 3 hours with evidence of single, non-aggregated proteins. As you increase the time to 5 hours, the density of proteins becomes very high with substantial aggregation on and off the DNA-CNTs.

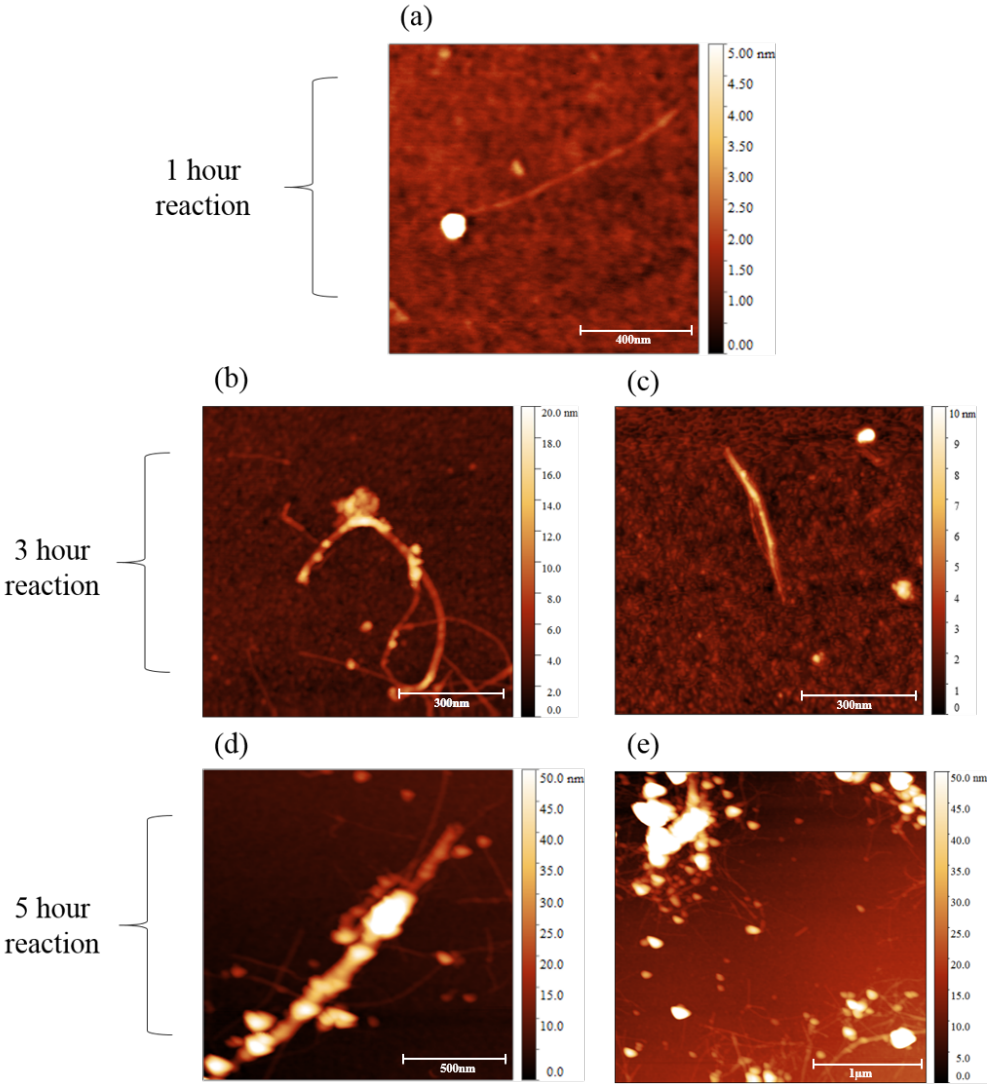

FIGURE 4.24: AFM images of SWNT-DNA-azide structures after SPAAC reaction with sfGFP-204SCO at different time intervals. (a) 1 hour reaction. (b,c) 3 hour reaction. (d,e) 5 hour reaction

These results show that this can be an effective way of producing protein-DNA-CNT hybrid structures in solution although the process would need to be refined. The 3 hour reaction showed the best results for protein attachment although there were still some aggregates in the solutions. This can be reduced with more vigorous filtering and post deposition rinsing procedures.

4.4 Summary

In this chapter, I have discussed the process of attaching various proteins in predefined orientations to CNTs. We have done this with a great deal of success, allowing us to decorate CNTs with a variety of proteins and apply them to an electronic device. Using an azide moiety to covalenlty cross-link proteins to CNTs under UV photo illumination, proved to be an effective method of attachment which could be applied to a variety of proteins with highly reproducible results. Defining the position of the chemical linker has also produced data indicating that the proteins assemble along the nanotubes under the influence of the orientation with respect to the nanotube, as well as how they stack along with neighbouring proteins as seen in Figure 4.8. This was primarily seen with SA-cyt b_{562} which always appeared to stack end to end in a tightly packed formation along the length of the CNT. sfGFP-204AzPhe also showed interesting stacking when bound, where they appear to be binding with their long axis pointing perpendicular to the direction of the CNT. This indicates the possibility of a dipole influence then the proteins align along the CNTs.

Attachment of proteins has shown to increase the electrical resistance of the SWNT devices, demonstrating the strong effect the introduction of these sp^3 defects has on the CNT's electronic structure. We were able to monitor this effect in real time using a simple potential divider circuit, observing distinct rises in the resistance of the devices when exposed to UV light in protein-azide solution. This rise was not observed when the devices were exposed to UV light in buffer solution, suggesting it's the protein binding event which is giving rise to this resistance increase.

Some progress has been made to study the protein post-deposition activity with electrical studies on the interaction between sfGFP-204AzPhe and SWNTs. Here I introduced the idea of possible charge trapping at CNT defect sites as a result of photo-induced exciton transfer of the fluorescent protein. This phenomenon could be further investigated at a wider range of wavelengths in order to understand the selectivity of the proteins response to light. This idea will be discussed further in the next chapter. Future work could be achieved with these devices, studying the

redox properties of cyt b_{562} through the use of cyclic voltammetry, and studying single molecule interactions with bound enzymes such as TEM β-lactamase.

We have explored the different possibilities that come from pre-functionalising proteins with uAAs which allows us to control their deposition on the nanoscale. With this we have been able to demonstrate the implementation of a non-covalent pyrene linker to an AzPhe uAA as well as the cyclo-octane uAA, used for DNA-Az CNT functionalisation. Although these have presented some additional experimental challenges; they do introduce extra degrees of control at the nanoscale with the potential of studying single molecule interactions using pristine SWNTs.

Chapter 5

Optical Studies of Protein-Carbon Nanotube Systems

5.1 Introduction

Optical properties of CNTs has been thoroughly investigated across many groups, resulting in vast amounts of information of their fluorescent properties, photo-absorption and Raman spectra. Each method characterises one or more of the fundamental properties of CNTs, including their structural and electrical properties. Using techniques such as Raman spectroscopy, we are able to investigate the bond network and structural properties of a large number of CNTs. This provides us with the information needed to understand the binding mechanism of each protein as well as possible electronic interactions which cause a shift or even splitting of the Raman vibrational modes.

The nanoscale structure of individual nanotubes makes it difficult to optically study each CNT with single molecule resolution. Understanding how the optical properties of CNTs change after protein functionalisation could provide a wealth of information about the electronic properties of the system and the mechanism of the inter-molecular interaction. However, with changing chirality between individual

CNTs comes variation in its electronic structure and therefore, changes in their absorption and emission spectra.

Proteins are widely studied using optical techniques, providing an insight into their structure and function at single molecule resolution. Furthermore, fluorescent proteins such as GFP can be selectively studied via their excitation wavelength using various techniques such as confocal microscopy and TIRFM. As GFP has a well defined emission peak around 510nm, we can filter out other wavelengths allowing us to only study the proteins. Gaining an understanding of the dynamics of the protein in question gives information into how these molecules may interact with nano-materials like CNTs.

In this chapter, I discuss the use of optical techniques to investigate the interaction between proteins and CNTs. Raman spectroscopy was used to characterise the binding of a protein to a CNT by monitoring its effect on the vibrational dynamics and electronic structure of the nanotube. In order to understand how the binding affects the protein, we have studied the fluorescent properties of sfGFP using TIRFM, giving us an insight into how the protein behaves once bound, and the electronic interaction between the protein and CNT.

5.2 Raman Spectroscopy of Protein-CNT Hybrids

As described in chapter 3, Raman spectroscopy is a powerful tool which can be used to probe the bond network of CNTs. By using this method, we have been able to measure small shifts in vibrational modes within the CNTs caused by the formation of a covalent bond with a protein molecule.

The modes most associated with CNT structural defects are the D mode, occurring at around 1340cm^{-1} and its overtone, the G$'$ mode at around 2670cm^{-1}. The relative strength of these peaks would scale with the number of defects. However, as our approach for covalently linking proteins does not introduce many defects

with respect to the number of carbon atoms present, we do not expect the relative intensities of these peaks to change much upon functionalisation. Nevertheless, these additional defects have an effect on the CNT modes which results in a shift and maybe even splitting of the peaks.

The D peak arises from a single localised phonon mode in the presence of a defect. To illustrate this process, we can plot the electronic Brillouin zone of sp^2 carbon with its electronic dispersion described as Dirac cones as seen in figure 5.1. Here, a phonon near the K point in the Brillouin zone inelastically scatters an electron to K′ then elastically back-scattered to the K point. In order to abide by the conservation of momentum, a defect must be present to account for this momentum difference of the back-scattered phonon[69][96].

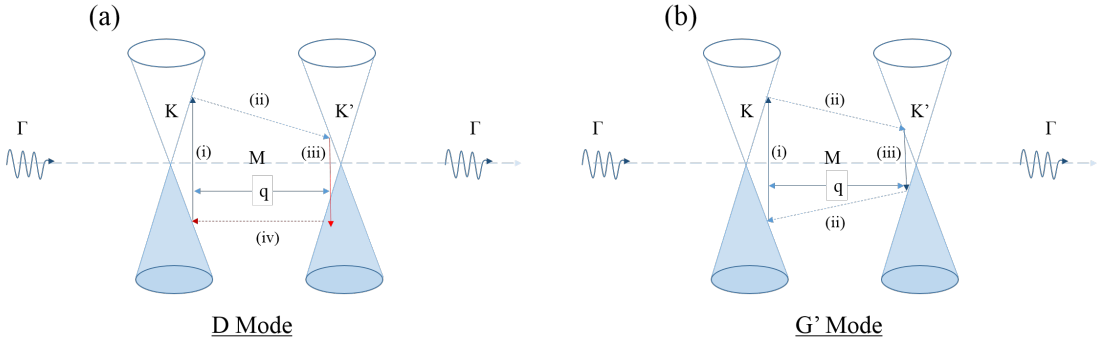

FIGURE 5.1: Raman scattering along the high symmetry direction between two Dirac cones at K and K′ separated by a wave vector q, in reciprocal space, representing the electronic dispersion.(a, b)(i) A photon excites an electron/hole from its occupied state (blue shaded region). (a, b)(ii)Inelastic scattering by a phonon. (a, b)(iii) Electron/hole recombination, (a)(iv) Red arrows indicate interaction with defect accounting for momentum conservation.

The G′ mode, also known as the 2D mode, is an overtone of the D mode arising from a 2 phonon interaction of the same nature. However, as this peak originates from a process where momentum is conserved, it can arise from self annihilating pairs of phonons. This means a defect is not required for this peak to appear. Therefore, these modes are present in pristine CNTs, though variations to this spectral peak follow the same set of rules as the D mode[96].

Both of these Raman modes are known as inter-valley scattering modes, in which phonons are scattered from one Dirac cone to the other. Therefore, the wave vector

is determined by the relative positions of these Dirac cones in reciprocal space (see figure 5.1) [97][69]. When an sp^3 bond is introduced though the cross-linking of an AzPhe molecule across the C=C double bond, this can result in a strain on the neighbouring bonds. This in turn can result in a shift in the Dirac cones which can change the inter-valley phonon wave vector. This symmetry breaking causes a movement which can result in peak broadening and splitting[96].

Using this theory, we can determine if a defect is present, and possibly infer the nature of this chemically induced defect.

5.2.1 Experimental Methods

All Raman measurements were taken by Prof. Monica Craciun at University of Exeter using a 532nm laser with a spot size of 2μm. The samples were prepared by drop casting a SWNT-SDS solution onto SiO_2 substrates and left to dry on ambient conditions before rinsing in de-ionised water and ethanol.

Initial experiments were conducted with TEM-165AzPhe at a concentration of 10nM. Some samples were illuminated with 305nm UV light at 18Wm^{-2} for 10 minutes in order to covalently bind the proteins to the CNTs, while others were left in the dark to provide a comparison between the two. Showing evidence of a difference between these Raman spectra can be used to determine the effect of the azide cross linking on the phonon modes.

Though these preliminary tests yielded some interesting results, the density of CNTs on the substrates were fairly low causing the spectra to be dominated by the SiO_2 as seen in figure 5.2. To resolve this, the density of CNTs was increased in further experiments.

Further experiments were conducted with sfGFP-204AzPhe and cyt b_{562}-50AzPhe at 1μM with a higher concentration of SWNTs to ensure strong CNT Raman peaks.

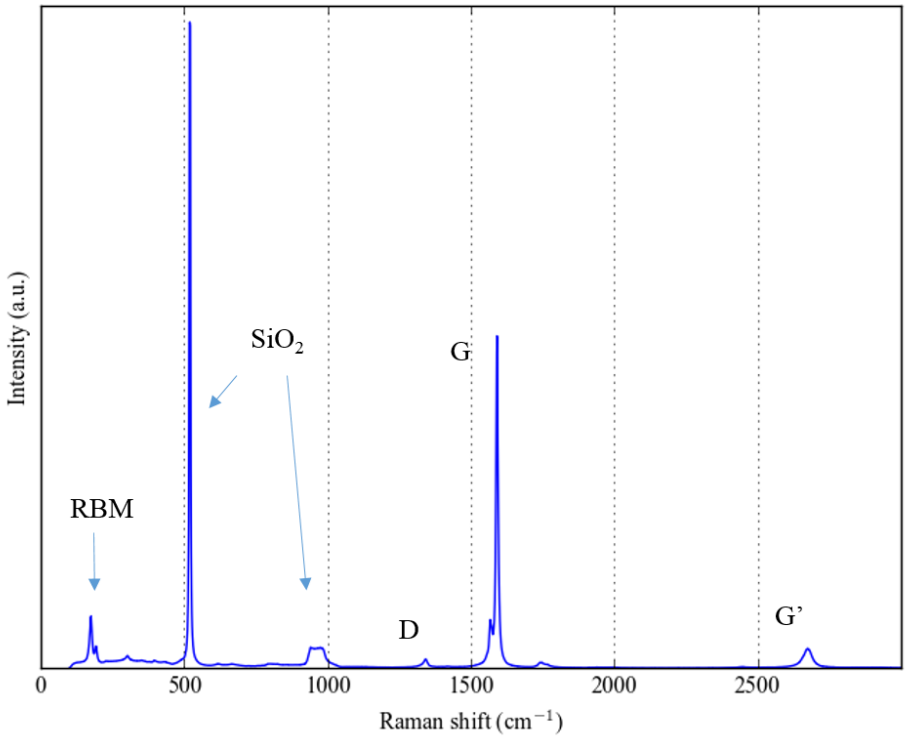

FIGURE 5.2: Full Raman spectra for a low concentration of sSWNTs on SiO_2. Due to the low number of CNTs, the low frequency spectra is dominated by the substrate causing reduced intensity of CNT modes.

5.2.2 Results and Discussion

A number of control tests were conducted on unmodified SWNTs, providing data on a range of Raman modes to compare with the protein functionalised SWNTs. The middle to high frequency modes for unmodified SWNTs can be seen in figure 5.3. The D peak shows up more prominent in sSWNT samples than mSWNT samples. As mentioned earlier, the G′ peak will still be present before functionalisation as it does not need defects to be observed.

The radial breathing modes (RBM) showed considerable variation in frequency due to a distribution of chiralities in both the semiconducting and metallic CNTs. These variations in chirality did not affect the higher frequency modes significantly.

For each Raman spectrum, a Lorentzian curve was fitted to the D and G′ peaks as shown in Figure 5.4. From this, we could obtain the positions and widths of

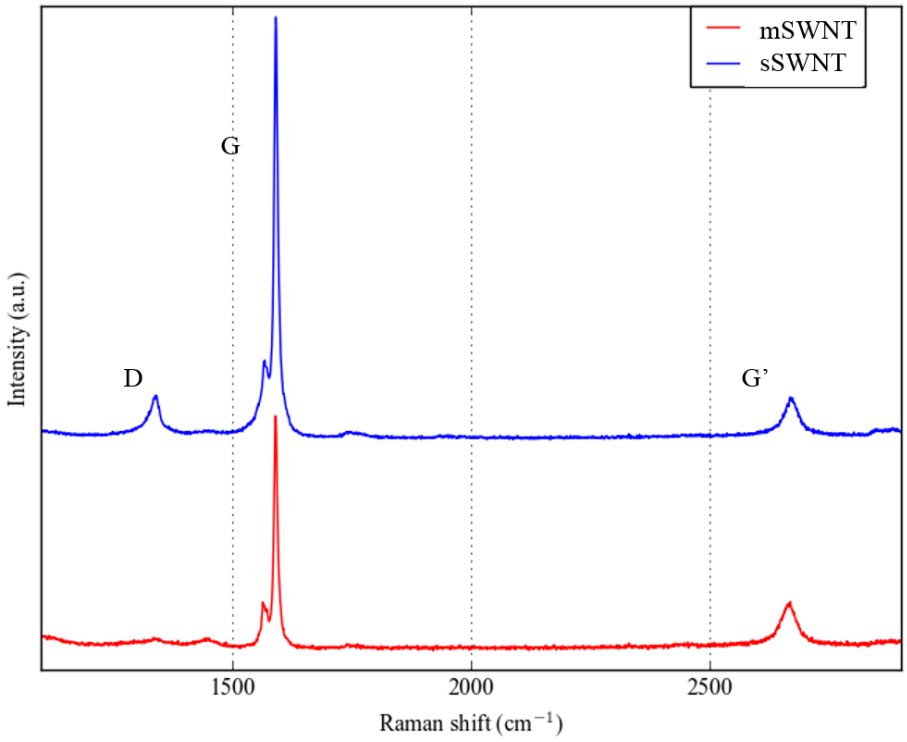

FIGURE 5.3: Raman spectra for non-functionalised mSWNTs and sSWNTs displaying the middle to high frequency modes.

each of these peaks. Due to the shape of the peaks, a Lorentzian fit was chosen over a Gaussian fit.

The preliminary data showed a larger variation between samples in terms of peak intensity as the low density of CNTs meant most of the data was overwhelmed by the peaks measured from the substrate. However, some interesting data was found from the TEM functionalisation of mSWNTs as seen in figure 5.5. Here, we measure a clear increase in intensity of the D mode when the CNTs are functionalised with TEM after UV illumination. This increase in D mode intensity is not seen when the same protein variant is deposited without the UV illumination. This indicates that the intensity increase comes as a result of photo-cross-linking, causing defects to be formed. In addition to this result, the G′ peaks show a position shift to higher wavelengths when functionalised with TEM as a result of sp^3 orbitals being formed. Moreover, the TEM samples without UV illumination display no significant shift in position from the unmodified sample. As mentioned

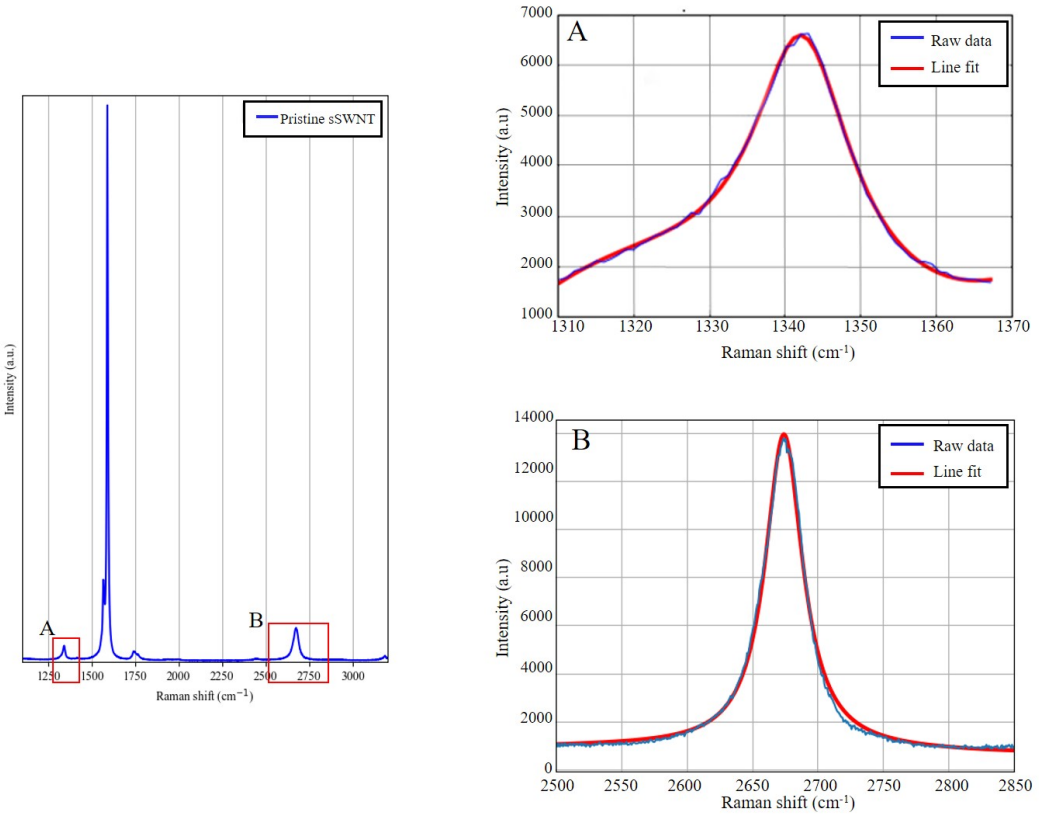

FIGURE 5.4: Raman spectrum at higher frequencies for pristine sSWNTs. Lorentzian curves were fitted to the D peak shown in region A, and the G′ peak shown in region B.

earlier, this could be a result of minor peak splitting from a chemically induced defect, producing strain on the CNT bond structure, increasing the observed Raman frequency.

This initial result was very encouraging, indicating that covalent bonds were being formed between the proteins and the CNTs. To further this investigation, the experiment was repeated with a higher concentration of SWNTs and proteins, this time using sfGFP-204AzPhe and cyt b_{562}-50AzPhe to test the versatility of the attachment method.

Both proteins showed a significant shift in the position of the D peak as seen in figure 5.6 where the protein functionalised samples show a similar shift to higher wavenumbers indicating an influence of strain as a result of sp^3 orbitals being formed. A shortening of the bond-length would stiffen the bond which could be

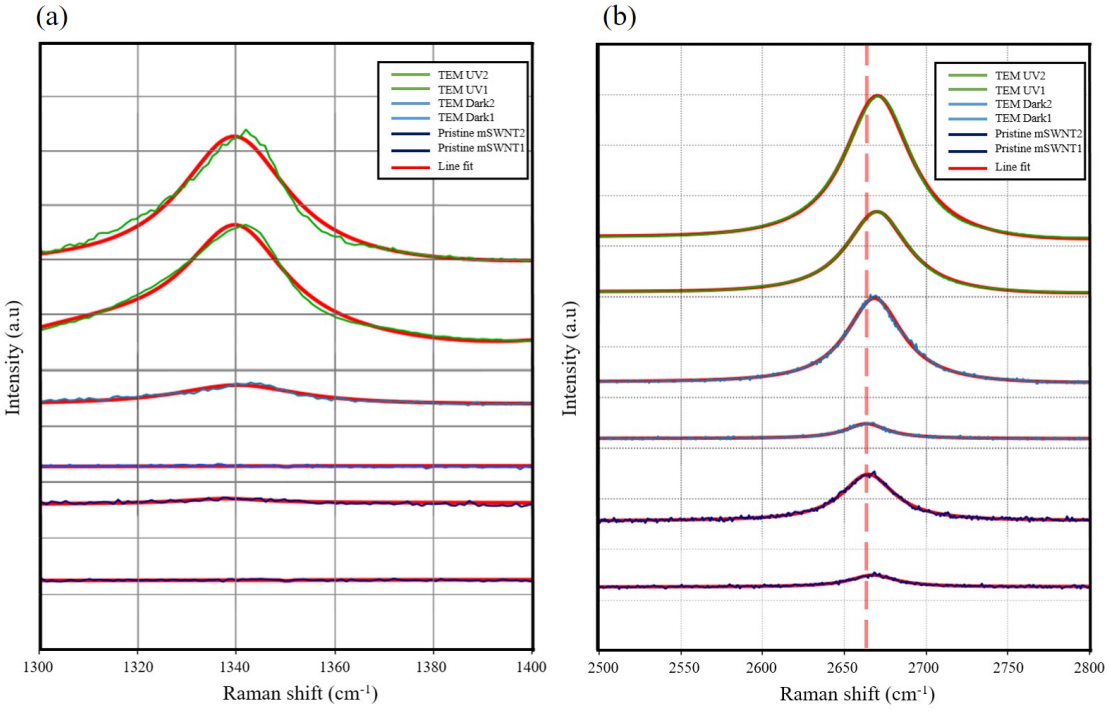

FIGURE 5.5: Comparison of the D and G′ modes between pristine mSWNTs, and ones funtionalised with TEM-165AzPhe with and without UV exposure. Each curve is fitted with a Lorentzian line fit (red curves). (a) Raman spectra around the D peak. (b) Raman spectra around the G′ peak. The red dotted line shows the position of the pristine mSWNT G′ peak.

the origin of the shift to higher frequencies. An example of where a large D mode shift is seen in a case analysed by Craciun et.al where a far higher percentage of the sp^2 carbon is converted to sp^3 carbon through fluorination of graphene[98].

Peak frequencies and full width half maximums (FWHM) were obtained by fitting each peak to a Lorentzian curve line-fit. From these values shown in figure 5.6, we can see that the protein functionalised samples not only show peak shifts to higher frequency from the un-modified SWNTs, but the FWHM also increase. This can reflect a spread in peak positions due to induced disorder.

These shifts in peak position are consistent across multiple samples, with measurements taken for 3 different areas on each sample. The peak frequency positions for both sSWNTs and mSWNTs are shown in figure 5.7. We see a narrow spread in the position of SWNTs modified with proteins which could be a result of a specific phonon mode caused by an abundance of a defect of a specific type. In this case

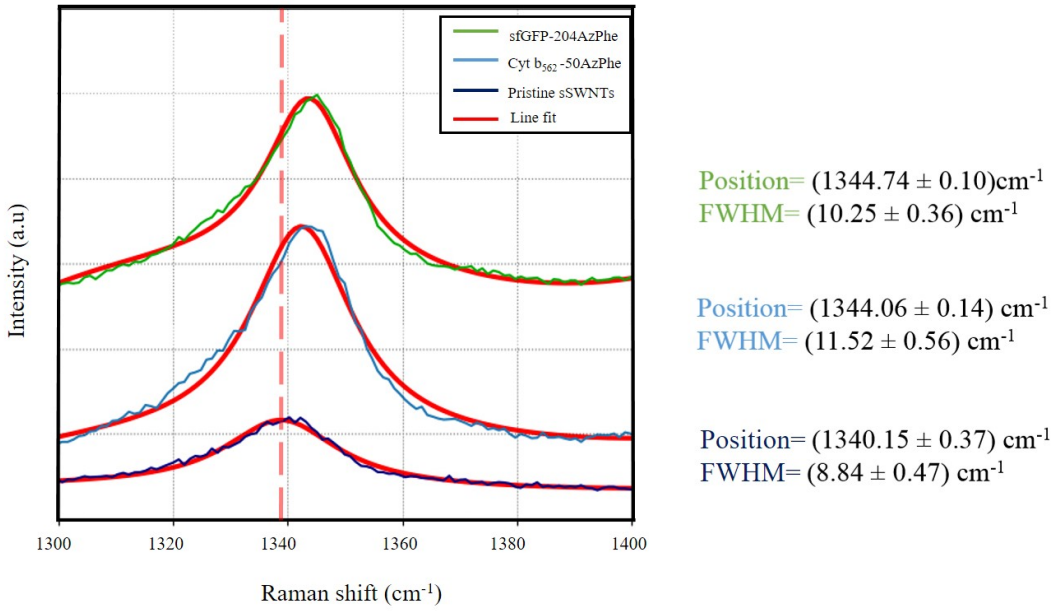

FIGURE 5.6: Raman spectra showing the shift in the D peak for protein decorated sSWNTs. Each curve is fitted with a Lorentzian line fit (red curves). The red dotted line indicates the position of the unmodified sSWNT D peak.

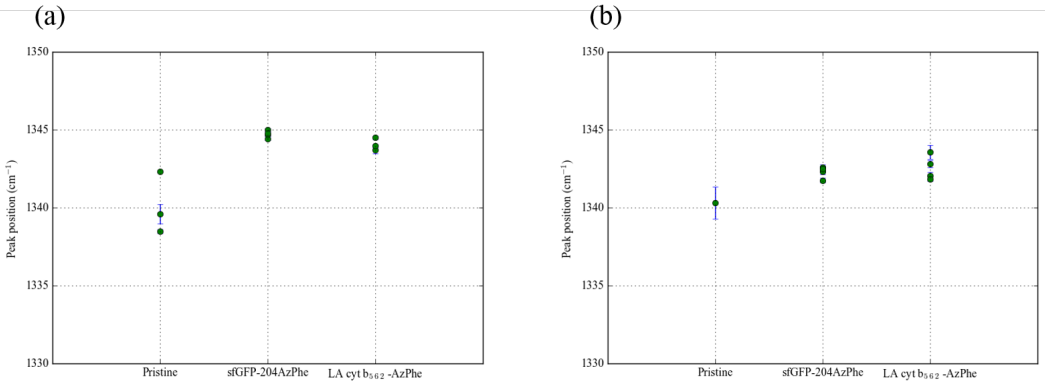

FIGURE 5.7: Positions of D peaks for unmodified SWNTs, sfGFP-204AzPhe on SWNTs and cyt b_{562}-50AzPhe on SWNTs for (a) sSWNTs and (b) mSWNTs.

it's the carbon binding through to the azide moiety. The pristine SWNTs show some variation in peak frequency across the surface. The pristine mSWNTs had no measurable D peak in two out of the three measurements taken, indicating a very low number of structural defects. Nevertheless, for both sfGFP and cyt b_{562}, the D mode is seen to consistently shift to higher frequency and broaden on functionalisation by azide binding.

Figure 5.8 displays the G′ peaks from the samples in the previous figure. As G′ is

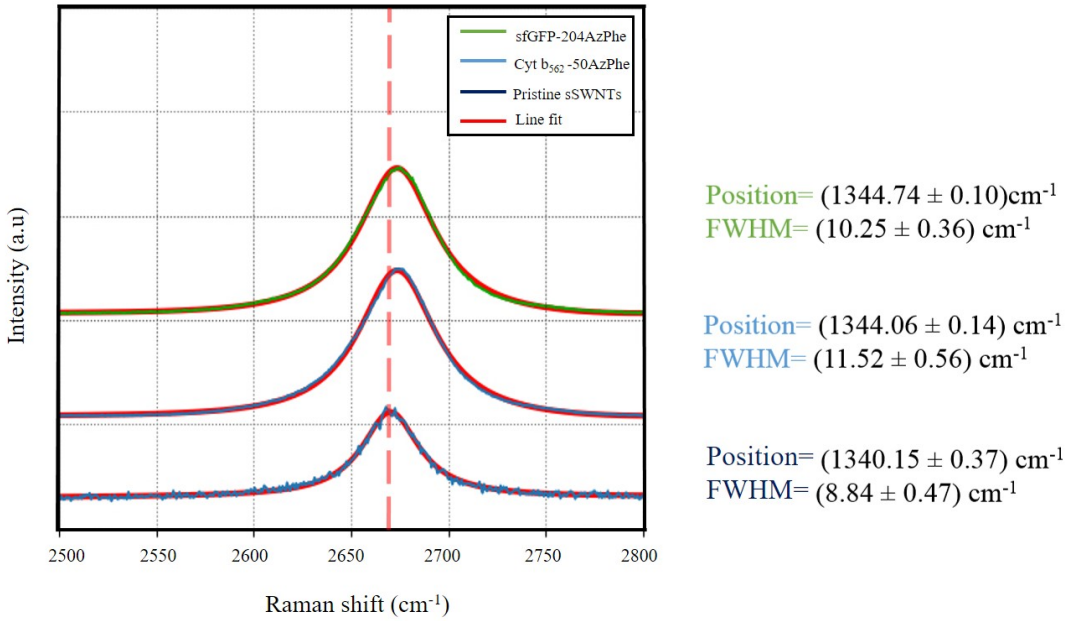

FIGURE 5.8: Raman spectra showing the shift in the G′ peak for protein decorated sSWNTs. Each curve is fitted with a Lorentzian line fit (red curves). The Red dotted line indicates the position of the unmodified sSWNT G′ peak.

an overtone of the D peak, we expect to see the resulting shift in frequency and broadening of the peaks compared with the pristine sample which is seen in the D peak. Here it is clearer to see with the G′ peak being more prominent than the D peak in the pristine samples.

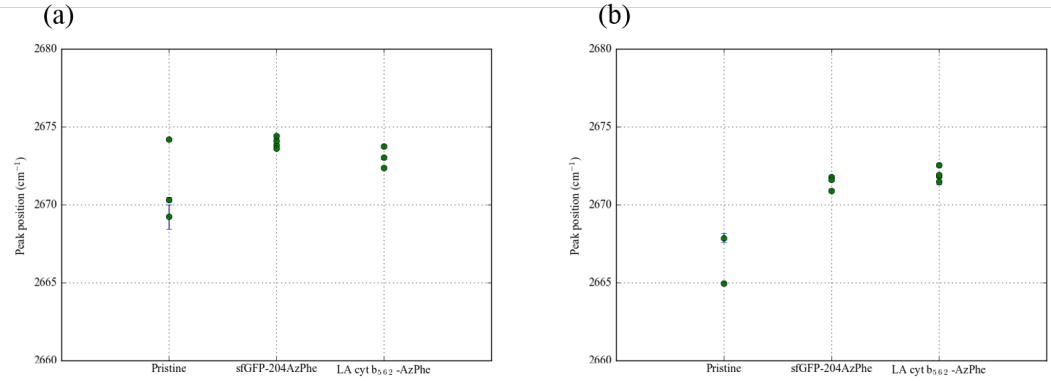

FIGURE 5.9: Positions of G′ peaks for unmodified SWNTs, sfGFP-204AzPhe on SWNTs and cyt b_{562}-50AzPhe on SWNTs for (a) sSWNTs and (b) mSWNTs.

Similar to with the D peaks, the G′ peaks also show a narrow spread of peak positions for protein-SWNT samples and a larger spread for the pristine sample as

see in figure 5.9. Here we can see the overall increase in position when the SWNTs are modified with proteins, characteristic of sp^3 forming.

Raman spectroscopy has proved to be an important tool for providing evidence of the binding mechanism of the AzPhe linker molecule with sp^2 carbon and allowing us to understand the effect this has on the structure of the SWNTs. We measure peak shifts to higher frequencies of the D and G′ modes for SWNTs functionalised with TEM, sfGFP and cyt b_{562}, indicating stiffer bonds, which is likely to relate to sp^3 coordination. Protein functionalisation also resulted in peak broadening which is likely to be a result of increased disorder in the CNT structure. Overall, Raman spectroscopy has provided strong evidence of covalent bonds being made when SWNTs are functionalised with azide linker molecules under UV illumination.

Now we have evidence of how the proteins bind to the SWNTs, we will discuss how the CNTs has affected the properties of the proteins using TIRFM.

5.3 TIRFM of sfGFP on SWNTs

Total internal reflection fluorescence microscopy (TIRFM) is a tool used to selectively excite molecules within a narrow region of the substrate in order to study emission from surface bound particles at a specific, predefined wavelength. This is used to record fluorescence data from large arrays of molecules over time which provides us with information on the dynamics and electronic properties of the system.

The fluorescent properties of CNTs vary with chirality giving them a wide range of emission wavelengths in the near infrared [44][42]. This makes them difficult to study when trying to understand single molecule interactions. Therefore, we chose to investigate how CNT functionalisation affects the fluorescent properties of sfGFP. From this we were able to gather a wealth of information on the protein intensities, photobleaching and blinking dynamics.

Photobleaching of the fluorescent molecule is a term used to describe when a fluorophore permanently loses its fluorescence due to over exposure to a photon source. Photo-excitation causes the fluorophore to undergo a number of excitation cycles as transitions between an electronic states[99]. This causes breaking in the covalent bonds around the fluorophore resulting in an irreversible modification to the molecule. In the case of GFP, the barrel structure protects the fluorophore from chemical reactants like oxygen, allowing it to undergo large numbers of excitation cycles. Typically, GFP will undergo 10^5 to 10^6 excitation/photon emission cycles before photobleaching[56][100].

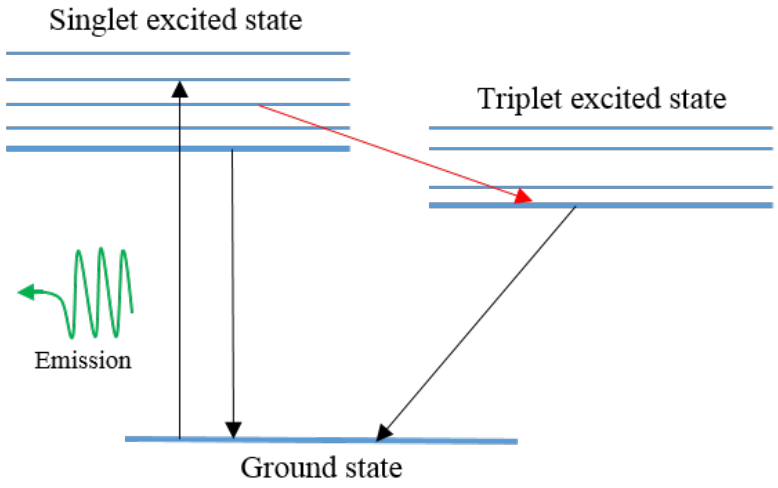

FIGURE 5.10: Diagram illustrating the electronic transitions between the ground state, the singlet excited state and the triplet excited state. The red arrow indicates the "forbidden" electronic transition to the triplet state.

Another phenomenon associated with fluorescent molecules such as GFP, is fluorescence blinking[101]. This is where the light emitted from the fluorophore cycles between on and off states[102]. Although this phenomenon is not fully understood, there are explanations which can shed some light on the mechanism taking place including electronic transitions from singlet to triplet states and protonation of the protein's chromophore.

As noted previously, photo-excitation will cause the fluorophore to go through a number of excitation and de-excitation cycles which will cause a continuous emission from the molecule resulting in an "on" state. Here, the cycles will be between the ground state of the electron and the singlet state of the electron,

where the spin of the excited electron is opposite to the spin of the ground state, fulfilling the Pauli exclusion principle. Another, less likely transition, is to the triplet state, where the spin of the excited electron matches that of the ground state. As these energy transitions are forbidden by the Pauli principle, the most likely transition for this to occur is when the level of the singlet and triplet states overlap, causing a transition between these states. This would mean little energy is gained or lost in the transition. However, as transitions are far less likely from this triplet state to the ground state, this can cause electrons to become trapped in this excited state, resulting in no emission and therefore an "off" state. These quantum jumps between levels run through a cycle becoming less probable over time resulting in a power law blinking phenomena[99].

For fluorescent proteins such as sfGFP, it is believed that protonation of the chromophore facilitates its fluorescence[103]. Protons are shuttled along water channels to the chromophore when activated by photo-excitation[104]. One of these water channels connects the chromophore to the external environment via the Ser205 residue, close to our AzPhe situated at the 204 position in the short axis variant[104][105]. The position of this molecule could be key to describing differences in fluorescent properties between the 204 and 132 sfGFP variants.

By recording intensities from these molecular light emitters at certain time intervals, we have been able to gather information on these processes to further our understanding on this protein-CNT electronic interaction.

5.3.1 Imaging of sfGFP on sSWNTs

Before attempting to understand how the fluorescent properties of sfGFP varied upon CNT functionalisation, we needed to perform a few preliminary studies. We needed to first find out if the UV exposure in the cross-linking reaction had any effect on the fluorescence of the proteins. Secondly, we needed to see if CNTs were visible in this "blue" range of the spectrum under TIRF. Finally, we needed to check if the attachment of proteins would act as fluorescent markers for the CNTs.

An important experiment to provide evidence of protein activity, prior to CNT modification was to image an area before and after the addition of proteins, and co-localising these images with AFM studies.

In this section, we discuss the results of these preliminary studies, allowing us to image sfGFP bound to CNTs using TIRFM.

5.3.1.1 Experimental Methods

In order for TIRFM to work, glass coverslips of a particular thickness must be used. The thickness is important as the incident light has to pass though a certain critical angle in order for total internal reflection to take place. For these experiments, the thickness of the coverslips were 0.13 to 0.16mm. These coverslips were first cleaned in an oxygen plasma to ensure all fluorescent contaminants are removed from the surface. This subsequently leaves the surface extremely hydrophilic, meaning any solution deposited on the surface will quickly disperse and spread over the cover slip.

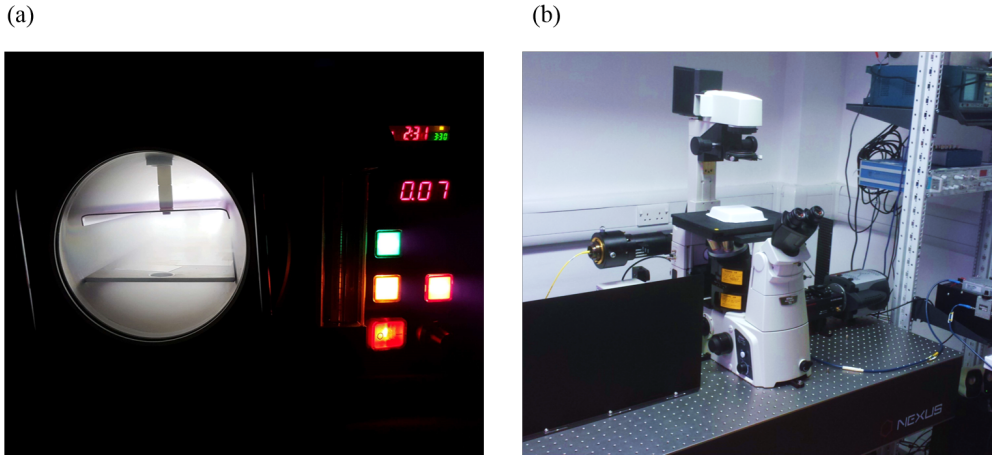

FIGURE 5.11: (a) Photo of coverslips being plasma treated in a plasma reactor. (b) Picture of the TIRF microscope.

As the spatial resolution of TIRFM is inferior to that of AFM, the concentration of SWNTs in the solution was reduced to 0.1mg/ml as the higher concentrations make it more difficult to distinguish between individual SWNTs. The surfaces of the coverslips were coated in sSWNT solutions and left for 10 minutes before

rinsing in a flow of de-ionised water. This ensured that the solutions did not have time to dry on the surface which can leave a drying pattern of potentially fluorescent contaminant material. The coverslips were then rinsed in ethanol for 60 minutes to remove the surfactant and residual contaminants from the surface.

Fluorescent micrographs and associated single molecule data were gathered using a Nikon Ti-U inverted microscope and Andor iXon ultra 897 EMCCD camera. Illumination was provided by a Ventus 473nm gallium(III) nitride (GaN) laser, used to excite sfGFP, with a power output of 100mW (laser power at the microscope stage averaged at 20mW). Laser coupling into the microscope was achieved via a custom built optical circuit followed by a single mode fibre-optic launch. The total internal reflection illumination angle was generated using a combination of fibre-optic micro-positioning and a high numerical aperture TIRF objective. The excitation and fluorescence emission wavelengths were separated using a dichroic mirror with a 488nm edge. Emitted wavelengths were further filtered using a 500nm edge long pass filter and a 525nm band pass filter. Acquisitions were controlled using the Andor Solis software package. Frame exposure times were set to 60ms and an electron-multiplying (EM) gain of 250 was used.

The proteins used for this investigation were the 132AzPhe and 204AzPhe variants of sfGFP as they have different distances between the fluorophore and the linker position. These were imaged on clean coverslips at 1-10pM in solution on order to obtain single molecule data of unbound sfGFP. For the sSWNT samples, they were imaged before protein modification, then functionalised with protein ranging from 10nM to 1μM with a 5 minute exposure to 305nm UV light at 18Wm^{-2}. Samples were rinsed with a flow of de-ionised water and dried before imaging. This allowed us to determine if the proteins maintained their fluorescent properties in ambient conditions. Further experiments regarding studies of protein-CNT systems in solution will be discussed in section 5.3.2.

Once the samples were analysed with TIRFM, we were able to image them with tapping mode AFM. Here we co-localised the TIRFM images using the marker made using the scalpel blade, and imaged various areas to match AFM to TIRFM.

All TIRFM experiments were done in collaboration with Dr. David Jamieson and Dr. Oliver Castell in the School of Pharmacy and Pharmaceutical Sciences in Cardiff University.

5.3.1.2 Results and Discussion

When dealing with fluorescent molecules, we must ensure limited exposure to light before investigating them with TIRFM. However, the attachment of proteins with the azide moiety to CNTs is done using prolonged exposure to UV light. Therefore, as a preliminary experiment, the effect of UV exposure on the fluorescence and potential photo bleaching was investigated and the results are shown in figure 5.12.

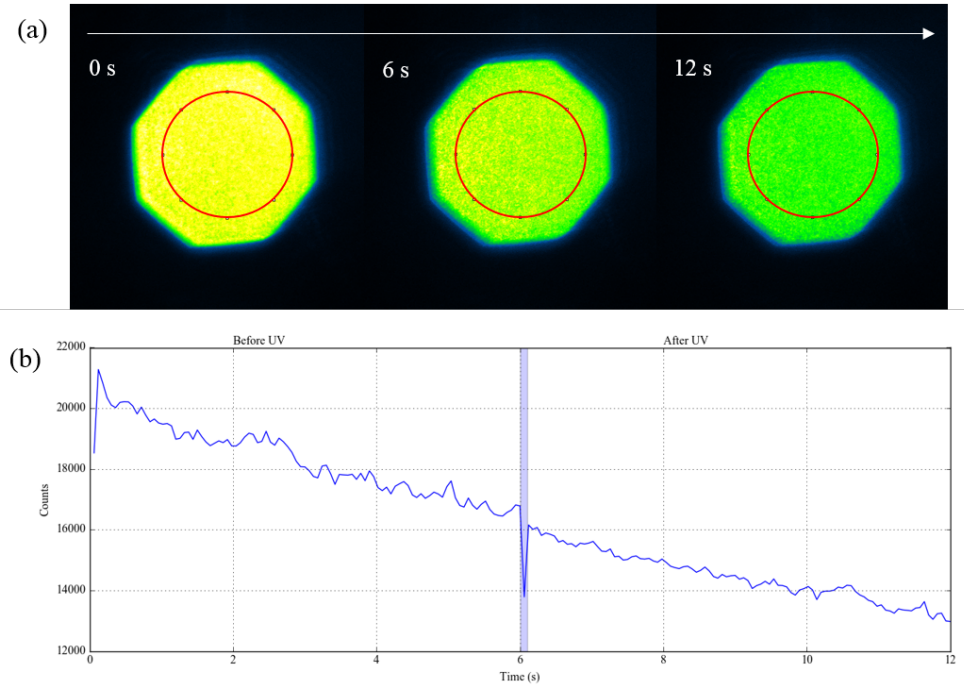

FIGURE 5.12: Photobleaching test of a dense array of sfGFP-204AzPhe with UV intermediate test. (a) TIRFM images displaying the relative intensities of the same area over time while being exposed to 473nm light. (b) Plot of intensity over time. At 6 seconds, TIRF is tuned off and a 305nm LED illuminates the sample for 5 minutes before TIRF is turned back on and records for a further 6 seconds. The dip in the midpoint of the plot comes from the aperture shutter opening and closing between measurements.

In this experiment, 10μL of 100nM sfGFP-204AzPhe was drop cast onto a plasma treated coverslip and imaged using a 30mW laser for 6 seconds. After this point the shutter to the laser was closed and the sample was illuminated with a 305nm

LED at 18Wm^{-2} for 5 minutes. These were the same conditions used for all the protein attachment experiments used for TIRFM. Once the UV LED was turned off, the same area was imaged using TIRFM for a further 6 seconds. As figure 5.12 shows, there is a linear decay in the intensity as a result of photo bleaching with no significant bleaching caused by the UV illumination step. This is a strong indication that the UV exposure has little to no effect on the fluorescent properties of sfGFP, which was expected as the photo bleaching and emission properties of the fluorophore depend on its specific excitation wavelength. As the excitation wavelength of sfGFP is about 475nm, the 305nm LED used for azide attachment should not have any significant effect on the fluorescent properties of the protein.

Another important prerequisite for these experiments was to image unmodified SWNTs in order to determine if they fluoresce under TIRFM with the same conditions used for sfGFP. We know from optical studies done on sSWNTs, that their excitation and emission wavelengths are longer than the wavelength of the laser used to illuminate the samples and the wavelength of the collected fluorescence data. Therefore, sSWNTs appear invisible under these TIRFM conditions. As the coverslips are plasma treated before CNT deposition, they are extremely hydrophilic. CNTs have a hydrophobic surface making them highly susceptible to interactions with non-polar contaminants which could make them show up under TIRF conditions. Therefore, more care was taken when preparing samples for TIRFM and time between preparation and experiment was made as short as possible to reduce the risk of contamination. To assess the possible fluorescence of sSWNTs, we marked an area of a sSWNT coated coverslip and imaged it before and after sfGFP modification, and studied the intensity of photons given off. These results are shown in figure 5.13.

The sSWNT samples were modified with 100nM sfGFP-204AzPhe under 305nm light for 5 minutes, followed by a rinse in a flow of de-ionised water and dried in air. The minimum counts for before and after the addition of sfGFP were very similar, giving a strong indication of comparable background intensities. The maximum and mean intensities in this region are significantly higher after protein modification giving us evidence of post modification protein activity as well as

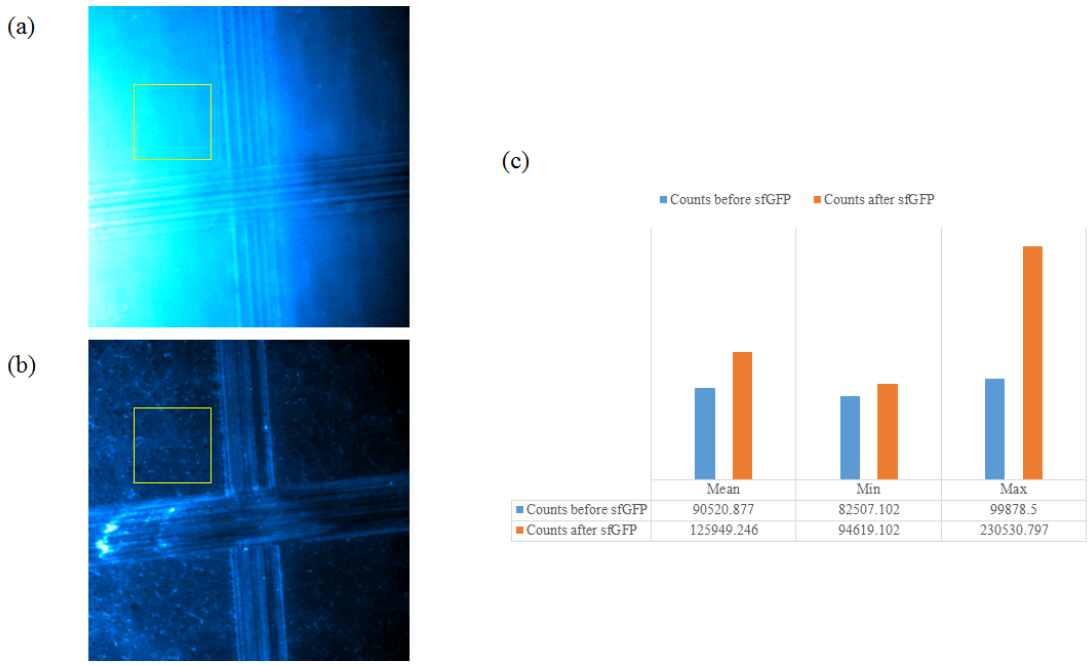

FIGURE 5.13: TIRFM images of a coverslip coated with sSWNTs. The cross is made using a scalpel blade post-sSWNT deposition as a marker for repeat analysis of the same area for (a) before the addition of sfGFP-204AzPhe and (b) after the addition of 100nM sfGFP-204AzPhe followed by induced photo cross-linking of the proteins to the sSWNTs. The variations in contrast between the two images is quantified by selecting an area within the yellow squares and measuring the number of counts recorded.(c) Differences in the mean, minimum and maximum counts between the same areas before and after the addition of sfGFP-204AzPhe.

successful attachment to CNTs. From the images, it is clear that after protein modification, fibre like structures have become visible on the surface as a result of protein-CNT hybrid structures being formed.

By taking a closer look into one of the corners of the marker, as shown in figure 5.14, you can see defined tube-like structures with varying coverage of sfGFP. There are still areas which look like they may contain contaminants, showing a dull fluorescent background in some areas. However, the rinsing procedure seems to have effectively removed the majority of unbound protein with most of the fluorescence coming from the hybrid structures. Further evidence of protein functionalisation and activity can be seen in figure 5.15, where we have been able to co-localise there TIRFM images with AFM studies.

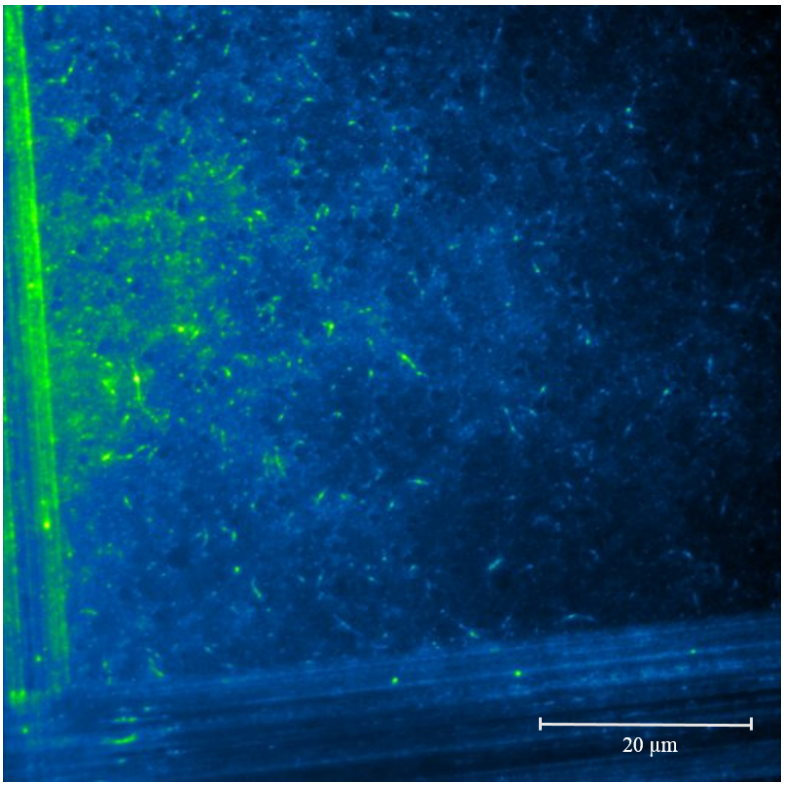

FIGURE 5.14: TIRFM image of marked area with sSWNTs decorated with sfGFP-204AzPhe molecules in air.

From these images we can confirm that these fluorescent fibres are sSWNTs decorated with sfGFP, with the higher density of proteins showing up much brighter in TIRFM. The AFM studies show very little unbound proteins around the CNTs meaning the additional background fluorescence must be coming from alternative contamination. One thing to note is the overall intensity of photons from low density areas of sfGFP is quite low and can be comparable to the background fluorescence. This low level of fluorescence is not expected from GFP, which suggests there is a large amount of fluorescent quenching between the proteins and the CNTs. In order to get a better idea of this phenomena and the mechanism causing this fluorescence drop, we decided to study the fluorescent properties of single molecule, unbound sfGFP (204 and 132AzPhe variants) and compare this with CNT bound protein.

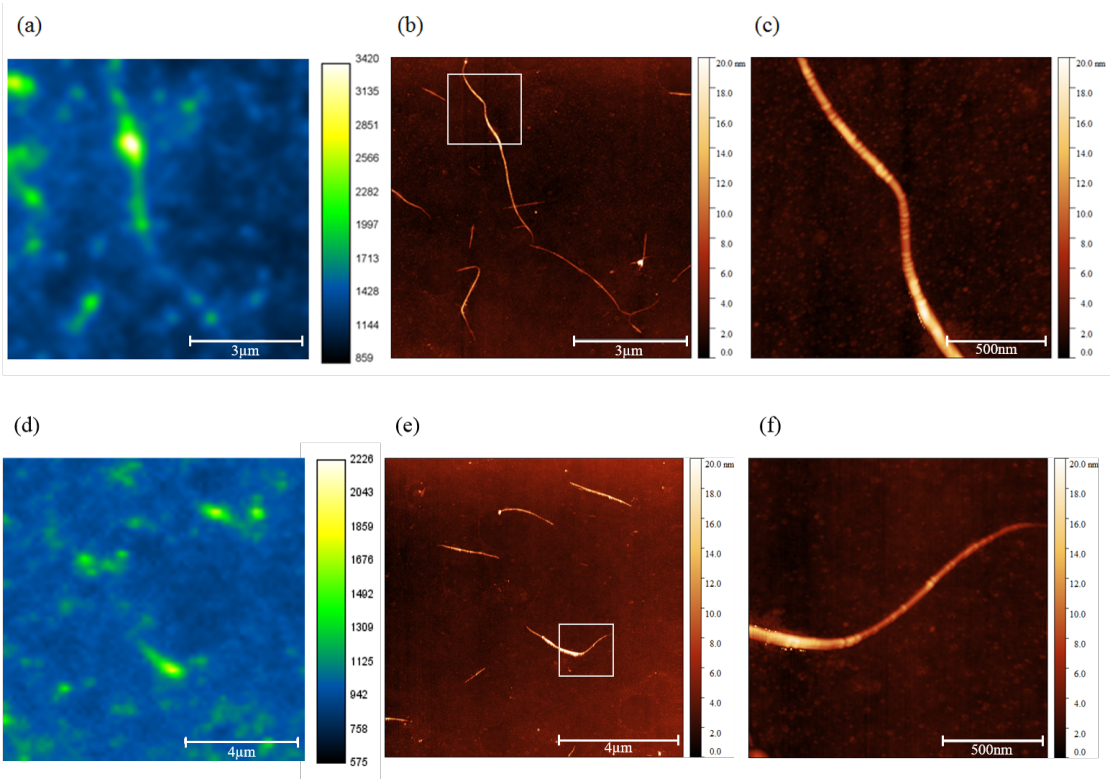

FIGURE 5.15: sSWNTs decorated with sfGFP-204AzPhe molecules. (a) and (d) TIRFM image showing lighter areas where there is a higher count of fluorescence compared with the darker background. This fluorescence comes from the inherent fluorescent properties of sfGFP. (b) and (e) AFM images showing topography of the area studied using TIRFM. The white boxes show the areas imaged in (c) and (f) respectably. The elongated structures are the sSWNTs with proteins along them. The proteins can be seen as small oval structures bound along the surface of the CNTs.

5.3.2 Photophysics of sfGFP on sSWNTs

With the system and experimental setup established, we turned our attention studying how the fluorescent intensity of sfGFP changes over time. By studying this intensity variation over time, we have gathered a wealth of information regarding photobleaching and blinking fluorophores, as well as the effect of the position of the protein's linker molecule on these fluorescent properties. This allows us to postulate possible mechanisms which govern these phenomena and the physical interactions between the proteins and the CNTs.

5.3.2.1 Experimental Methods

The proteins used for this investigation were the 132AzPhe and 204AzPhe variants of sfGFP as they have different distances between the fluorophore and the linker position. Single molecule data was acquired by drop casting 1μl of 1nM sfGFP solution onto plasma-treated coverslips. The concentration needed to be low enough to allow us to distinguish between individual protein molecules when analysing fluorescent characteristics.

For the data acquired from proteins bound to sSWNT to be compared with single molecule data, we needed to maintain the same imaging conditions. This meant all the images were to be taken in solution in order to study proteins in the same environmental conditions. Furthermore, if we were to change from imaging in solution to imaging in air, we would change the refractive index above the coverslip which would strongly affect the observed evanescent wave. Therefore, all protein-sSWNT samples were prepared by depositing protein solution onto the sSWNT coated coverslips, illuminating with 305nm UV light, followed by a solution dilution stage. This stage was done by applying a flow of de-ionised water over the sample, while the coverslip was resting on a 3D printed TIRFM stage with a reservoir channel as seen in figure 5.16. The excess solution would drain into the channel, allowing us to rinse the protein solution away, whilst maintaining a water solution on top of the coverslip.

5.3.2.2 Results and Discussion

Figures 5.17 and 5.18 shows time averaged TIRFM images of sfGFP-132AzPhe and sfGFP-204AzPhe respectively with examples of fluorescence intensity traces over a sequence of 60ms frames.

These intensity traces share very similar properties between each protein sample in terms of photobleaching times. Here we can see evidence of rapidly blinking fluorophores which switch between a fluorescent state of high intensity, to that of low intensity near the background level. One difference we note from these traces

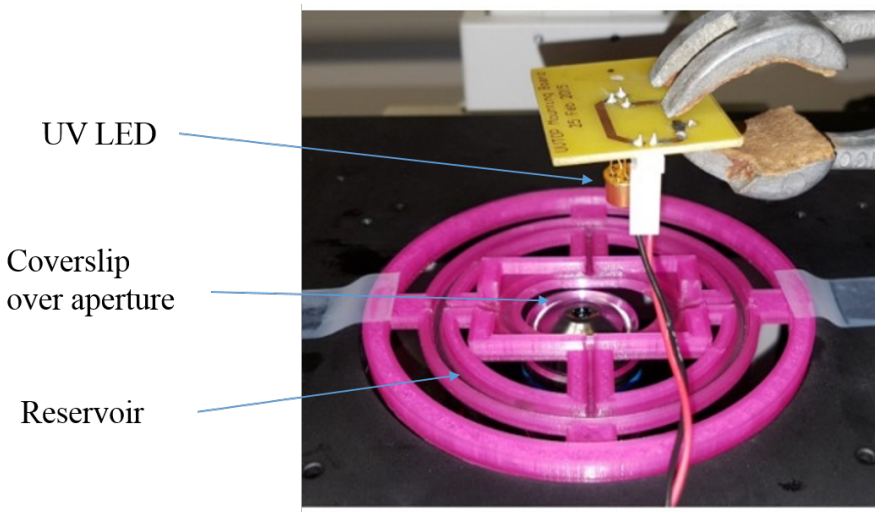

FIGURE 5.16: TIRFM stage for protein-CNT imaging. The UV LED is positioned above the coverslip and used for protein photo cross-linking in between TIRFM measurements. The 3D printed stage allows liquid to drain into a surrounding reservoir.

is the different fluorescent blinking rates before photobleaching. sfGFP-132AzPhe undergoes more "on/off" cycles in quick succession whereas the 204 variant tends to stay in its "on" state for much longer. This could be a consequence of having the linker molecule next to a water channel, close to the chromophore in the 204 variant as I briefly mentioned earlier in this chapter. The 204AzPhe variant is also significantly brighter than its counterpart. It is unclear at the moment what causes these differences.

Photobleaching occurs at the point when the fluorescence intensity drops suddenly to background level without recovery. For individual sfGFP molecules, the time it takes to photo-bleach is very short with the majority of the proteins bleached after about 20 seconds as we can see in the overall average intensity plots over time shown in Figure 5.19.

The wavy background seen in the TIRFM images is an artefact of the CCD and is only observed when averaging all frames and applying a low intensity scale. To acquire these decay curves, intensity data were selected from the brightest points which displayed single molecule characteristics. Pixels were selected based on a threshold intensity, chosen based on the average fluorescence of the brightest pixels, filtering out low-level fluorophores from the fluorescence decay calculation.

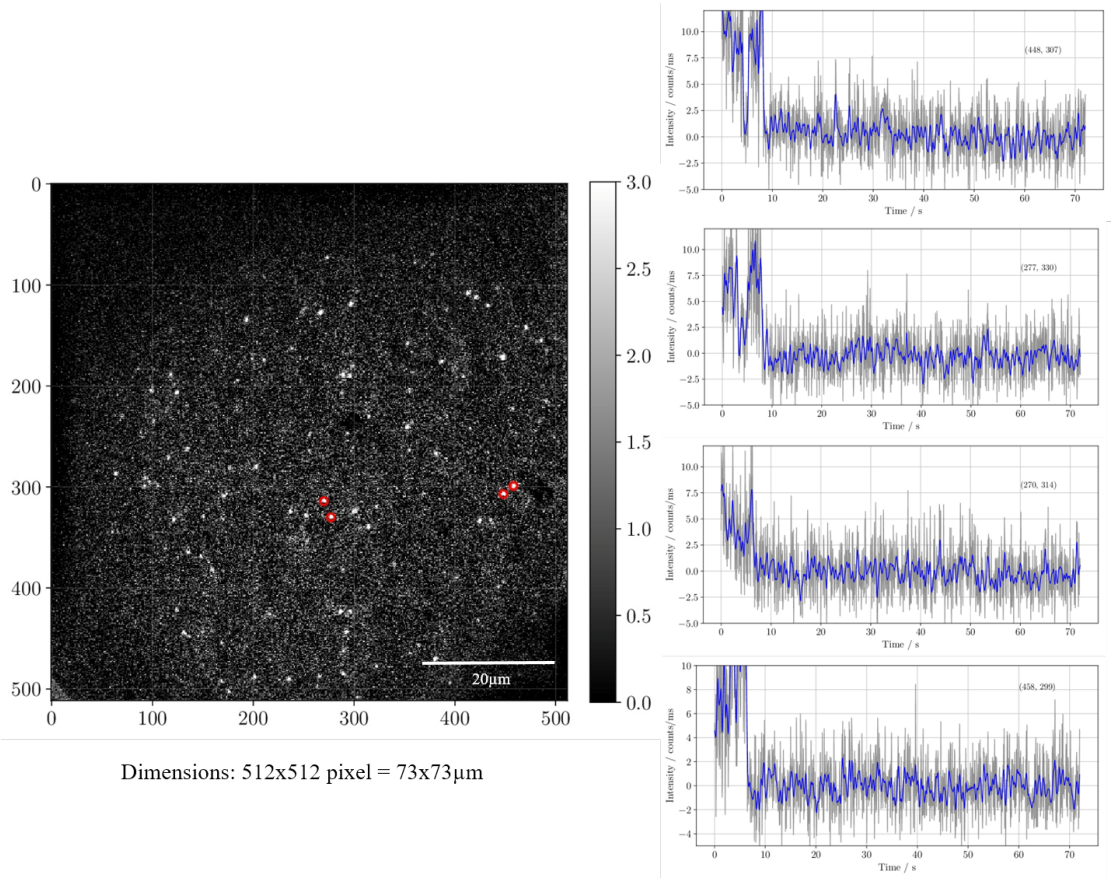

FIGURE 5.17: TIRFM image for the 100th frame of unbound sfGFP-132AzPhe in buffer solution. The red circles on the image show selected single molecules, from which the intensity/time traces on the right were taken. A Gaussian filter was applied to individual pixels, to smooth noisy data. This is shown as a blue line over the observed data shown in grey.

By collecting the average fluorescent intensity over time for the brightest 100 molecules, we were able to form decay curves shown in Figure 5.19, from which we applied an exponential line-fit to and solved for the time constant τ, using the following equation:

$$N(t) = N_0 e^{-t/\tau} \tag{5.1}$$

where *N(t)* is the average number of counts per pixel at time t, which decays exponentially from it's initial number of counts at start of the trace N_0. The fluorescence decays with respect to it's time constant τ, which is commonly known as the mean lifetime. We use this value to determine the average lifetime of the sfGFP fluorescence before photobleaching.

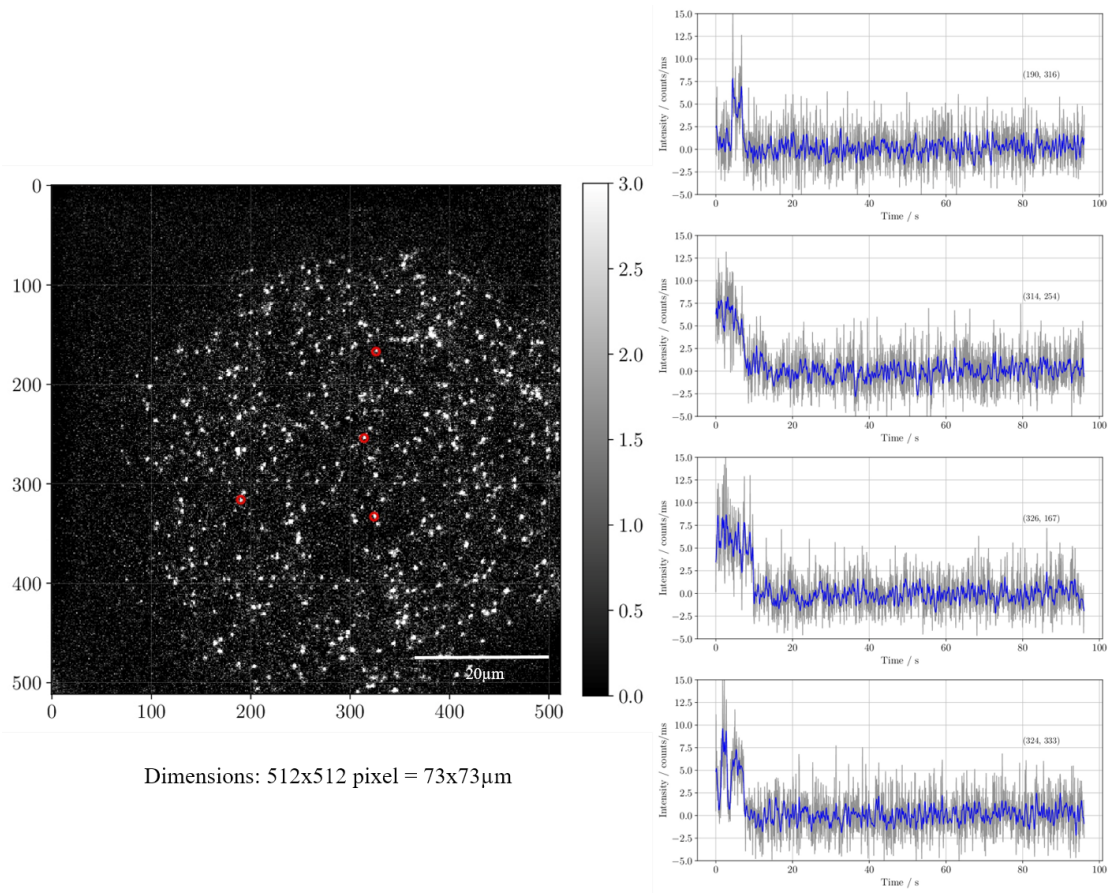

FIGURE 5.18: TIRFM image for the 100th frame of unbound sfGFP-204AzPhe in buffer solution. The red circles on the image show selected single molecules, from which the intensity/time traces on the right were taken. A Gaussian filter was applied to individual pixels, to smooth noisy data. This is shown as a blue line over the observed data shown in grey.

The mean lifetimes for sfGFP-132AzPhe and sfGFP-204AzPhe are (3.07±0.02)s and (3.67±0.01)s respectively. This is an interesting result as it means sfGFP-204AzPhe remains fluorescent for longer on average than the 132 variant. They are both as bright as each other as we can see from their initial intensities which suggests that the 204 variant is more stable under excitation.

We can now compare these results with data acquired from sfGFP variants bound to sSWNTs in solution.

Figures 5.21 and 5.22 show time averaged images of sfGFP-132AzPhe on sSWNTs and sfGFP-204AzPhe on sSWNTs respectively, with examples of individual time traces obtained from single fluorophores. The first thing we notice when comparing these traces to the earlier ones for unbound proteins, is the large drop in intensity

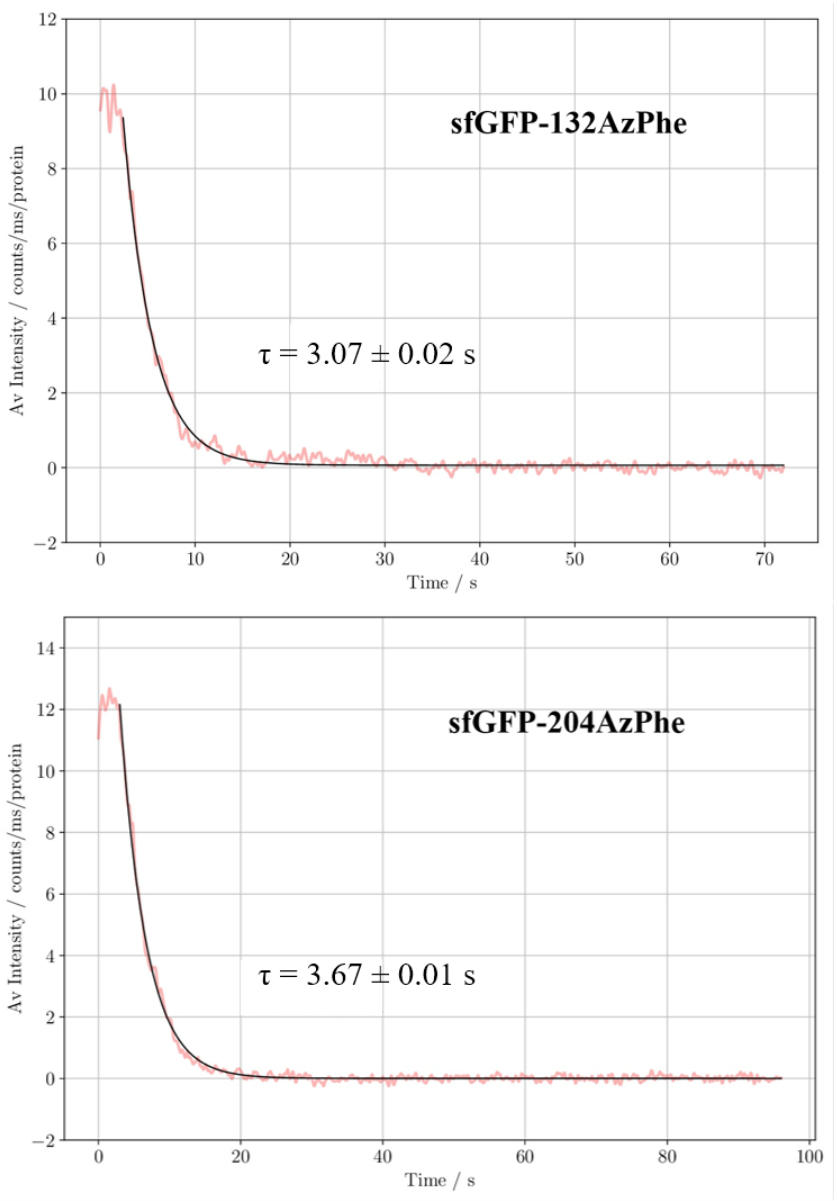

FIGURE 5.19: Fluorescent intensity decay curves for sfGFP-132AzPhe and sfGFP-204AzPhe. These were made from the intensity/time traces of 100 single molecules and fitted to an exponential to determine the decay constant.

seen for these individual proteins attached to CNTs. This makes it hard to distinguish between an on state and the background noise, also making it extremely difficult to analyse the blinking behaviour of the individual fluorophores. Overall, the fluorophores seen in these images remain in their "on" state throughout most of the time exposed in TIRF for both protein variants. This is a key observation which could relate to the CNT's electronic interaction with each protein molecule, though it is difficult to say how they are interacting. There are some short lived

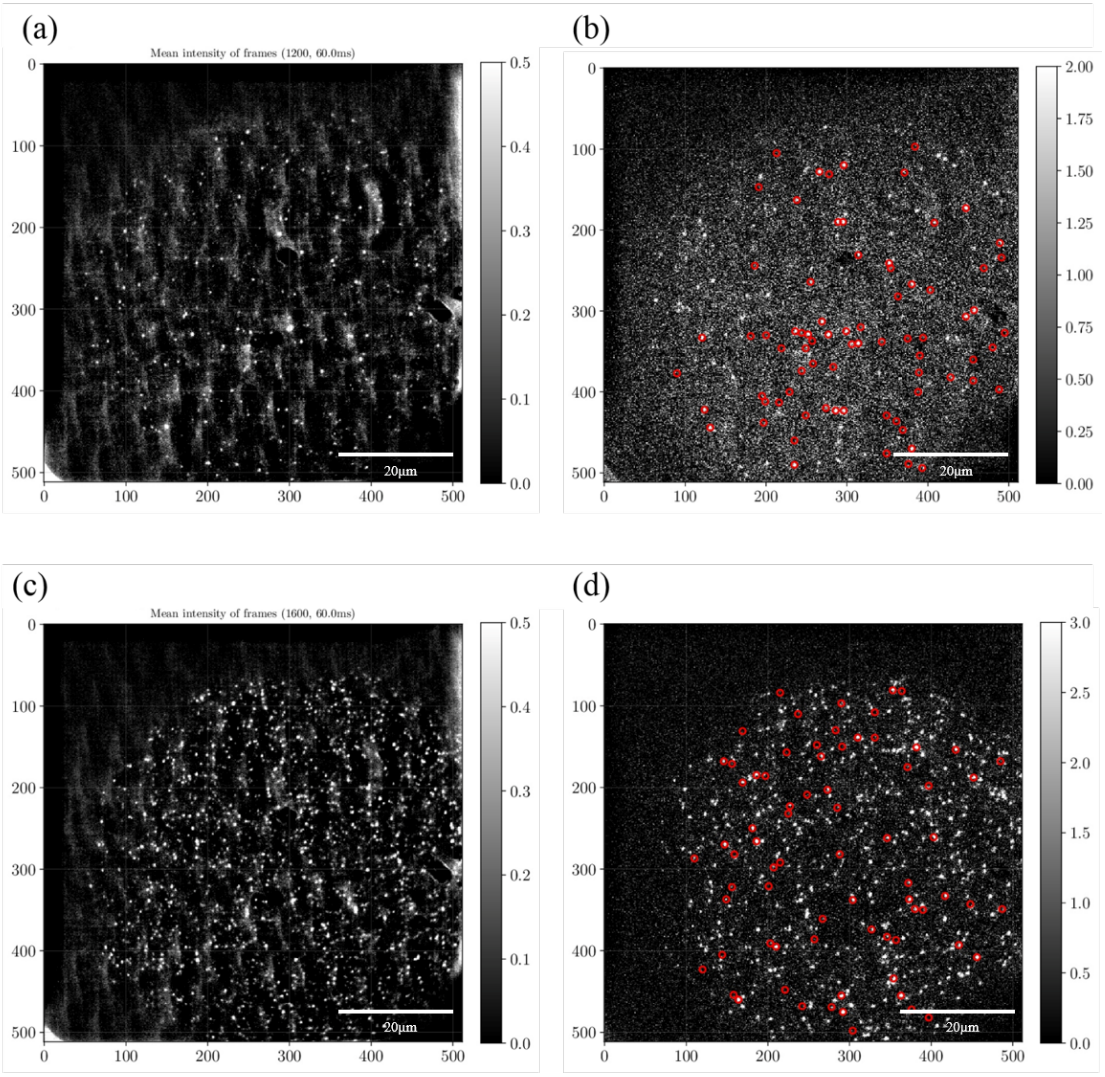

FIGURE 5.20: TIRFM images for (a)time averaged sfGFP-132AzPhe with (b) the 100 selected bright molecules in red circles, and (c)time averaged sfGFP-204AzPhe with (d) the 100 selected bright molecules in red circles.

fluorescent molecules of a higher overall fluorescent intensity than the the majority of the molecules in the image. These could be non-specifically bound proteins as they still have lower intensities than that of unbound proteins, but are more prone to photobleaching than the other "specifically bound" proteins.

When comparing the time averaged images of sfGFP-132AzPhe and sfGFP-204AzPhe, we can see that the 204 variant has more visible protein coverage of CNTs making more visible in the field of view than the 132 variant. Post-TIRFM analysis of these coverslips using AFM showed us that both samples had similar densities of

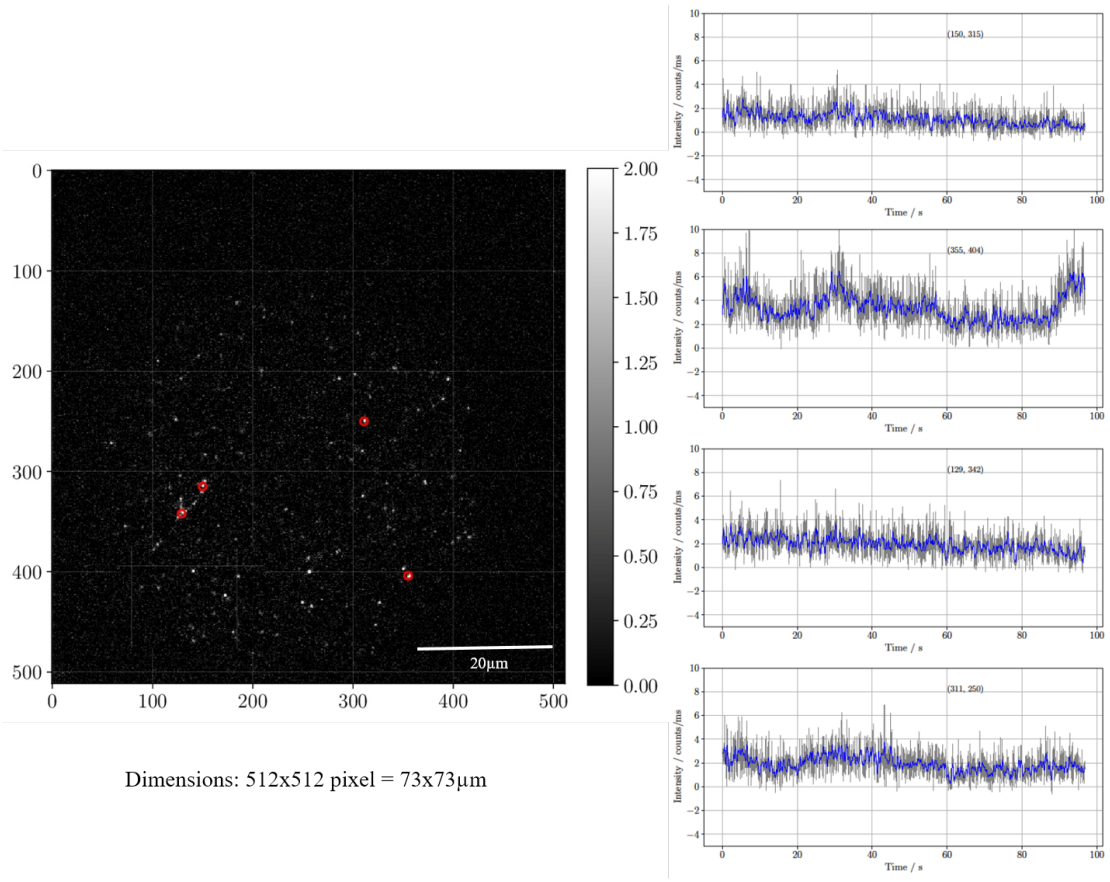

FIGURE 5.21: Time averaged TIRFM image sfGFP-132AzPhe bound to sS-WNTs in solution. The red circles on the image show selected single molecules, from which the intensity/time traces on the right were taken. A Gaussian filter was applied to individual pixels, to smooth noisy data. This is shown as a blue line over the observed data shown in grey.

CNTs bound to them, but lower numbers of proteins for the sfGFP-132AzPhe bound to the CNTs. This was an observation we noticed in previous experiments and we believe this 132 variant is less prone to cross-linking with the side-walls of CNTs than the 204 variant. A possible explanation to this is the tendency for the azide group to react with the surrounding solvent solution. As the 132AzPhe linker molecule is situated on the end of a loop in the protein structure, it has a low density of neighbouring residues, leaving it exposed to the surrounding solvent (water/ buffer). The 204AzPhe group is situated on the side of the β-barrel, and is therefore only partially exposed to the surrounding solvent. When the azide group is photo-activated in UV light, it will look for an electron rich environment by which to react with. Therefore, if the azide is more exposed to a solvent, it will tend to react with that solvent under UV exposure, thus limiting its possibility of

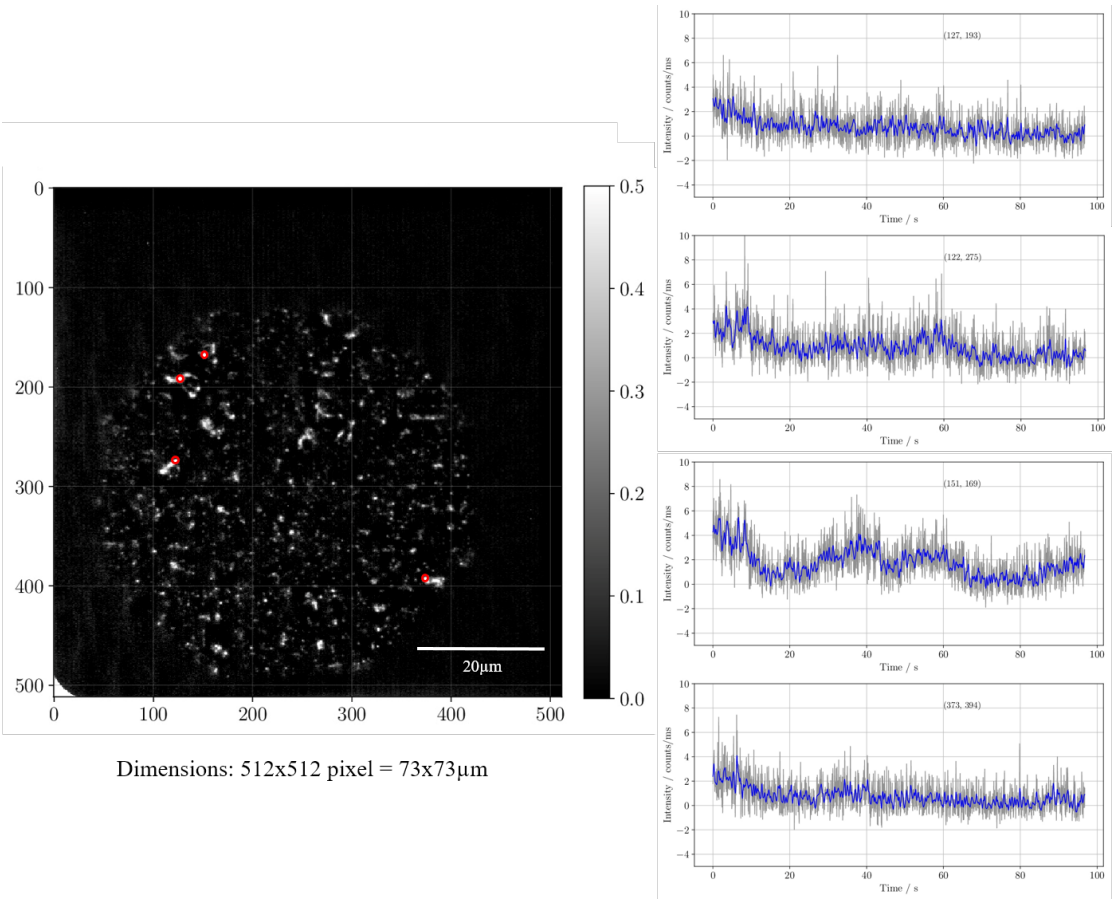

FIGURE 5.22: Time averaged TIRFM image sfGFP-204AzPhe bound to sSWNTs in solution. The red circles on the image show selected single molecules, from which the intensity/time traces on the right were taken. A Gaussian filter was applied to individual pixels, to smooth noisy data. This is shown as a blue line over the observed data shown in grey.

binding to CNTs.

Figures 5.23 and 5.24 show the average decays of selected fluorescent molecules on SWNTs for sfGFP-132AzPhe and sfGFP-204AzPhe respectively.

As expected from the individual time traces, the intensities are far lower on average for proteins attached to SWNTs than on their own. This has allowed them to emit photons for a much longer period of time. We were not able to fully photo-bleach these fluorophores within the acquisition time with the decay curves not showing typical exponential decays. Instead, we see much noisier fluorescent behaviour over time (red lines) when compared with the background (black lines). In some cases, we see some recovery of the fluorescence, shown as an increase in average intensity over time. These increases can be attributed to prolonged dark states

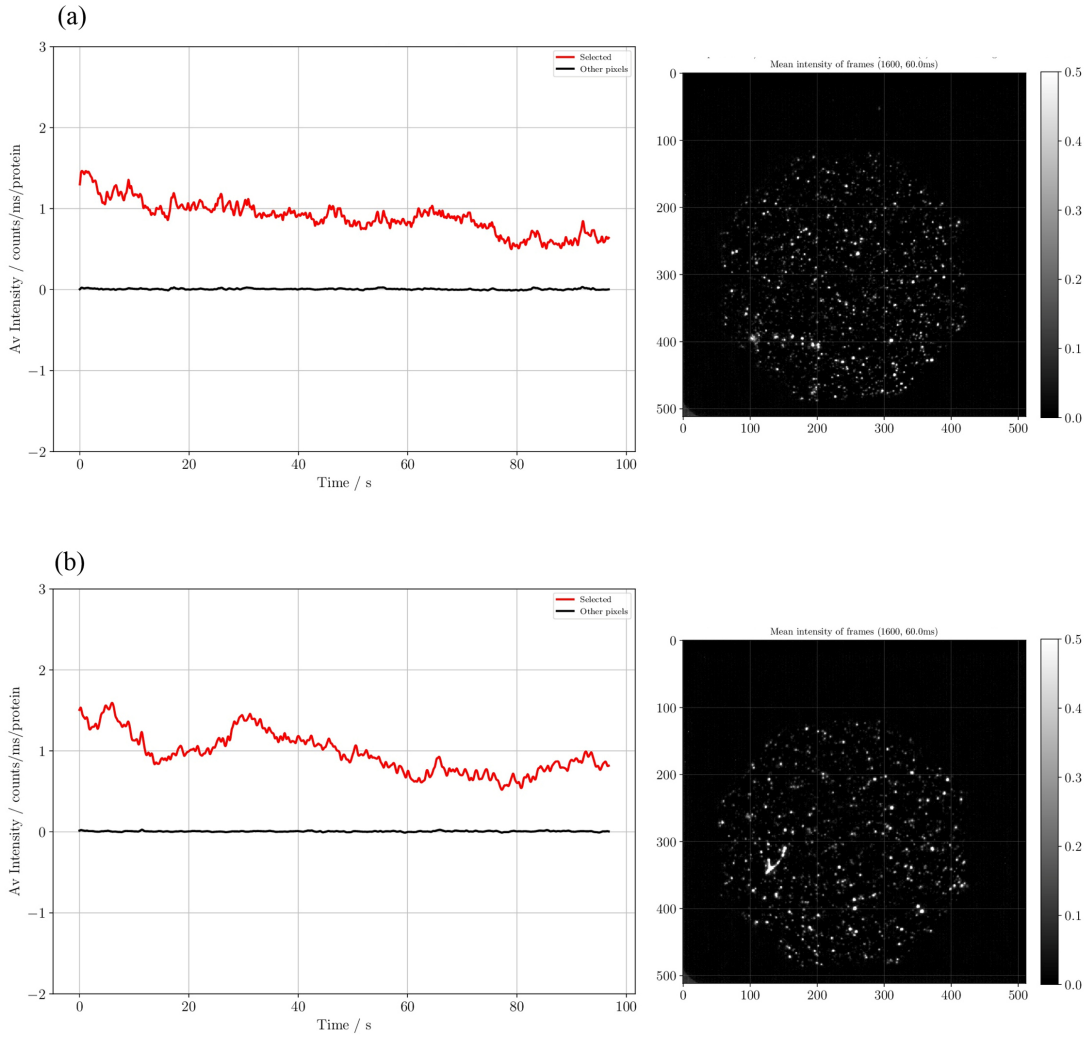

FIGURE 5.23: Fluorescent decays of sfGFP-132AzPhe on sSWNTs 2 different regions (a and b) with their respective time averaged TIRFM images. The red lines in the decay plots depict the fluorescent data gathered from the proteins bound to CNTs with the black line showing the background fluorescence.

where the fluorophore switches to a "off" state for a longer time than usual before returning to an "on" state. Interestingly, this phenomena appears to occur around the same time on average for the sfGFP-204AzPhe sample in different areas. This occurs at around 20 to 30 seconds before it returns to a steady decay. A similar recovery is seen in figure 5.23 (b).

Another interesting finding is that although the starting intensities of each protein variant bound to CNTs are around that same value, as seen with the unbound protein data, the 204AzPhe variant appears to decay to near zero much faster than

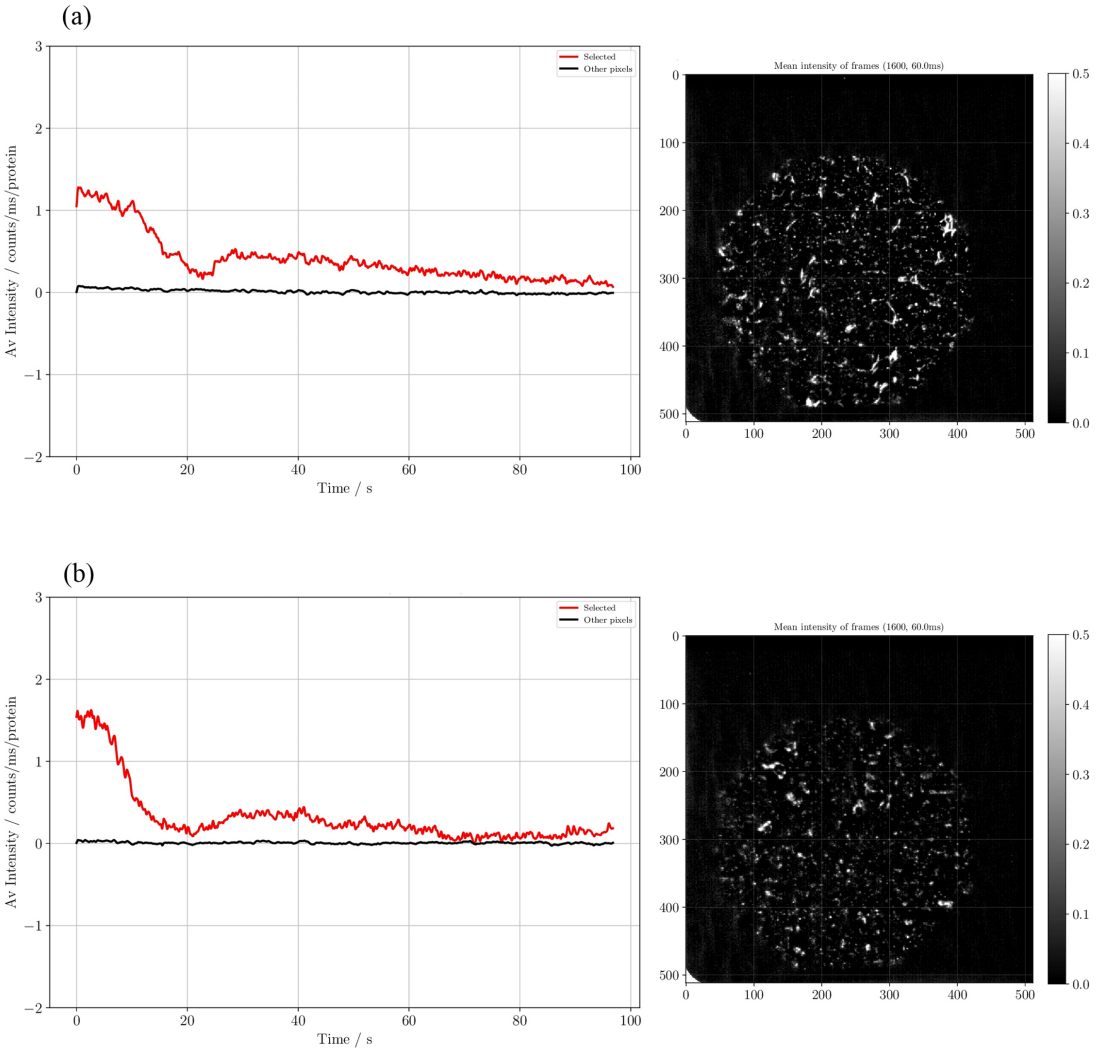

FIGURE 5.24: Fluorescent decays of sfGFP-204AzPhe on sSWNTs 2 different regions (a and b) with their respective time averaged TIRFM images.The red lines in the decay plots depict the fluorescent data gathered from the proteins bound to CNTs with the black line showing the background fluorescence.

that of the 132AzPhe variant. For the unbound protein data, the 132AzPhe variant had the shorter decay time which must mean the position of this linker molecule on the protein has a very strong influence on the protein-CNT interaction. One possibility is that with the distance between the chromophore and the CNT has a strong influence on the electronic interaction between the structures. This would reduce the distance for electron transfer, which could increase the possibility of electron hopping or tunnelling, upon photo-excitation. In the previous chapter, we briefly discussed possible charge trapping sites at the point of a CNT defect. This could act to quench the electrons from the protein, reducing the number

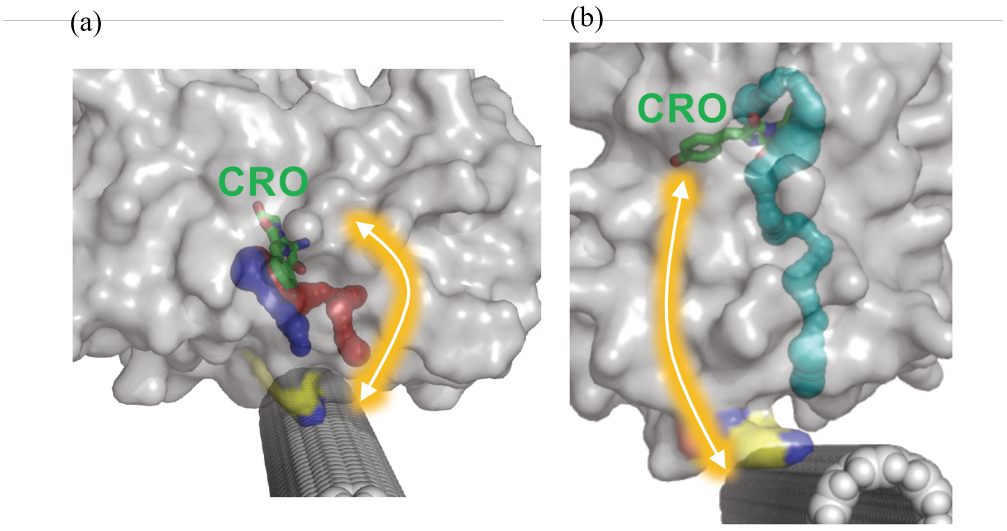

FIGURE 5.25: Models of water channels between the chromophore and the CNT, calculated in CAVER. (a) Tunnels between the CNT and sfGFP-204AzPhe, shown in blue and red. (b) Tunnel between the CNT and sfGFP-132AzPhe, shown in cyan. All CAVER calculations were performed by Harley Worthy of the School of Biosciences, Cardiff University.

of electronic cycles over a period of time. An alternative explanation is that the protein-CNT interaction is blocking the water channel at the 204 position, preventing protonation of the chromophore[104], thus reducing the rate of photo-cycles and therefore, reduce the fluorescence. However, this does pose the question as to why the starting fluorescence of the 132AzPhe variant is the same as the 204AzPhe variant. Figure 5.25 shows the possible water channels between the chromophore of the protein and the CNT for both variants of sfGFP, calculated by Harley Worthy (School of Biosciences, Cardiff University) in molecular modelling program, CAVER. Given the presence of these channels, this may indicate possible routes of communication between the chromophore and the CNT. These proton channels may play a part in the charge transfer mechanism with the 204 variant having a much shorter route to couple with the CNT than the 132 variant.

It isn't completely clear what is the mechanism of electronic interaction between sfGFP and CNTs, but it has produced some interesting results. We have concluded that the position of the linker molecule on the protein is not only important of binding, but also has a large effect on how the protein interacts electronically with the CNT.

5.4 Summary

In this chapter, we've presented data suggesting effecting covalent binding of proteins to CNTs with further evidence to show an electronic interaction between the two structures. Raman spectroscopy was used to confirm covalent cross linking of various proteins to carbon nanotubes by observing shifts in their Raman spectra compared with that of pristine CNTs. Using TIRFM, we have been able to show protein activity post deposition, both in solution and in ambient conditions. This was a key experiment to determine that this method of covalent cross-linking to CNTs via pheyl-azide chemistry was viable to form protein-CNT hybrid structures.

The evidence gathered from the Raman plots shows a strong indication of covalent binding between the AzPhe moiety in the protein and both metallic and semiconducting SWNTs. This complements the results from the AFM imaging and resistance plots, with clear evidence of control over the method of protein-SWNT cross linking.

Here, we have concluded that the increase in peak frequency and FWHM of the D and G′ peaks is evidence of sp^3 carbon forming with the presence of an azide group.

In the second half of this chapter, we discussed the use of TIRFM to analyse protein-CNT interactions by using sfGFP as a fluorescent marker. The use of TIRFM also allowed us to see fluorescent proteins decorating CNTs as well as studying their dynamic photo-physical properties. Attachment and post-attachment activity was confirmed by co-localising TIRFM images with AFM. Here, higher densities of proteins showed up much brighter under TIRFM, with much of the fluorescence being quenched by the CNT.

We conclude that covalent attachment to CNTs greatly reduces the fluorescence of the proteins giving evidence of a clear interaction. We also concluded that the position of the linker molecule can greatly affect the fluorescent properties of the protein with the 204AzPhe variant (closer to the chromophore), had a greater decay rate than the 132AzPhe variant when attached to the CNTs. Though distance

between the chromophore and the CNT does not explain all the effects seen; it does highlight the importance of position of the protein for potential coupling and communication along intramolecular networks within the biomolecule.

Chapter 6

Conclusions

The research presented in this thesis was driven by our recent advances in single molecule electrical studies with protein structures. This work introduced a level of control over the deposition and orientation of protein structures when bound to gold[106][31]. The main idea was to use this novel method of biomolecular control to build a sensor platform that enables us to develop an understanding of bioelectronics at the nanoscale and the electron transfer characteristics of individual proteins. To do this, we used CNTs as the interface material allowing us to have control of our structures at the nanoscale and it in turn, provided us with a reactive, compatible surface upon which to cross link individual proteins.

The main goals of this study were to establish the basis upon which to build a sensor device and understand the mechanism from which proteins interact with the carbon surface. To do this, we have employed numerous techniques and investigated multiple proteins in order to develop a broader picture to explain the interactions taking place on the nanoscale.

To build a platform from which to study electronic interactions between CNTs and proteins, we needed to produce CNT based electrical devices and establish an effective and reproducible method of attaching proteins to the CNT sidewalls. The devices were successfully created by bridging SWNTs, separated between sSWNTs and mSWNTs, across gold electrodes via DEP. This method aligned the CNTs and

proved to be a reliable way of bridging neighbouring electrodes with a high success rate.

The next step was establishing nanoscale control over protein deposition and effective cross linking to CNTs. This was achieved by incorporating the uAA, AzPhe into the sequence which formed the protein structures. This provided a method of covalently cross linking the proteins across the sp^2 C=C double bond forming a single sp^3 defect site per protein attached. By pre-defining the position of the linker molecule in the protein structure, we were able to define the point at which the protein interacts with the CNT surface. This has been demonstrated with sfGFP and cyt b_{562} for linker molecules in orthogonal positions and the heights of these proteins when bound to CNTs were analysed using AFM. We found that the long axis and short axis variants of sfGFP were measured to extend (3.1±0.4)nm and (2.4±0.5)nm above the CNTs respectively which was good evidence of defined orientation upon chemical linking. This result was also demonstrated with the long axis and short axis variant of cyt b_{562}, with heights of (3.1±0.4)nm and (2.8±0.4)nm respectively.

These experiments also showed some evidence that the proteins have a tendency to align themselves in a specific orientation dependent on the orientation of the CNT. This was observed with both the short axis variants of sfGFP, which aligned perpendicular to the length of the CNT, and cyt b_{562} which aligned parallel to the length of the CNT. The same phenomena was observed with the pyrene variant of cyt b_{562} which suggested it was an inherent property of the protein. A likely explanation is that the alignment comes from the hydrogen bond network within the proteins, causing a small dipole moment within the biomolecule which aligns to the length of the CNT when it comes into close proximity. Another interesting finding was the difference in tendency of sfGFP-132AzPhe and sfGFP-204AzPhe to bind to the sidewall of CNTs, with the 204AzPhe variant binding more frequently than the 132AzPhe variant. We hypothesised that this was caused by differences in solvent exposure to the AzPhe molecule with the 132 position allowing a large amount of exposure to solvents whereas the 204 position is on the β-barrel, making it only partially exposed to solvents.

Aside from the AzPhe covalent linking, we managed to briefly investigate the use of non-covalent linker methods by using pyrene or short-strand DNA. The pyrene moiety was cross-linked to the azide molecule in the modified protein via CuAAC, which, although this can be detrimental to the structure of the protein, allowed us to non-covalently bind cyt-b_{562} in two different orientations to CNTs via π-π stacking.

We had some minor success in binding proteins to a linker molecule present on a modified DNA strand, wrapped around a CNT. This would provide a way of linking proteins to CNTs in solution without the need for a surfactant. This is a process which could be developed to produce reproducible, reliable results, however we did not manage to further this investigation in the scope of this project.

In order to study how the proteins interacted with CNTs when covalently cross-linked, we used the optical techniques Raman spectroscopy and TIRFM. Raman spectroscopy provided information about the binding mechanism to help confirm the covalent nature of the bond between the proteins and CNTs. We were able to demonstrate a clear induced D peak in Raman spectra upon addition of TEM-165AzPhe to pristine mSWNTs with UV exposure, which was not seen in the same samples without UV exposure. This information provided evidence of defect sites being produced in the sp^2 carbon surface through covalent attachment of the azide group. We went further to demonstrate clear shifts on the D and G′ modes to higher frequencies upon covalent cross linking of sfGFP-204AzPhe and cyt b_{562}-50AzPhe. This is evidence of an induced strain in the sp^2 as a result of sp^3 orbitals being formed. When combining this evidence with that found from AFM imaging and CNT resistance measurements, we can conclude that we have successfully covalently cross-linked proteins to CNTs with control over the position of protein-CNT interaction.

TIRFM provided a powerful method of detecting single molecule fluorescence dynamics on and off CNTs. By using sfGFP as a biological fluorescent marker, we were able to image CNTs using optical microscopy methods, demonstrating both effective cross-linking and post deposition activity of the protein on the nanotubes.

These experiments were conducted both in solution and in ambient conditions, demonstrating the stability and versatility of such a system. In addition to this, We were able to use TIRFM data to measure the decay times of sfGFP-132AzPhe and sfGFP-204AzPhe, as well as observing their dynamics as unbound molecules and when bound to SWNTs. There was a clear difference in fluorescence and decay times between the two sfGFP variants, with sfGFP-132AzPhe having the shorter decay time and the lower fluorescent intensity. Although we are unsure of the exact reason of these differences, it does highlight the importance of the position of the linker molecule to the dynamics of the protein. When bound to the SWNTs, we saw very different results to the unbound protein data, with sfGFP-204AzPhe decaying much quicker than sfGFP-132AzPhe. We can hypothesise that this difference was caused by a combination of the shorter distance between the chromophore and the CNT, as well as the possibility of the CNT blocking a water channel around Ser205. These processes would suggest a combination of proton shuttling and electron transfer in determining the nature of the fluorescent dynamics of the protein. Nevertheless, we have shown in intimate electronic interaction between proteins and CNTs with the position of the linker molecule with respect to the active centre of the protein being a key variable when developing protein-CNT hybrid systems.

6.1 Future work

With the growing demand for fast, intimate diagnostic techniques for disease and drug delivery, this work can be developed to meet the requirements for real-time diagnostic measurements. Although we didn't test this platform for use as a biomedical detector, our efforts in attaching proteins such as TEM β-Lactamse to CNTs can developed in the attempt to detect electrical changes upon interactions with an inhibitor protein. We can improve the electrical setup by reducing the size of the electrodes and fine tuning the DEP conditions, to enable us to bridge far fewer CNTs (less than 10) across the electrodes in order to measure single

molecule interaction events, without the electrical signal being suppressed by the signal from the ensemble of CNTs.

This work can also be taken in a different direction, with the possibility to use CNTs to try to further our understanding of protein electrical dynamics. We touched upon this when studying the dynamics with TIRFM. Though further analysis could be done, incorporating more protein variants and fine tuning the system with single chirallity CNTs. Furthering our understanding of the blinking dynamics of a protein could shed light on the mechanisms which govern the protein's function.

While our efforts in developing protein-CNT hybrids with DNA as the intermediate material were short lived, this work can be developed further to produce CNT-protein-CNT junction systems. This work has been demonstrated by our collaborators in Queen Mary University, London. By incorporating this structure into an electrical device, we could perform single molecule electrical measurements to develop our understanding of the electron transfer phenomenon in individual protein structures. We have been successful in providing a reliable method of cross-linking a variety of proteins to CNTs in pre-defined orientations using a variety of linking techniques. This work has stressed the importance of the position of the linker molecule while demonstrating the versatility of such a platform. With further development, this platform can be used to perform real-time single molecule measurements for understanding fundamental protein dynamics, electron transfer, medical diagnostics and physiology.

Bibliography

[1] Douglas W. Wilmore. Growth Hormone. *Encyclopedia of Gastroenterology*, pages 257–261, 2004.

[2] Y. Takahashi, D. M. Kipnis, and W. H. Daughaday. Growth hormone secretion during sleep. *The Journal of clinical investigation*, 47(9):2079–2090, 1968.

[3] Sibhghatulla Shaikh, Jamale Fatima, Shazi Shakil, Syed Mohd Danish Rizvi, and Mohammad Amjad Kamal. Antibiotic resistance and extended spectrum beta-lactamases: Types, epidemiology and treatment. *Saudi Journal of Biological Sciences*, 22(1):90–101, 2015.

[4] André Matagne, Josette Lamotte-Brasseur, and Jean-Marie Frère. Catalytic properties of class A β-lactamases: efficiency and diversity. *Biochemical Journal*, 330:581–598, 1998.

[5] Kannan Balasubramanian and M Burghard. Biosensors based on carbon nanotubes. *Analytical and Bioanalytical Chemistry*, 385(3):452–468, jun 2006.

[6] Xuefeng Guo. Single-molecule electrical biosensors based on single-walled carbon nanotubes. *Advanced materials (Deerfield Beach, Fla.)*, 25(25):3397–408, jul 2013.

[7] Kenzo Maehashi, Taiji Katsura, Kagan Kerman, Yuzuru Takamura, Kazuhiko Matsumoto, and Eiichi Tamiya. Label-Free Protein Biosensor Based on Sptamer-Modified carbon Nanotube Field-Effect Transistors. *Analytical Chemistry*, 79(2):782–787, 2007.

[8] Robert a. Croce Jr, Sagar Vaddiraju, Pik-Yiu Chan, Rea Seyta, and Faquir C. Jain. Label-free protein detection based on vertically aligned carbon nanotube gated field-effect transistors. *Sensors and Actuators B: Chemical*, 160(1):154–160, dec 2011.

[9] Debjit Chattopadhyay, Izabela Galeska, Fotios Papadimitrakopoulos, V Uni, and Recei V April. Metal-Assisted Organization of Shortened Carbon Nanotubes in Monolayer and Multilayer Forest Assemblies Institute of Materials Science Dense arrays of single-wall carbon nanotubes (SWNTs) aligned normal to substrates has been envisioned to enhance perfo. *Journal of the American Chemical Society*, (20):9451–9452, 2001.

[10] Yani Chen, Guy Royal, Emmanuel Flahaut, Saioa Cobo, Vincent Bouchiat, Laëtitia Marty, and Nedjma Bendiab. Light Control of Charge Transfer and Excitonic Transitions in a Carbon Nanotube/Porphyrin Hybrid. *Advanced Materials*, 29(18), 2017.

[11] Jason J Davis, Karl S Coleman, Bobak R Azamian, Claire B Bagshaw, and Malcolm L H Green. Chemical and biochemical sensing with modified single walled carbon nanotubes. *Chemistry (Weinheim an der Bergstrasse, Germany)*, 9(16):3732–9, aug 2003.

[12] Cristina García-aljaro, Lakshmi N Cella, Dhamanand J Shirale, Miso Park, and Francisco Javier. Biosensors and Bioelectronics Carbon nanotubes-based chemiresistive biosensors for detection of microorganisms. *Biosensors and Bioelectronics*, 26:1437–1441, 2010.

[13] Alexandra M Münzer, Zachary P Michael, and Alexander Star. Carbon Nanotubes for the Label-Free Detection of Biomarkers. *ACS nano*, (9):7448–7453, 2013.

[14] Yongki Choi, Tivoli J Olsen, Patrick C Sims, Issa S Moody, Brad L Corso, Mytrang N Dang, Gregory a Weiss, and Philip G Collins. Dissecting single-molecule signal transduction in carbon nanotube circuits with protein engineering. *Nano letters*, 13(2):625–31, 2013.

[15] Mb Lerner, Jimson D'Souza, and Tatiana Pazina. Hybrids of a genetically engineered antibody and a carbon nanotube transistor for detection of prostate cancer biomarkers. *Acs Nano*, 6(6):5143–9, 2012.

[16] V Georgakilas and K Kordatos. Organic functionalization of carbon nanotubes. *Journal of the American Chemical Society*, 124(5):760–761, 2002.

[17] Qing Hua Wang, Zhong Jin, Ki Kang Kim, Andrew J. Hilmer, Geraldine L. C. Paulus, Chih-Jen Shih, Moon-Ho Ham, Javier D. Sanchez-Yamagishi, Kenji Watanabe, Takashi Taniguchi, Jing Kong, Pablo Jarillo-Herrero, and Michael S. Strano. Understanding and controlling the substrate effect on graphene electron-transfer chemistry via reactivity imprint lithography. *Nature Chemistry*, 4(9):724–732, 2012.

[18] Sung Min Seo, Tae June Kang, Youndong Kim, Namyeon Kim, Jay Ahn, Tae Woo Kim, Yong Hyup Kim, Sung Ho Ryu, and Young June Park. Electrode asymmetry driven self-gating effect on the electrical detection of protein. *Sensors and Actuators, B: Chemical*, 191:800–805, 2014.

[19] J. Ozhikandathil, S. Badilescu, and M. Packirisamy. Plasmonic Gold Decorated MWCNT Nanocomposite for Localized Plasmon Resonance Sensing. *Scientific Reports*, 5:1–11, 2015.

[20] Mitchell B. Lerner, Jennifer Dailey, Brett R. Goldsmith, Dustin Brisson, and A. T. Charlie Johnson. Detecting Lyme disease using antibody-functionalized single-walled carbon nanotube transistors. *Biosensors and Bioelectronics*, 45(1):163–167, 2013.

[21] B.L. Allen, P.D. Kichambare, and a. Star. Carbon Nanotube Field-Effect-Transistor-Based Biosensors. *Advanced Materials*, 19(11):1439–1451, jun 2007.

[22] Christopher A. Hunter and Jeremy K.M. Sanders. The Nature of π-π Interactions. *Journal of the American Chemical Society*, 112(14):5525–5534, 1990.

[23] Kihwan Nam, Kilho Eom, Jaemoon Yang, Jinsung Park, Gyudo Lee, Kuewhan Jang, Hyungbeen Lee, Sang Woo Lee, Dae Sung Yoon, Chang Young Lee, and Taeyun Kwon. Aptamer-functionalized nano-pattern based on carbon nanotube for sensitive, selective protein detection. *Journal of Materials Chemistry*, 22(44):23348, 2012.

[24] Yuki Yamamoto, Tsuyohiko Fujigaya, and Naotoshi Nakashima. Fundamental properties of oligo double-stranded DNA / single-walled carbon nanotube nanobiohybrids . *The Royal Society of Chemistry*, 2:1767–1772, 2010.

[25] Yu Wang, Dian Ming Zhou, Zhan Wu, Li Juan Tang, and Jian Hui Jiang. Terminal protection of small molecule-linked ssDNA-SWNT nanoassembly for sensitive detection of small molecule and protein interaction. *Chinese Chemical Letters*, 24(2):107–110, feb 2013.

[26] Benjamin S Flavel, Manfred M Kappes, Ralph Krupke, and Frank Hennrich. Separation of Single-Walled Carbon. *ACS nano*, (4):3557–3564, 2013.

[27] B.J. Bauer, M.L. Becker, V. Bajpai, J.a. Fagan, E.K. Hobbie, K. Migler, C.M. Guttman, and W.R. Blair. Measurement of Single-Wall Nanotube Dispersion by Size Exclusion Chromatography. *Journal of Physical Chemistry C*, 111(48):17914–17918, dec 2007.

[28] Aravind Vijayaraghavan. Bottom-up assembly of nano-carbon devices by dielectrophoresis. *Physica Status Solidi (B)*, 250(12):2505–2517, dec 2013.

[29] Lifeng Dong, Vachara Chirayos, Jocelyn Bush, Jun Jiao, Valery M Dubin, Ramanan V Chebian, Yoshi Ono, John F Conley, and Bruce D Ulrich. Floating-Potential Dielectrophoresis-Controlled Fabrication of Single-Carbon-Nanotube Transistors and Their Electrical Properties. *ACS Physicsl Chemistry*, 109(27):13148–13153, 2005.

[30] Samuel Reddington, Peter Watson, Pierre Rizkallah, Eric Tippmann, and D Dafydd Jones. Genetically encoding phenyl azide chemistry: new uses and ideas for classical biochemistry. *Biochemical Society Transactions*, 41(5):1177–1182, 2013.

[31] Eduardo Antonio, Della Pia, Qijin Chi, J Emyr Macdonald, Jens Ulstrup, D Dafydd, and Martin Elliott. Fast electron transfer through a single molecule natively structured redox protein. *The Royal Society of Chemistry*, 4:7106–7113, 2012.

[32] Eduardo Antonio, Della Pia, Qijin Chi, Martin Elliott, and J Emyr Macdonald. ChemComm Redox tuning of cytochrome b 562 through facile metal porphyrin substitution w. pages 10624–10626, 2012.

[33] Andrew M Hartley, Athraa J Zaki, Adam R Mcgarrity, Cecile Robert-ansart, Andriy V Moskalenko, Gareth F Jones, Monica F Craciun, Saverio Russo, Martin Elliott, J Emyr, and D Dafydd Jones. Functional modulation and directed assembly of an enzyme through non-natural post-translation modification. *Chemical Science*, 6:3712–3717, 2015.

[34] R Saito ; G Dresselhaus ; M S Dresselhaus ;. *Physical Properties of Carbon Nanotubes*. Imperial College Press, 5 edition, 1998.

[35] S Iijima. Helical microtubules of graphitic carbon. *Nature*, 354:56–58, 1991.

[36] P R Bandaru. Electrical properties and applications of carbon nanotube structures. *Journal of Nanoscience and Nanotechnology*, 7(4):1239–1267, apr 2007.

[37] Feng Zhang, Peng-xiang Hou, Chang Liu, Bing-wei Wang, Hua Jiang, Maolin Chen, Dong-ming Sun, Jin-cheng Li, Hong-tao Cong, Esko I Kauppinen, and Hui-ming Cheng. Growth of semiconducting single-wall carbon nanotubes with a narrow band-gap distribution. *Nature Communications*, 7:1–8, 2016.

[38] Wei Hung Chiang and R. Mohan Sankaran. Linking catalyst composition to chirality distributions of as-grown single-walled carbon nanotubes by tuning Ni x Fe 1x nanoparticles. *Nature Materials*, 8(11):882–886, 2009.

[39] Hang Woo Lee, Yeohoon Yoon, Steve Park, Joon Hak Oh, Sanghyun Hong, Luckshitha S. Liyanage, Huiliang Wang, Satoshi Morishita, Nishant Patil,

Young Jun Park, Jong Jin Park, Andrew Spakowitz, Giulia Galli, Francois Gygi, Philip H.S. Wong, Jeffrey B.H. Tok, Jong Min Kim, and Zhenan Bao. Selective dispersion of high purity semiconducting single-walled carbon nanotubes with regioregular poly(3-alkylthiophene)s. *Nature Communications*, 2(1):541–548, 2011.

[40] Yehai Yan, Mary B Chan-Park, and Qing Zhang. Advances in carbon-nanotube assembly. *Small (Weinheim an der Bergstrasse, Germany)*, 3(1):24–42, jan 2007.

[41] Kannan Balasubramanian and Klaus Kern. 25th Anniversary Article: Label-Free Electrical Biodetection Using Carbon Nanostructures. *Advanced Materials*, 26(8):n/a–n/a, mar 2014.

[42] Sebastian Kruss, Andrew J. Hilmer, Jingqing Zhang, Nigel F. Reuel, Bin Mu, and Michael S. Strano. Carbon nanotubes as optical biomedical sensors. *Advanced Drug Delivery Reviews*, 65(15):1933–1950, 2013.

[43] Michael S. Strano, Stephen K. Doorn, Erik H. Haroz, Carter Kittrell, Robert H. Hauge, and Richard E. Smalley. Assignment of (n, m) Raman and optical features of metallic single-walled carbon nanotubes. *Nano Letters*, 3(8):1091–1096, 2003.

[44] R B Weisman and P V Subramoney. Carbon Nanotubes. *The Electrochemical Society interface*, 15(2):42–46, 2006.

[45] Jeremy M. Berg, John L. Tymoczko, and Lubert Stryer. *Biochemistry.* Freeman, fifth edit edition, 2002.

[46] David L. Nelson and Michael Cox. *Lehninger Principles of Biochemistry, 3rd Ed.* Worth Publishers Inc., 2000.

[47] M F Perutz. Electrostatic Effects in Proteins. *AAAS*, 201(September), 1978.

[48] Alexi V. Finkelstein and Oleg B. Ptitsyn. *Protein Physics.* Academic Press, 2002.

[49] Clemens B Winkelmann, Irina Ionica, Xavier Chevalier, Guy Royal, Christophe Bucher, and Vincent Bouchiat. Optical Switching of Porphyrin-Coated Silicon Nanowire Field Effect Transistors. *Nano Letters*, 7(6):1454–1458, 2007.

[50] David S Hecht, Robert J A Ramirez, Mikhail Briman, Erika Artukovic, Kelly S Chichak, J Fraser Stoddart, and George Gr. Bioinspired Detection of Light Using a Nanotube Field Effect Transistor. *Nano Letters*, 6(9):2031–2036, 2006.

[51] Hareem T Maune, Si-ping Han, Robert D Barish, Marc Bockrath, William A. Goddard III, Paul W K Rothemund, and Erik Winfree. Self-assembly of carbon nanotubes into two-dimensional geometries using DNA origami templates. *Nature Nanotechnology*, 5(1):61–66, 2010.

[52] a. B. Dalton, a. Ortiz-Acevedo, V. Zorbas, E. Brunner, W. M. Sampson, S. Collins, J. M. Razal, M. Miki Yoshida, R. H. Baughman, R. K. Draper, I. H. Musselman, M. Jose-Yacaman, and G. R. Dieckmann. Hierarchical Self-Assembly of Peptide-Coated Carbon Nanotubes. *Advanced Functional Materials*, 14(12):1147–1151, dec 2004.

[53] Ole Hammerich, Jens Ulstrup, Richard J Nichols, Wolfgang Haiss, David G Fernig, Harm Van Zalinge, and David J Schiffrin. *In Situ Stm Studies Of Immobilized Biomolecules At The Electrodeelectrolyte Interface*. Bioinorganic Electrochemistry, 2008.

[54] Lisa Scullion, Thomas Doneux, Laurent Bouffier, David G. Fernig, Simon J. Higgins, Donald Bethell, and Richard J. Nichols. Large conductance changes in peptide single molecule junctions controlled by pH. *Journal of Physical Chemistry C*, 115(16):8361–8368, 2011.

[55] Stacy L Springs, Susanna E Bass, and George L Mclendon. Cytochrome b 562 Variants : A Library for Examining Redox Potential Evolution . *ACS Biochemistry*, 39:6075–6082, 2000.

[56] Roger Y Tsien. THE GREEN FLUORESCENT PROTEIN. *Annual Rev. Biochem*, (67):509–44, 1998.

[57] Andre Matagne, Josette Lamotte-Brasseur, and Jean-Marie Frere. Catalytic properties of class A β-lactamases: efficiency and diversity. *Biochem J*, 330:581–598, 1998.

[58] Mats Ormö and Andrew B. Cubitt. Cristal Structure of the Aequorea victoria Green Fluorescent Protein. *Science*, 273(September):1392, 1996.

[59] P Hager. Studies on Cytochrome b562 of Escherichia. *The Journal of Biological Chemistry*, 242(9):2272–2277, 1967.

[60] Takahito Mukai, Akiko Hayashi, Fumie Iraha, Aya Sato, Kazumasa Ohtake, Shigeyuki Yokoyama, and Kensaku Sakamoto. Codon reassignment in the Escherichia coli genetic code. *Nucleic Acids Research*, 38(22):8188–8195, 2010.

[61] Samuel C Reddington, Eric M Tippmann, and D Dafydd Jones. Residue choice defines efficiency and influence of bioorthogonal protein modification via genetically encoded strain promoted Click chemistry. *Chemical communications (Cambridge, England)*, 48(67):8419–21, 2012.

[62] Li Li and Zhiyuan Zhang. Development and applications of the copper-catalyzed azide-alkyne cycloaddition (CuAAC) as a bioorthogonal reaction. *Molecules*, 21(10):1–22, 2016.

[63] Erika Penzo, Matteo Palma, Risheng Wang, Haogang Cai, Ming Zheng, and Shalom J Wind. Directed Assembly of End-Functionalized Single Wall Carbon Nanotube Segments. *Nano Letters*, 15:6547–6552, 2015.

[64] Shalom J Wind, Erika Penzo, Matteo Palma, Risheng Wang, Teresa Fazio, Danny Porath, Dvir Rotem, Gideon Livshits, and Avigail Stern. Integrating DNA with Functional Nanomaterials. *Journal of Self-Assembly and Molecular Electonics*, 1:177–194, 2013.

[65] G Binnig and C.F. Quate. Atomic Force Microscope. *Physical Review Letters*, 56(9), 1986.

[66] Nader Jalili and Karthik Laxminarayana. A review of atomic force microscopy imaging systems: Application to molecular metrology and biological sciences. *Mechatronics*, 14(8):907–945, 2004.

[67] B Cappella and G Dietler. Force-distance curves by atomic force microscopy. *Surface Science Reports*, 34:1–104, 1999.

[68] Q. Zhong, D. Inniss, K. Kjoller, and V.B. Elings. Fractured polymer/silica fiber surface studied by tapping mode atomic force microscopy. *Surface Science*, 290(1-2):L688–L692, jun 1993.

[69] M.S. Dresselhaus, G. Dresselhaus, R. Saito, and a. Jorio. Raman spectroscopy of carbon nanotubes. *Physics Reports*, 409(2):47–99, 2005.

[70] Anne Crawford, Edmir Silva, Karen York, and Chenxiang Li. Raman Spectroscopy : A Comprehensive Review. *Department of Textile Engineering, Chemistry and Science*.

[71] Kenneth N Fish. Total Internal Reflection Fluorescence (TIRF) Microscopy. *Curr Protoc Cytom*, (2):1–21, 2009.

[72] Michael Jermyn, Joannie Desroches, Kelly Aubertin, Karl St-Arnaud, Wendy Julie Madore, Etienne De Montigny, Marie Christine Guiot, Dominique Trudel, Brian C. Wilson, Kevin Petrecca, and Frederic Leblond. A review of Raman spectroscopy advances with an emphasis on clinical translation challenges in oncology. *Physics in Medicine and Biology*, 61(23):R370–R400, 2016.

[73] a. Ferrari and J. Robertson. Interpretation of Raman spectra of disordered and amorphous carbon. *Physical Review B*, 61(20):14095–14107, 2000.

[74] V. Brar, Ge. Samsonidze, M. Dresselhaus, G. Dresselhaus, R. Saito, a. Swan, M. Ünlü, B. Goldberg, a. Souza Filho, and a. Jorio. Second-order harmonic and combination modes in graphite, single-wall carbon nanotube bundles,

and isolated single-wall carbon nanotubes. *Physical Review B*, 66(15):1–11, 2002.

[75] By Daniel Axelrod. Total Internal Reflection Fluorescence Microscopy in Cell Biology. *Methods in enzymology*, 361(1996), 2000.

[76] Daniel Axelrod. Cell-substrate Contacts Illuminated by Total-Internal Reflection Fluorescence. *Journal of Cell Biology*, 89(9):141–145, 1981.

[77] Thi Thuy Nguyen, Sy Uan Nguyen, Dinh Tam Phuong, Duc Chien Nguyen, and Anh Tuan Mai. Dispersion of denatured carbon nanotubes by using a dimethylformamide solution. *Advances in Natural Sciences: Nanoscience and Nanotechnology*, 2(3):035015, aug 2011.

[78] Panagiotis Angelikopoulos and Andrei Gromov. Dispersing individual single-wall carbon nanotubes in aqueous surfactant solutions below the cmc. *The Journal of Physical Chemistry C*, pages 2–9, 2009.

[79] PC Ma, JK Kim, and BZ Tang. Functionalization of carbon nanotubes using a silane coupling agent. *Carbon*, pages 1–18, 2006.

[80] Yan Yan Huang and Eugene M. Terentjev. Dispersion of Carbon Nanotubes: Mixing, Sonication, Stabilization, and Composite Properties. *Polymers*, 4(4):275–295, jan 2012.

[81] P Stokes and SI Khondaker. Directed assembly of solution processed single-walled carbon nanotubes via dielectrophoresis: from aligned array to individual nanotube devices. *Journal of Vacuum Science & Technology B*, 28(6), 2010.

[82] Evgeniy E. Tkalya, Marcos Ghislandi, Gijsbertus de With, and Cor E. Koning. The use of surfactants for dispersing carbon nanotubes and graphene to make conductive nanocomposites. *Current Opinion in Colloid and Interface Science*, 17(4):225–232, aug 2012.

[83] Zhi-Bin Zhang, Juan Cardenas, Eleanor E. B. Campbell, and Shi-Li Zhang. Reversible surface functionalization of carbon nanotubes for fabrication of field-effect transistors. *Applied Physics Letters*, 87(4):043110, 2005.

[84] JM Bonard, Thierry Stora, and JP Salvetat. Purification and size-selection of carbon nanotubes. *Advanced Materials*, (10):827–831, 1997.

[85] Herbert A. Pohl. *Dielectrophoresis*. Syndics of the Cambridge University Press, 1978.

[86] Ralph Krupke, Frank Hennrich, Hilbert V Löhneysen, and Manfred M Kappes. Separation of metallic from semiconducting single-walled carbon nanotubes. *Science (New York, N.Y.)*, 301(5631):344–7, jul 2003.

[87] Ming Lin Li, Siu Ling Leung, Yan Li Qu, Zai Li Dong, and Wen J. Li. Dielectrophoretic assembly of 2 nm gold particles for nano-sensing applications. *2010 IEEE 5th International Conference on Nano/Micro Engineered and Molecular Systems, NEMS 2010*, pages 932–936, 2010.

[88] Brian R Burg and Dimos Poulikakos. Review Large-scale integration of single-walled carbon nanotubes and graphene into sensors and devices using dielectrophoresis : A review. *Materials Research Society*, 26(13):1561–1571, 2011.

[89] M. Grujicic, G. Cao, a. M. Rao, T. M. Tritt, and S. Nayak. UV-light enhanced oxidation of carbon nanotubes. *Applied Surface Science*, 214:289–303, 2003.

[90] M. Grujicic, G. Cao, and R. Singh. The effect of topological defects and oxygen adsorption on the electronic transport properties of single-walled carbon-nanotubes. *Applied Surface Science*, 211:166–183, 2003.

[91] Alexey M. Bogdanov, Alexander S. Mishin, Ilia V. Yampolsky, Vsevolod V. Belousov, Dmitriy M. Chudakov, Fedor V. Subach, Vladislav V. Verkhusha, Sergey Lukyanov, and Konstantin A. Lukyanov. Green fluorescent proteins are light-induced electron donors. *Nat. Chem. Biol.*, 5(7):459–461, 2010.

[92] Masashi Ishii, Bruce Hamilton, and Nigel Poolton. Imaging of charge trapping in distorted carbon nanotubes by x-ray excited scanning probe microscopy. *Journal of Applied Physics*, 104(10):1–5, 2008.

[93] Sohye Jang, Kalme Sachin, Hui-jeong Lee, Dong Wook Kim, and Hyun Soo Lee. Development of a Simple Method for Protein Conjugation by Copper-Free Click Reaction and Its Application to Antibody-Free Western Blot Analysis. *Bioconjugate Chemistry*, 23(11):2256–2261, 2012.

[94] Tilman Plass, Sigrid Milles, Christine Koehler, Carsten Schultz, and Edward A. Lemke. Genetically encoded copper-free click chemistry. *Angewandte Chemie - International Edition*, 50(17):3878–3881, 2011.

[95] Jean François Lutz. Copper-free azide-alkyne cycloadditions: New insights and perspectives. *Angewandte Chemie - International Edition*, 47(12):2182–2184, 2008.

[96] Andrea C. Ferrari and Denis M. Basko. Raman spectroscopy as a versatile tool for studying the properties of graphene. pages 1–26, 2013.

[97] Mingyuan Huang, Hugen Yan, Tony F. Heinz, and James Hone. Probing strain-induced electronic structure change in graphene by Raman spectroscopy. *Nano Letters*, 10(10):4074–4079, 2010.

[98] F Withers, S Russo, M Dubois, and M F Craciun. Tuning the electronic transport properties of graphene through functionalisation with fluorine. *Nano Res Letts*, 6:1–11, 2011.

[99] Thomas Basche. Fluorescence intesity fluctuations of single atoms , molecules and nanoparticles. *Journal of Luminescence*, 77:263–269, 1998.

[100] Robert M Dickson, Andrew B Cubitt, and Roger Y Tsien. On / off blinking and switching behaviour of single molecules of green fluorescent protein. *Letters To Nature*, 388(July):355–358, 1997.

[101] C R Bagshaw and D Cherny. Blinking fluorophores : what do they tell us about protein dynamics ? *Proteins: Structure and Function*, pages 979–982, 2006.

[102] Fernando D Stefani, Jacob P Hoogenboom, and Eli Barkai. Beyond quantum jumps : Blinking nano - scale light emitters. *Physics today*, pages 34–39, 2009.

[103] Christian Blum and Vinod Subramaniam. Single-molecule spectroscopy of fluorescent proteins. *Analytical and Bioanalytical Chemistry*, 393(2):527–541, 2009.

[104] Ai Shinobu and Noam Agmon. Proton wire dynamics in the green fluorescent protein. *Journal of Chemical Theory and Computation*, 13(1):353–369, 2017.

[105] Ai Shinobu, Gottfried J. Palm, Abraham J. Schierbeek, and Noam Agmon. Visualizing proton antenna in a high-resolution green fluorescent protein structure. *Journal of the American Chemical Society*, 132(32):11093–11102, 2010.

[106] Eduardo Antonio, Della Pia, Qijin Chi, D Dafydd Jones, J Emyr Macdonald, Jens Ulstrup, and Martin Elliott. Single-Molecule Mapping of Long-range Electron Transpot for a Cytochrome b562 Variant. *Nano Letters*, 11:176–182, 2011.